Time and Frequency Offsets in All Optical OFDM Systems

by

Mumtaz Ali

A thesis submitted in partial fulfilment for the degree of
Doctor of Philosophy

at

Heriot-Watt University
Institute of Photonics and Quantum Sciences,
School of Engineering and Physical Sciences

September 2014

Abstract

Ultra-high-speed data transmission (terabit-per-second per channel) is urgently required in optical communication systems to fulfill the emerging demands of 3D multimedia applications, cloud computing, and bandwidth-hungry applications. In one way by using single-carrier optical communication systems for the data transmission rates $\geq$ 1 Tb/s, we need the high baud rate and/or the high-order modulation formats (i.e. 512-QAM, 1024-QAM). Another way is to group the data carrying subcarriers without a guard bands (tightly spaced) to form a *superchannel* which gives increase in channel capacity. In a superchannel, the requirements of high-order modulation formats and high baud rates are relaxed. In an all-optical orthogonal frequency division multiplexing (AO-OFDM) system, the subcarriers are orthogonal and closely packed which gives more suitability to form superchannel. This thesis focuses on the time and frequency offsets in AO-OFDM systems.

A theoretical model to investigate the performance of on-off-keying (OOK) modulated AO-OFDM system is developed for analytical simulation. The analytical (statistical) model considers the random characteristics of time and frequency offsets in adjacent subcarriers as well as the common noise sources such as shot and thermal noises to calculate the interference variances for evaluating the BER performance. The effects of time and frequency offsets on the BER performance of AO-OFDM system is evaluated with the number of optical subcarriers (N_{SC}), receiver bandwidth (BW_{RX}), and cyclic prefix (CP)

We further develop an analytical model to evaluate the performance of AO-OFDM system with advanced modulation format (M-QAM) in the presence of time and frequency offsets, and the performance is compared with numerical simulations of other emulation setups (odd-and-even subcarriers and decorrelated systems). The performance is investigated with N_{SC}, BW_{RX}, and CP in AO-OFDM system. A delay-line interferometer based all-optical method to reduce the effects of time and frequency offsets is proposed and evaluated.

Finally, performance of demultiplexed subcarriers from an optical discrete Fourier trans-

form (O-DFT) in AO-OFDM system in the presence of chromatic dispersion and limited modulation bandwidth is evaluated. The fiber Bragg grating (FBG) based passive device is proposed to reduce the interference and the results are compared with existing method using sampling gates. The proposed method using FBG for interference reduction provides a cost-effective design of AO-OFDM system.

Acknowledgements

I would like to thank my supervisor Dr. Xu Wang for generous help, constant support, and high quality advices throughout my Ph.D. studies. I am also thankful for providing me the exposure to international events such as 15^{th} International Conference on Transparent Optical Networks (ICTON 2013) in Cartagena Spain, and 8^{th} International Workshop on Optical signal processing and Optical switching (IWOO 2013) in Edinburgh UK.

I would like to acknowledge Dr. Bo Dai (Postdoctoral Researcher) for useful advices and tips during my research work. I am grateful to all my colleagues, Mr. Xuhua Wang and Mr. Yu Liang, in the OCPN group for fruitful discussions.

I am thankful to the Heriot-Watt University for providing Ph.D. scholarship funding and professional training opportunities. Also, I am grateful to the academics of Heriot-Watt University for providing me the opportunities of working in state-of-art labs of Optoelectronics, Digital Signal Processing Lab (TMS32C6713 DSK), Digital Design (Altera Quartus II), Computer Architecture and Embedded Systems (PIC microcontroller), Electrical Energy Systems, Mobile Communication, Advanced Analog Electronics, Electric Circuits, Signal and Systems, Engineering Mathematics with Matlab. Ultimately, the working in these labs not only helped me in my Ph.D. research but also in future works.

I would like to thank my mother and late father who guided me in every season of my life. Last but not the least, my wife and my daughter, Maryam, whose love always encouraged me to follow my dreams.

ACADEMIC REGISTRY
Research Thesis Submission

Name:	MUMTAZ ALI		
School/PGI:	Engineering & Physical Sciences		
Version: *(i.e. First, Resubmission, Final)*	Final	Degree Sought (Award **and** Subject area)	Ph.D. (Electrical Engineering)

Declaration

In accordance with the appropriate regulations I hereby submit my thesis and I declare that:

1) the thesis embodies the results of my own work and has been composed by myself
2) where appropriate, I have made acknowledgement of the work of others and have made reference to work carried out in collaboration with other persons
3) the thesis is the correct version of the thesis for submission and is the same version as any electronic versions submitted*.
4) my thesis for the award referred to, deposited in the Heriot-Watt University Library, should be made available for loan or photocopying and be available via the Institutional Repository, subject to such conditions as the Librarian may require
5) I understand that as a student of the University I am required to abide by the Regulations of the University and to conform to its discipline.

* *Please note that it is the responsibility of the candidate to ensure that the correct version of the thesis is submitted.*

Signature of Candidate:		Date:	30th September 2014

Submission

Submitted By *(name in capitals)*:	MUMTAZ ALI
Signature of Individual Submitting:	
Date Submitted:	

For Completion in the Student Service Centre (SSC)

Received in the SSC by *(name in capitals)*:			
Method of Submission *(Handed in to SSC; posted through internal/external mail)*:			
E-thesis Submitted ***(mandatory for final theses)***			
Signature:		Date:	

Please note this form should bound into the submitted thesis.

Updated February 2008, November 2008, February 2009, January 2011

Table of Contents

List of Tables

List of Figures

Acronyms

- **ADC** Analog-to-Digital Converters
- **AO-OFDM** All-Optical OFDM
- **AWG** Arrayed Waveguide Grating
- **B2B** Back-to-Back
- **BER** Bit Error Rate
- **BW** Bandwidth
- **CD** Chromatic Dispersion
- **CFO** Carrier Frequency Offset
- **CMA** Constant Modulus Algorithm
- **CO-OFDM** Coherent Optical OFDM
- **CP** Cyclic Prefix
- **CPE** Common Phase error
- **CW** Continuous Wave
- **DAC** Digital-to-Analog Converter
- **DEMUX** Demultiplexer
- **DFT** Discrete Fourier Transform
- **DI** Delay Interferometer
- **DLI** Delay Line Interferometer
- **DQPSK** Differential Quadrature Phase Shift Keying
- **DSP** Digital Signal Processor
- **EAM** Electro Absorption Modulator
- **EDFA** Erbium Doped Fibre Amplifier
- **EVM** Error Vector Magnitude
- **FBG** Fiber Bragg Grating
- **FEC** Forward Error Correction
- **FFT** Fast Fourier Transform
- **FIR** Finite Impulse Response
- **FPGA** Field-Programmable Gate Array
- **GVD** Group Velocity Dispersion
- **ICI** Intercarrier Interference
- **IDFT** Inverse Discrete Fourier Transform
- **IFFT** Inverse Fast Fourier Transform
- **IM/DD** Intensity Modulation/Direct Detection

- **ISI** Intersymbol Interference
- **LD** Laser Diode
- **LO** Local Oscillator
- **MLLD** Mode-Locked Laser Diode
- **MUX** Multiplexer
- **MZM** Mach-Zehnder Modulator
- **NRZ** Non Return-to-Zero
- **OCDMA** Optical Code Division Multiple Access
- **OFDM** Orthogonal Frequency Division Multiplexing
- **OFDMA** Orthogonal Frequency Division Multiple Access
- **OOK** On-Off Keying
- **OTN** Optical Transport Network
- **P/S** Parallel-to-Serial
- **PAPR** Peak to Average Power Ratio
- **PD** Photodetector
- **PON** Passive Optical Network
- **PRBS** Pseudo Random Binary Sequence
- **PS** Phase Shifter
- **QAM** Quadrature Amplitude Modulation
- **RX** Receiver
- **S/P** Serial-to-Parallel
- **ScFO** Subcarrier Frequency Offset
- **SG** Sampling Gate
- **SMF** Single Mode Fiber
- **SNR** Signal-to-Noise Ratio
- **SSB** Single Side Band
- **SSFBG** Superstructured Fiber Bragg Grating
- **STM** Symbol Time Misalignment
- **STO** Symbol Time Offset
- **WDM** Wavelength Division Multiplexing
- **WLAN** Wireless Local Area Networks

Chapter 1

Introduction

1.1 Evolution of optical transport networks

In the last two decades, the expansion of the internet has increased a growth of transport network bandwidth [1]. In Figure 1.1 (red circles), the growth rate is 60% per year from 2001 to 2010, with the total network traffic of 20 Tb/s for the US network in year 2010 [2]. Similar trends can be seen in regions in the rest of world (Australia, Hong Kong, Japan, South Korea, and Western Europe) [3]. Due to future data-centric cloud applications, which takes the role of distributed system, the growth rates may be accelerated. As per Amdahl's rule of thumb [4, 5], the processor's bandwidth is proportional to its power of processing. These two things binds the growth in network traffic and have evolution of supercomputers with the scaling slope of 2.7 dB/year, as shown in Figure 1.1 (green squares). Furthermore, the multimedia application requiring the large network bandwidth is gaining importance.

For large amounts of data traffic, a high-speed optical interfaces at an access network and a transmission network (including intermediate nodes in the core networks) are required [1]. For point-to-point serial interfaces, the rates of multiplexed interfaces are scaled at 0.5 dB

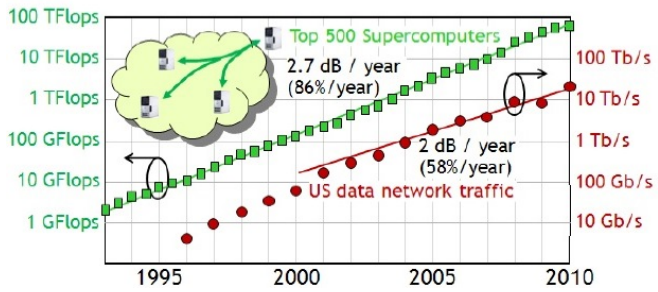

Figure 1.1: Evolution of Optical Transport Networks [2].

per year which is proportional to speed of the semiconductor devices, as shown in Figure 1.2. From 2005 to 2010, the transmission rates are nearly constant at 100 Gbps but there is transition to advanced modulations (quadrature phase shift keying (QPSK) and quadrature amplitude modulation (QAM)) with coherent detection [6], in order to get the high spectral efficiencies in wavelength division multiplexing (WDM). With the use of advanced modulation formats, the scaling of physical interfaces to high data rates is not easier due to the requirements of high effective number of bits of data converters (DAC and ADC) [7]. Comparing the scaling trends in Figure 1.2, the interface rate of 200 Gbps per polarization has already been demonstrated but the electronic multiplexed serial transmissions of signals of 1 Tbps are still in research.

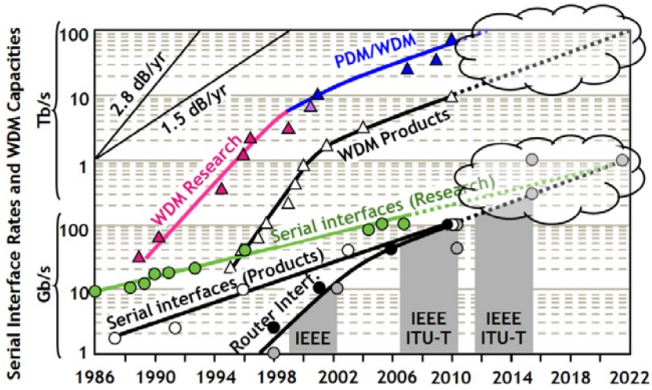

Figure 1.2: Evolution of serial interfaces and WDM systems in research and products [1].

Until 2006, the optical networks normally operates on circuit-switched serial interfaces, and with the new 100 Gb/s standards (IEEE and ITU-T) the networks are moved to packet switched parallel interfaces. The upgradation of switching networks (circuit to packet) allows the technological development in OTN data rates, for e.g. SONET/SDH/OTN (white), WAN devices (black) and ethernet devices (grey) are shown in Figure 1.2.

1.2 Advanced Modulation Formats for High Spectral Efficiency

The evolution of spectral efficiency in research is recorded at 1.2 dB per year, as shown in Figure 1.3(a) [1]. Furthermore, the use of polarization division multiplexing (PDM) allows to maintain the same rate of scaling. Due to the fundamental reason of direct relationship between the spectral efficiency of system and required signal-to-noise ratio, increasing the level of modulation format from 4 QAM to 16 QAM (twice) requires the SNR of 3.8 dB more. Further increase in level of modulation format from 16 QAM to 256 QAM incurs SNR penalty 8.8 dB, as shown in Figure 1.3(b). The SNR penalties associated with the use of higher level modulation formats reduce the transmission distances [8]. Further, with the short system's reach the cost and energy consumption of a system increases due to more electro-optic regenerations at the intermediate nodes. In [8], the spectral efficiency limitation is estimated in 1000 km fiber link is nearly 16 b/s/Hz by using PDM. With the decrease in transmission distance to half gives improvement in the spectral efficiency of 2 b/s/Hz.

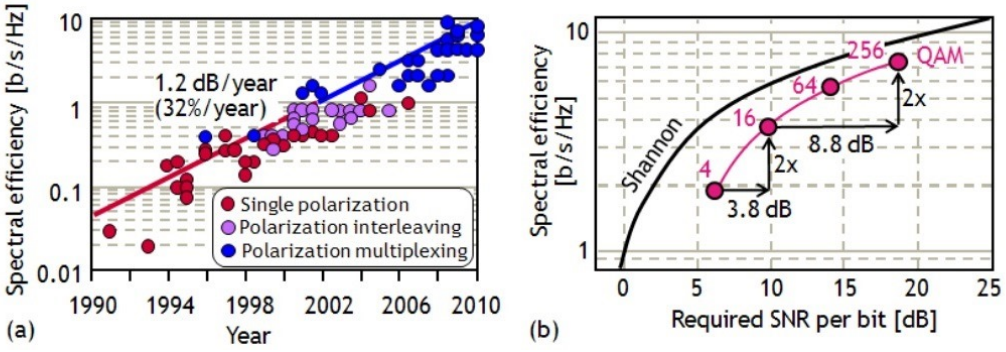

Figure 1.3: Spectral efficiency in research (a) evolution and (b) required SNR [1].

1.3 Single-carrier versus multi-carrier approaches

In a single carrier approach, only one carrier frequency carries the data information while in a multicarrier approache, information is transmitted in parallel on low data-rate subcarriers.

Orthogonal frequency division multiplexing (OFDM) technique is a one of the approach of multicarrier data transmission. In OFDM, the spectrum of an orthogonal subcarriers are overlapped. For information transmission, single-carrier and multi-carrier transmission systems (coherent optical-OFDM) has advantages and disadvantages given as follows [10, 11]:

1.3.1 Single-Carrier Approach

- Channel estimation is purely based on blind equalization algorithms like constant modulus algorithm (CMA). The CMA is normally used for phase modulation and not easily be implemented for multi-level modulations (like M-ary QAM).

- With the increase in order of the multi-level modulation formats, design of optical modulation part becomes complex due to a serial or parallel configurations of optical modulators. Due to rise in single-carrier system complexity with order of multi-level modulation format, the cost of system increases.

- Encodes the data on full available spectrum makes difficult the system scalability in a bandwidth.

- Implementation is easier and requires low cost of system, and an achieved spectral efficiency $\leq$ 1 b/s/Hz in comparison to multi-carrier approach.

1.3.2 Multi-Carrier Approach

- Multicarrier systems have shifted the capabilities of signal processing to the transmitter by using software-defined optical transmission which gives an adaptivity to transmitter. The important processing capabilities are the estimation and compensation of channel and phase. By using pilot symbols or pilot subcarriers in multicarrier system give easier to an estimation of channel and phase.

- For high-level modulation formats (8-PSK or 8-QAM and above), reduces the system

cost due to only reconfiguration required in digital signal processor (DSP) and data converters.

- The spectrum is tighter and signal is generated in frequency domain which makes easier to partition the rectangular-shaped OFDM spectrum into small multiple bands and each band can be processed separately.

- Recorded data transmission rates $\geq$ 1 Tbps in research with an achieved spectral efficiency $\geq$ 1 b/s/Hz. The important condition for data rates $\geq$ 1 Tbps (in an optical OFDM systems) is orthogonality among subccarriers have to be maintained.

- Optical components commercially available at lower speeds, and an integration of components is comparatively complex.

On the basis of above comparisons, multicarrier approaches offers the advantages in terms of bandwidth scalability, adaptability of transponders, high spectral efficiency and high data rates. In a multicarrier approaches we have disadvantages of a high peak to average power ratio which poses the challenges of channel (fiber) nonlinearity, and a strict synchronization requirements in order to avoid frequency, time and phase offsets.

1.4 Multiplexing Techniques for Optical Superchannels Scheme

The superchannel of a desired capacity is the combination of several independent data-modulated optical subcarriers, and the subcarriers are either from single source or multiple continuous wave (CW) laser sources [12]. For the single laser source (mode-locked laser diode) generating multiple subcarriers, the phase control is normally not required but for other case stabilized laser sources are required [13].

The combined subcarriers in a superchannel offers the highest spectral efficiency, and it can be achieved by using a higher order modulation format (like 16-QAM) with coherent

detection at receiver [14] and a pulse shaping techniques. Previously, return-to-zero pulse shape technique and its variants were used for the requirements of high sensitivity, interference reduction and increase in tolerance to nonlinearity of transmission medium. Now-a-days, orthogonal frequency division multiplexing (OFDM)[11], [12], Nyquist-WDM[15] - [17], and coherent-WDM (CoWDM) [18] are used for (de) multiplexing with less crosstalk at high spectral efficiency. In AO-OFDM system, the complex-data symbols are modulated on an orthogonal optical subcarriers. In Nyquist-WDM system (N-WDM), the complex data symbols are modulated on temporal sinc-shaped subcarriers. In coherent WDM (CoWDM), the closely packed rectangular-spectra shaped subcarriers carry the complex data symbols. As shown in Figure 1.4, in an OFDM transmitter no phase control or pulse shaping filter required while in other two system we need a tight control of phase (in CoWDM) or an optical filter (in N-WDM) is required to reduce an interchannel interference or fulfill the condition of Nyquist principle.

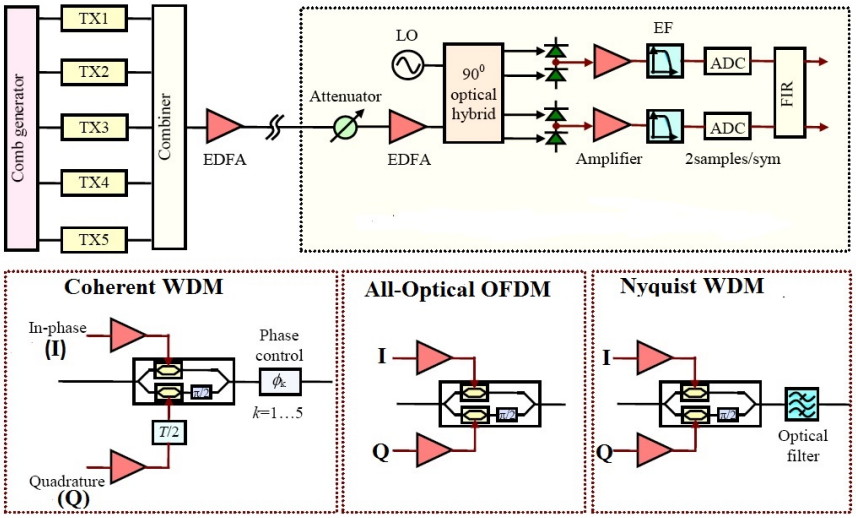

Figure 1.4: Superchannels multiplexing types [18].

In Figure 1.5, the spectrums of transmitted superchannels are shown, where Δf, and M_{BW} are subcarrier spacing, and total bandwidth of subcarrier. In AO-OFDM, the electrical signal is the baseband M-QAM signal which is modulated on optical subcarrier. The spacing between optical subcarriers is Δf and is less than M_{BW} . In the spectrum of Co-WDM, the

phase control is used to ensure $\Delta f = M_{BW}$ with no guard bands. In Co-WDM, we need a tight control of phase among data carrying subcarrier in order to minimize an interference [18]. In a N-WDM, a condition of $\Delta f > M_{BW}$ is required and subcarriers have a rectangular spectral shape.

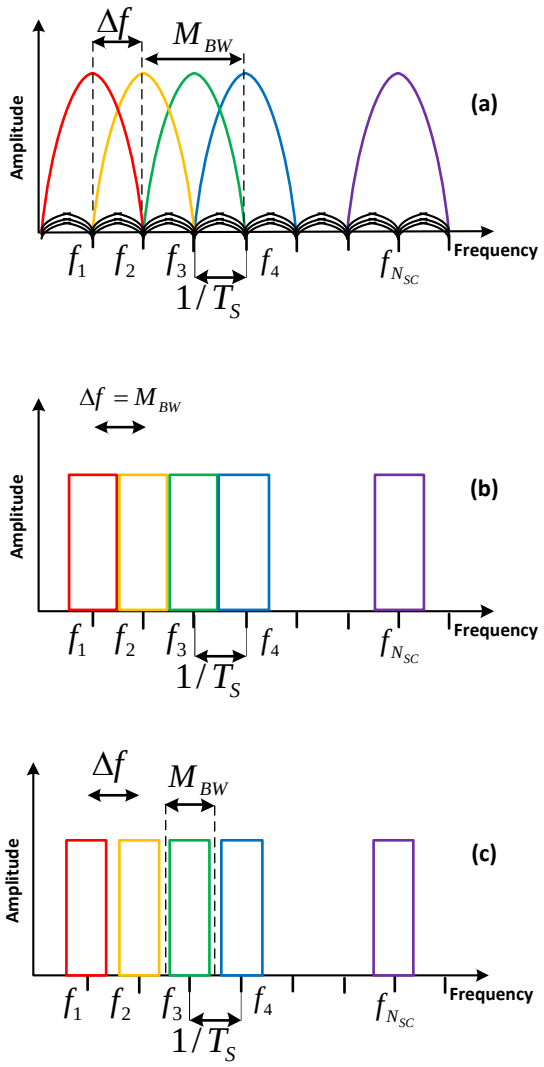

Figure 1.5: Spectrum of multiplexing techniques for superchannels (a) all-optical OFDM (b)coherent WDM (c) Nyquist WDM [18].

1.5 Motivation

In the needs of 3D multimedia applications, cloud computing and applications which requires the fat-pipes, the Tbit/sec superchannels are emerged to fulfill the needs of bandwidth hungry applications [19]. In a traditional time division multiplexing (TDM), multiple data streams are transmitted in an assigned time slot. The data transmission of 10.2 Tbit/sec is possible with TDM scheme but the challenges posed on the requirements of optical pulses with short duration [20]. In optical pulse sources, the spectrum of signal is broader which needs a precise dispersion compensation [21]. Another way is to use the WDM based superchannels scheme which allows the several channel transmissions in parallel. With the WDM based superchannels transmission, the needs of the short temporal pulse durations and the precise dispersion compensation are relaxed with the compromise on spectral efficiency and dedicated laser sources are required for each channel which increases the cost of system [13].

Optical OFDM in optical communications systems offers high spectral efficiency, tolerance to chromatic dispersion (CD), and the data information is encoded on subcarriers which are normally > 100, [22] - [27]. With the increased interest in this multicarrier transmission technique, it is applied to access and long-haul networks for high data rates [28] - [32]. As well as OFDM based data transmission have several advantages, it is sensitive to synchronization in time, frequency and phase [11]. In the presence of any of the above sensitivity to synchronization, the orthogonality among overlapped subcarrier is destroyed and the performance of OFDM system is seriously degraded.

AO-OFDM system implementation offers the highest aggregated data transmission with high spectral efficiency [12]. In the experimental demonstrations [33], AO-OFDM system comprises of one or two modulators to show the proof of concepts. In these demonstrations, the modulated optical subcarriers carry same data symbols, and the effects of channel impairments and synchronization issues are nearly scaled. Ultimately, the performance measures (BER and OSNR) are clearly not reflecting an actual system performance [34].

1.6 Contributions and List of Publications

The key contributions of this work are summarized below.

Chapter 3

- We propose OOK-modulated AO-OFDM model to investigate the symbol time misalignment and subcarrier frequency offsets.
- An analytical model is developed to evaluate the BER performance of AO-OFDM system
- Evaluate the performance for AO-OFDM system design parameters.

Chapter 4

- We propose analytical and numerical (Monte-Carlo) models for the performance evaluations of M-QAM AO-OFDM system.
- Develop numerical models of emulation setups of AO-OFDM systems.
- Propose a DLI based interference reduction method.

Chapter 5

- We propose a numerical (Monte-Carlo) model for the performance evaluation of OOK-modulated AO-OFDM system in the presence of CD and limited modulation bandwidth.
- Propose the FBG-assisted interference reduction method and the results are compared with SG based optical sampling method.

List of Publications The work presented in this thesis has led to the following publications:

- M. Ali, and X. Wang, "FBG-Assisted ICI Reduction for AO-OFDM Demultiplexed Signal", Microwave and Optical Technology Letters, vol. 56, pp. 23202324, 2014.
- M. Ali, B. Dai, and X. Wang, "Time and Frequency Synchronization in OOK AO-OFDM System", Accepted in IET Communications in 2014.
- M. Ali, B. Dai, and X. Wang, "M-QAM All-Optical OFDM System Performance Evaluation with Frequency and Timing Offsets", Submitted in Microwave and Optical Technology Letters in 2014.
- M. Ali and X. Wang,"Effects of symbol time misalignment and frequency offset on performance of realistic all-optical OFDM system", 15th International Conference on Transparent Optical Networks (ICTON 2013), Cartagena, Spain, July, 2013.
- M. Ali, B. Dai, and X. Wang, "Performance Evaluation of Superchannels Using All-Optical M-QAM OFDM and Coherent Receiver in the Presence of Time and Frequency Offsets", Accepted Full Paper (ID:255601) in Chinacom2014, Maoming, China, 2014.

1.7 Thesis Outline

The remainder of this thesis is organized as follows:

Chapter 1: Introduction In this chapter, we introduces our research work and highlight the importance of superchannels in a Tbit/sec data transmissions. Furthermore, it provides a motivation of choosing this research topic.

Chapter 2: Background of OFDM for Optical Communication System In this chapter, we illustrated the principles of OFDM based data transmission with mathematical expressions, highlighted the advantages over single-carrier approach. The three variant of OFDM in

optical communication systems, IM/DD OFDM, CO-OFDM and AO-OFDM, are discussed and compared their advantages with their limitations. Existing methods of detection of a composite AO-OFDM signal are discussed. Finally, the requirements of synchronization in OFDM systems are discussed.

Chapter 3: Time and Frequency Synchronization in OOK AO-OFDM System In this chapter, we have investigated the performance of OOK-modulated AO-OFDM system in the presence of symbol time misalignment and subcarrier frequency offset. In AO-OFDM system, the superchannel at the transmitter is based on optical subcarriers are independently OOK-modulated and combined to form the composite AO-OFDM signal, and the coherent detection at receiver. We have developed an analytical simulation model and evaluated a BER performance for two cases: numbers of subcarriers (N_{SC}) from 8 to 512, and from 3 to 128 at the data rate 10 Gbit/sec. Further, the system performance is evaluated with N_{SC}, receiver bandwidth, and cyclic prefix.

Chapter 4: M-QAM All-Optical OFDM System Performance Evaluation with Frequency and Timing Offsets This chapter provides AO-OFDM system (AO-OFDM transmitter and coherent detection) performance evaluation for advanced modulation format (M-QAM). For performance evaluations, we have first developed an analytical model and the simulation results are compared with the results of existing emulation setups. Our model considered not only the effects of interferences due to time and frequency offsets but also the receiver's shot and thermal noises. Further, an existing method of interference reduction (cyclic prefix) is also discussed. Finally, we have proposed a DLI based interference reduction method for AO-OFDM system.

Chapter 5: FBG-Assisted ICI Reduction for AO-OFDM Demultiplexed Signal In this chapter, the effects of CD and limited modulation bandwidth are evaluated on the performance of O-DFT based receiver in AO-OFDM system. FBG based passive device for inter-

ference reduction is proposed and results are compared with SG based existing method of optical sampling for all four subcarriers.

Chapter 6: Conclusions and Future Works This chapter summarizes the work in this thesis with future work.

Chapter 2

Background of OFDM for Optical Communication Systems

Orthogonal frequency division multiplexing (OFDM) is much mature type of multicarrier transmission in wired and wireless communication systems [32]. The main reason of using OFDM is the tolerance to an intersymbol interference (ISI) caused by dispersion of transmission medium. This effect important for high data rates and a traditional serial modulation formats like quadrature amplitude modulation (QAM) or non-return to zero (NRZ), which requires equalization in time domain. Another advantage of OFDM is that the multicarrier transmitter and receiver implementations are in digital domain rather than in analog domain. Due to these advantages of OFDM based data transmission, it has been adopted in a high-end symmetrical digital subscriber lines (DSL), digital television (TV), broadcasting of high-definition TV (HDTV), wireless local area network such as 802.11 a/g, long term evolution (LTE), and IEEE 802.16 [31], [39]. It has also been deployed in power line systems (PLC) [40], cognitive systems [41] and free-space optical systems [42]-[44]. Furthermore, OFDM has been introduced in optical communication systems for multiple carrier transmissions in parallel [35] - [37].

In OFDM system, the parallel transmission of original data symbols on multiple subcarriers have different frequencies which results the extension of original symbol duration. The resultant OFDM symbol duration is larger than the original data symbol duration of a serial transmission system. Due to longer OFDM symbol duration, it is more tolerable to ISI and ultimately the equalization circuit complexity reduces. Furthermore, the residual ISI can be

removed by using cyclic prefix (CP) [32].

When the existing multicarrier transmission techniques are used in wireless and optical communication systems like frequency division multiplexing (FDM) and wavelength division multiplexing (WDM), then a simultaneous data is also transmitted on a number of different frequency channels. In FDM and WDM systems, the guard bands are used between subcarriers in order to reduce the spectral overlap. The main difference in OFDM system from FDM/WDM system is the subcarriers frequencies are chosen in such a way that there are no guard bands among subcarriers and the subcarriers are orthogonal to each other. The inverse Fourier transform (IFT) is used to multiplex in a digital domain which reduces the implementation cost and complexity of system design. In FDM/WDM system, an analog filter is used to recover the desired subcarrier. In Figure 2.1, the graphical illustration of FDM, WDM and OFDM spectra are shown [31]. In OFDM, the subcarriers are overlapped (for bandwidth efficiency) and orthogonal, and they can be demultiplexed at a receiver with only single Fourier transform (FT) block. The shape of subcarriers' is a sinc form and have many side lobes. This is the main drawback of OFDM system which causes the system sensitive to frequency and phase offsets [32].

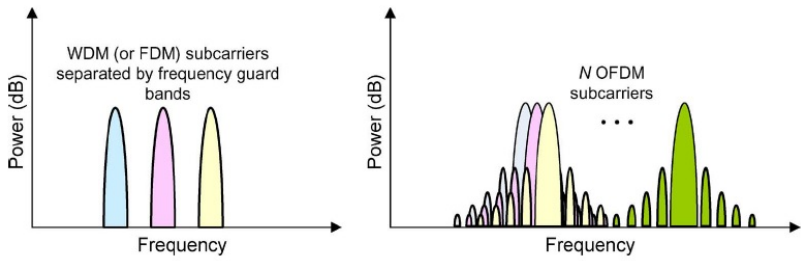

Figure 2.1: Graphical illustration of spectra of FDM, WDM, and OFDM [31].

2.1 OFDM transmitter and receiver

In OFDM system, the transmitter first maps the digital bits information into a waveforms of particular modulation format, like phase shift keying (PSK) or QAM symbols. The serial

modulated symbols are converted to N parallel data streams by a serial-to-parallel (S/P) converter. After S/P conversion, N different subcarriers carry N data symbols. Consider $X_l[k]$ denote the k^{th} subcarrier carried by l^{th} symbol, where k = 1, 2, ... , N, l = 1, 2, ... , ∞. After S/P conversion, the symbol duration is increased to NT_s which will ultimately the duration of OFDM symbol, $T_{sym} = NT_s$. Consider $\Psi_{l,k}(t)$ denote the k^{th} subcarrier carried by l^{th} OFDM symbol, which is given as

$$\Psi_{l,k}(t) = \begin{cases} e^{j2\pi f_k(t-lT_{sym})}, & 0 < t \leq T_{sym} \\ 0, & elsewhere \end{cases} \tag{2.1}$$

The relationship between the low frequency and the high frequency signals can be expressed as

$$x_l(t) = \sum_{l=0}^{\infty} \sum_{k=0}^{N-1} X_l[k] e^{j2\pi f_k(t-lT_{sym})} \tag{2.2}$$

and

$$x_l(t) = \mathrm{Re}\left\{ \frac{1}{T_{sym}} \sum_{l=0}^{\infty} \left\{ \sum_{k=0}^{N-1} X_l[k] \Psi_{l,k}(t) \right\} \right\}, \tag{2.3}$$

It is noted that $x_l(t)$ is the IFT of PSK or QAM symbols. The received OFDM signal, $y_l(t) = \sum_{l=0}^{\infty} \sum_{k=0}^{N-1} X_l[k] e^{j2\pi f_k(t-lT_{sym})}$, is processed to reconstruct $X_l[k]$ by FT operation which is given as

$$\begin{aligned} Y_l[k] &= \frac{1}{T_{sym}} \int_{-\infty}^{\infty} y_l(t) e^{-j2\pi f_k(t-lT_{sym})} dt \\ &= \frac{1}{T_{sym}} \int_{-\infty}^{\infty} \left\{ \sum_{i=0}^{N-1} X_l[i] e^{j2\pi f_i(t-lT_{sym})} \right\} e^{-j2\pi f_k(t-lT_{sym})} dt \\ &= \sum_{i=0}^{N-1} X_l[i] \left\{ \frac{1}{T_{sym}} \int_{0}^{T_{sym}} e^{j2\pi(f_i-f_k)(t-lT_{sym})} dt \right\} \\ &= X_l[k] \end{aligned} \tag{2.4}$$

At the OFDM receiver, the FT algorithms are used to efficiently demodulate the subcar-

rier. The graphical illustration of above mathematical expressions for OFDM modulation and demodulation process is shown in Figure 2.2 (a) [10]. The symbol, in frequency domain, $X[k]$ is modulated on the k^{th} subcarrier. In this illustration, six subcarriers, with k^{th} subcarrier frequency is $f_k = k/T_{sym}$, are used for OFDM signal transmission. In the demodulation process, an orthogonality property is used to demodulate the subcarriers. The sketch between transmitter and receiver shows the total OFDM symbol duration, T_{sym}, is longer than the original symbol, $X[k]$, duration which is T_s. Actually, OFDM symbol is a composite signal of N symbols which have total duration of T_{sym}. In Figure 2.2 (b), the spectra of overlapped OFDM subcarriers is shown. The overlapping of OFDM subcarriers is used for bandwidth efficiency. In Figure 2.3, the multicarrier modulation and demodulation in an OFDM is implemented by IFFT and FFT blocks at the transmitter and receiver sides.

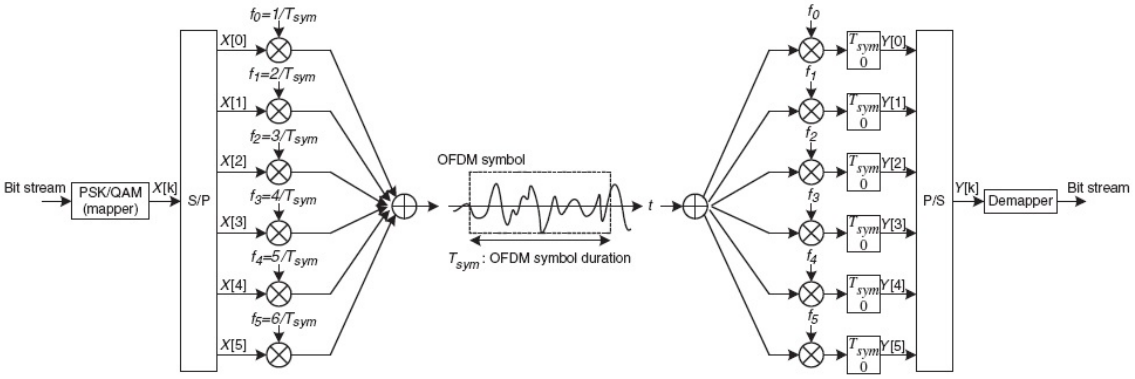

(a) OFDM modulation/demodulation

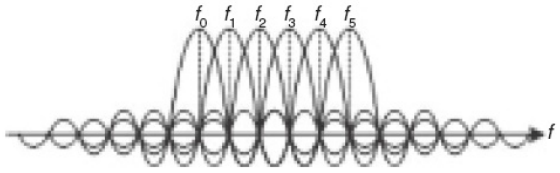

(b) Realization of subcarrier orthogonality

Figure 2.2: Graphical illustration of OFDM system [10].

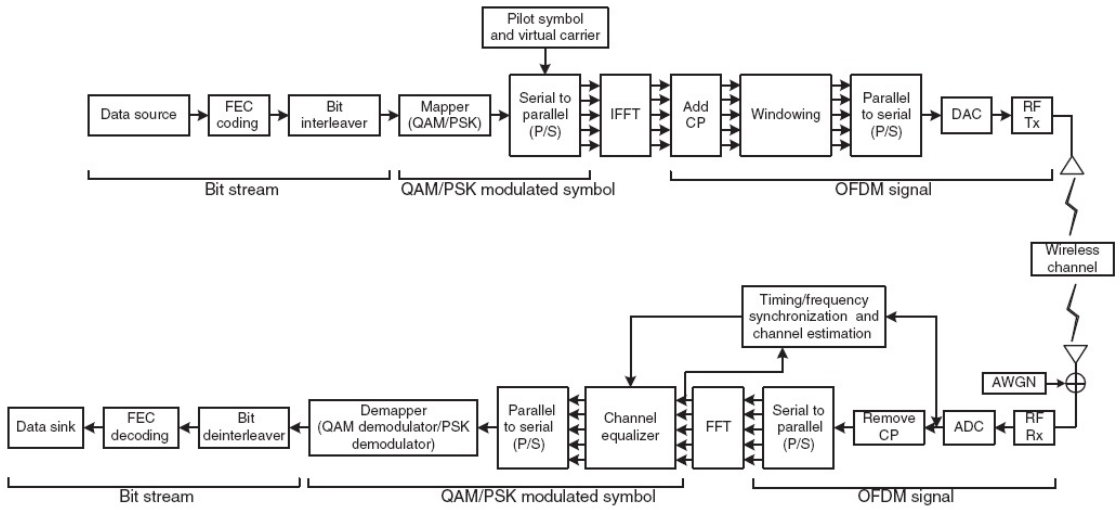

Figure 2.3: Block diagram of OFDM system [10].

2.2 Orthogonality condition in OFDM

The orthogonality condition is required in OFDM system in order to be intercarrier interference (ICI)-free [10]. In a given OFDM signal, $\left\{e^{j2\pi f_k t}\right\}_{k=0}^{N-1}$, where $0 \leq t \leq T_{sym}$, the k^{th} subcarrier have the frequency $f_k = k/T_{sym}$. The subcarriers are orthogonal if the integration of the products is zero, which is given as

$$\begin{aligned}\frac{1}{T_{sym}}\int_0^{T_{sym}} e^{j2\pi f_k t}e^{-j2\pi f_k t}dt &= \frac{1}{T_{sym}}\int_0^{T_{sym}} e^{j2\pi\frac{k}{T_{sym}}t}e^{-j2\pi\frac{i}{T_{sym}}t}dt \\ &= \frac{1}{T_{sym}}\int_0^{T_{sym}} e^{j2\pi\frac{(k-i)}{T_{sym}}t}dt \\ &= \begin{cases} 1, & \forall \text{int} \quad k=i \\ 0, & otherwise \end{cases}\end{aligned} \tag{2.5}$$

2.3 OFDM in an optical domain

An optical signal of a continuous wave (CW) laser source offers wide range of data modulations like modulation of its amplitude, phase, polarization, intensity, or amplitude and a

phase combined. Same variants of detection schemes are available at receiver. By introducing OFDM in an optical domain, new ways of transmitter and receiver implementations are possible. In this section, we discuss three related modulation/detection schemes. These are optical intensity/field modulation with direct-detection (IM/DD), coherent optical modulation with coherent detection (CO-OFDM), and all-optical OFDM (AO-OFDM), as shown in Figure 2.4 - Figure 2.6 [38].

2.3.1 IM/DD-OFDM

In this scheme, the multicarrier signal as OFDM signal in an electrical domain is generated by digital signal processor (DSP) and converted to an analog signal by digital-to-analog converter (DAC). An analog electrical OFDM signal is upconverted with radio-frequency (RF) front-end, as shown in Figure 2.4 [38]. An electrical OFDM signal (complex valued data signals) conversion to optical domain using optical modulation (OM) can be done by either an intensity modulation or a field modulation.

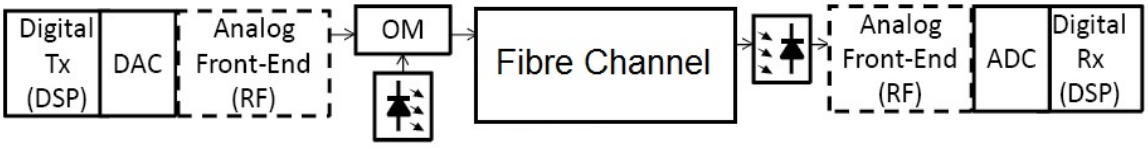

Figure 2.4: Block diagram of IM/DD optical OFDM scheme [38].

For field modulation case, an optical I/Q modulator can be used which translate the complex OFDM signal on an optical field. In an intensity modulation case, the modulated optical signal is directly proportional to the electrical OFDM signal. As an optical intensity have to be real and non-negative, the electrical OFDM signal must also needs to be real and positive in order to avoid distortion. In an optical intensity modulation, the real electrical OFDM signal can be obtained by an electrical I/Q modulator or a Hermitian symmetry (at the output of IFFT). In a Hermitian symmetry, there are no issues of I/Q multiplexing so we have no problem of I/Q imbalance. On the other side of using Hermitian symmetry, we have to discard the second half of OFDM symbol frame which ultimately reduces the data rate by

half. Another requirement for intensity modulation is to operate a modulator at its point of quadrature. For this purpose, a high dc bias have to be added to the RF signal in order to be positive RF OFDM signal. In this way, an optical carrier, which have no information, contain much optical power in an optical OFDM signal transmission. As a result, system operates at cost with low performance. Further, fiber nonlinearity poses a challenges for high optical carrier power. Different ways of OFDM signal clipping and a dividing the optical power of an optical carrier with sidebands have been proposed to reduce these effects of high power in OFDM systems [46], [47].

After optical OFDM signal transmission through fiber channel, a direct photodetection of double-side band (with linear phases) would gives a destructive interference at receiver. This effect can be avoided by using optical single sideband (OSSB) filter at transmitter. By using the OSSB filter in optical OFDM transmission system, the effects of chromatic dispersion (CD) reduces to a phase shift in only one sideband [48]. The advantage of linear phase shift is the correction at the receiver side is easier by the use of cyclic prefix (CP) and frequency domain equalization (FDE).

At the receiver side, the direct detection by using single photodiode translates the optical intensity to a beating terms of desired carrier with sideband RF term, and undesirable mixing products of sidebands (baseband/low frequency). The mixing product of sidebands have spectral width of 0 Hz to OFDM subcarrier of maximum frequency. In order to avoid the performance degradation of an IM/DD optical OFDM system, the frequency of RF is chosen to be much high to have guard band between the desired and undesired frequency components [47] [49]. With this technique of avoiding the performance degradation, the spectral efficiency of a system is compromised. Another disadvantage of using an IM/DD OFDM technique in an optical domain is the need of high optical power. In spite of the above disadvantages, for the next-generation of an optical access networks, an IM/DD optical OFDM provides a cost-effective solution with the use of off-the-shelf optical components.

2.3.2 Coherent Optical-OFDM

In a coherent optical-OFDM system (CO-OFDM), an inphase/quadrature (I/Q) modulator is used to modulate the optical field of an optical signal with an electrical multicarrier signal (OFDM). As an optical I/Q modulator generates only one sideband so we don't have to use the OSSB filter at the transmitter side but we need to use a local oscillator (LO) at the receiver side, as shown in Figure 2.5 [38]. At a transmitter side, the power requirements of an optical carrier is low as it will be suppressed and only power is allocated to the modulated OFDM sideband. So in a CO-OFDM system, we have more resilience to a SNR performance degradation. As a guard band is required in IM/DD OFDM system to avoid the mixing products at the detection, there is no need in CO-OFDM system due to the linear capturing of an optical field by using coherent detection at receiver side [50]. Without guard bands, CO-OFDM system offers a higher bandwidth/spectral efficiency if compared with IM/DD OFDM system. With the use of LO at receiver, the sensitivity of receiver increases which ultimately increases the reach of the system.

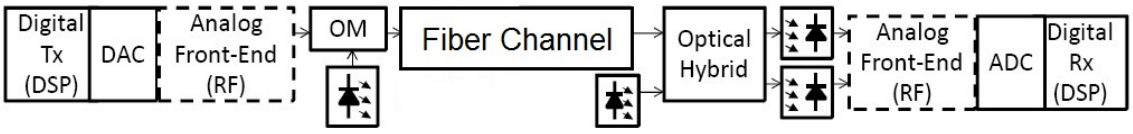

Figure 2.5: Block diagram of coherent optical OFDM scheme [38].

As shown in Figure 2.5 [38], after an electrical multicarrier signal generated from DSP, an optional analog RF front-end is used for electrical I/Q multiplexing before optical modulation. An OSSB is used to filter one sideband in case of intensity modulation, as discussed in the scenario of an IM/DD OFDM system. As described above that there is no need of guard bands in a CO-OFDM system but by considering the sharp edges of an OSSB filter's passband for OFDM signal modulated on an optical carrier, we still need small guardband. After optical signal propagated through fiber channel, a CW laser as a LO, an optical hybrid, and balanced detection are required for coherent detection of OFDM signal. For a downcon-

version from OFDM signal to baseband signal, an analog front-end is used. For the case of homodyne detection, the signal after coherent detection doesn't need an analog front-end.

Due to requirements of LO in a CO-OFDM system, the cost of a system increases. Moreover, the needs of LO poses a system's sensitivity to a phase offset and a frequency offset. In a CO-OFDM system, the DSP algorithms to estimate and compensate these offsets are the major requirements.

2.3.3 AO-OFDM

In an all-optical OFDM (AO-OFDM) system, the inverse discrete Fourier transform (IDFT) is implemented in an optical domain, as shown in Figure 2.6 [38], which is main difference between an AO-OFDM system and an IM/DD OFDM and a CO-OFDM systems, where FFT/IFFT is implemented in an electrical domain by using DSP. In AO-OFDM system, an optical subcarriers, generated from a comb laser source or CW laser sources, are separated by demultiplexer, like arrayed waveguide grating (AWG). After separation of an optical subcarriers or tones, each tone is independently modulated with a complex baseband signal, like M-QAM [12], [51]. For AO-OFDM system with N optical tones, N independent I/Q modulators are required. After N I/Q modulators, the modulated parallel optical streams are combined by multiplexer, such as AWG, and transmitted through fiber channel as a composite AO-OFDM signal. At the receiver side, the composite AO-OFDM signal is demultiplexed and a coherently detected.

In [52], AO-OFDM based superchannel of 1.5 Tbit/sec over transmission distance of 1200km is reported, as shown in Figure 2.7. In an experimental setup, 15 phase-locked subcarriers at the spacing of 12.5 GHz are 16-QAM modulated by using two I/Q modulators in an odd-and-even configuration. The spectra of modulated odd-and-even subcarriers are shown in Figure 2.8 (a). For the alignment of symbols, a tunable optical delay line is used after modulation of odd-and-even subcarriers. After combining the odd-and-even subcarriers, the modulated signal is splitted by 3 dB coupler and one signal path is delayed by 100

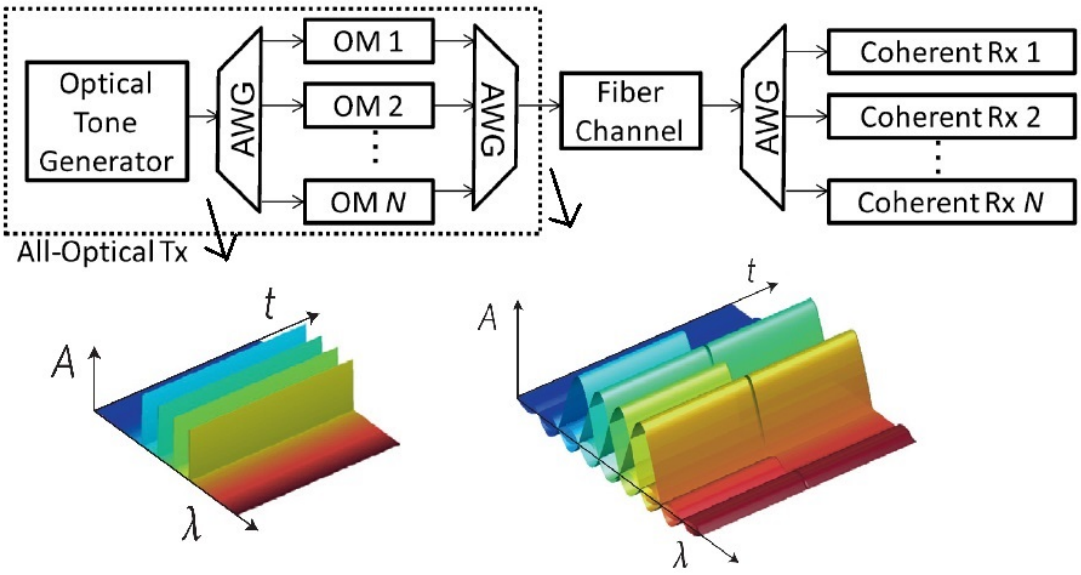

Figure 2.6: Block diagram of all-optical OFDM scheme [38].

symbols. After delaying, the polarization of signal (Y) is rotated by 90^o and combined with other path (X) by using polarization beam combiner. The composite signal of 15 subcarriers dual-polarization 16-QAM modulated is transmitted over 1200 km ($3 \times 5 \times 80$ km) with spectra shown in Figure 2.8 (b).

For demodulation of received composite AO-OFDM signal, LO is used as down-converter of superchannel to desired band. After downcoversion, 90^o optical hybrid with polarization diversity is used to separate the X and Y polarizations before photodetectors. In an investigation of limited receiver bandwith and sampling rate of ADC, the symbol rate of 12.5 Gbaud with varied $2\times$ to $6\times$ analog-to-digital converters (ADC) sampling rate is used in [52]. The bandwidth of sampling scope is set to 30 GHz and in range of 8 GHz to 26 GHz is the cut-off of low pass filter (LPF) in order to investigate the effects of using commercial low-grade photodetectors and ADC. In an experiment, $4\times$ oversampling is the minimum requirement to get the BER $< 10^{-3}$ and larger ADC bandwidth leads to better BER performance. Further in cases of $5\times$ and $6\times$ oversampling, the BER performance achieved is much better than $4\times$ oversampling case. For BER threshold of 10^{-3}, the minimum required bandwidth of ADC is 17.3 GHz for $4\times$ to $6\times$ oversampling range.

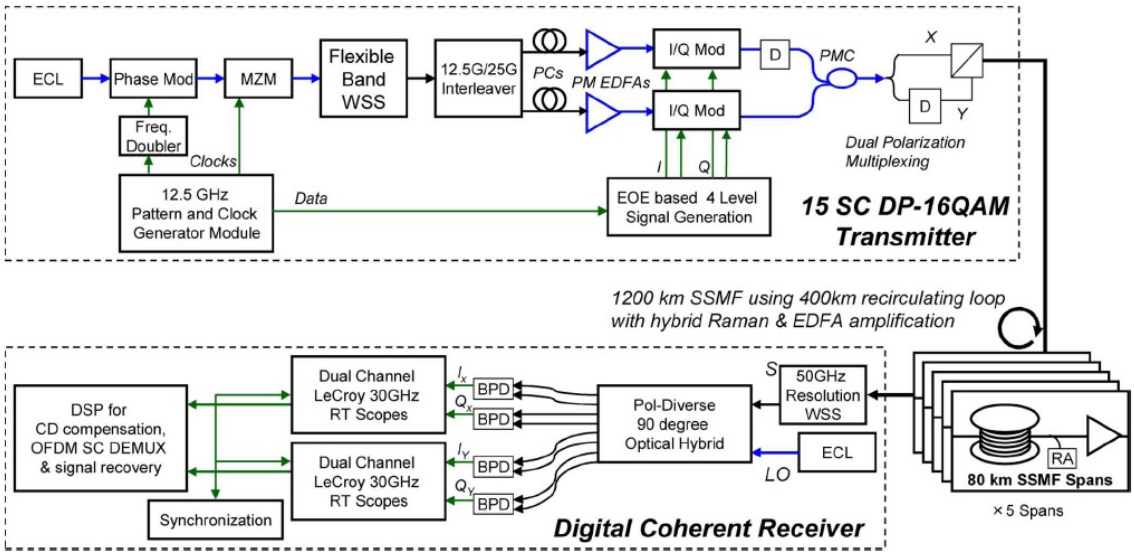

Figure 2.7: Experimental setup of 1.5 Tbit/sec AO-OFDM Transmission and Digital Coherent Receiver [52].

In an experimental results, the launch power of 2 dBm is required for 1.5 Tbit/sec data transmission over 1200 km for BER = 10^{-3} (achieved spectral efficiency of 7 b/s/Hz), as shown in Figure 2.9(a). Furthermore, the BER performance of all 15 subcarriers shows below the threshold of FEC, as shown in Figure 2.9 (b).

Optical receivers in an AO-OFDM systems

In Figure 2.6, the coherent receivers comprises of an analog-to-digital converters (ADC) which can sample the incoming analog signal upto four times the sampling rates of an digital-to-analog converters (DAC) at transmitter side. For the higher rates of transmission, it is required to process the incoming composite signal in an optical domain before photodetection in order to reduce it to a lower-rate. Optical DFT provides this preprocessing in an optical domain which comprises of optical time-delay lines to first convert the serial incoming data to parallel data and then phase shifters, as per DFT principle, to demultiplex the subcarriers. The DFT operation in an optical domain is a continuous process (different from electrical OFDM counterpart), and the output of optical DFT is continuous due to DFT window moves in time domain. In order to correctly detect the received signal after DFT operation for a given

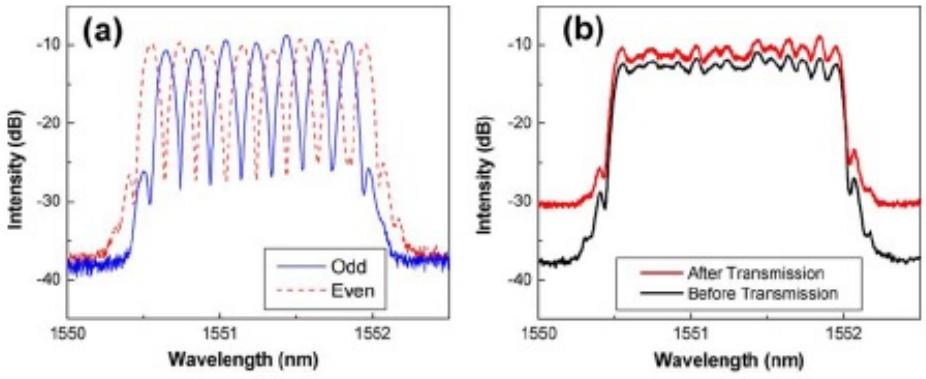

Figure 2.8: Output spectra (a)after modulation (b) superchannel before and after 1200 km [52].

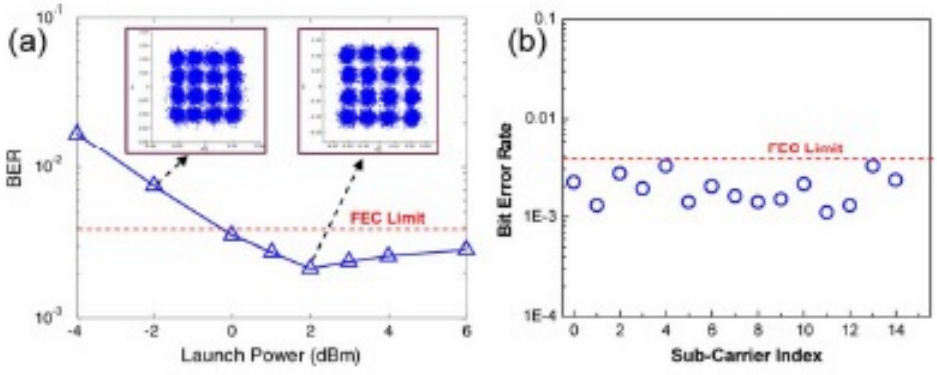

Figure 2.9: BER performance versus (a) launch power (dBm), and (b) optical subcarriers [52].

OFDM symbol, a sampling gates are required. In Figure 2.10, the schematic of optical FFT (O-FFT) is shown which have combined the functions of S/P conversion and FFT operation in an optical domain. The O-FFT operation is implemented by using delay lines, phase shifters, and 3 dB optical couplers. For correct symbol detection of desired subcarrier after O-FFT, electro-absorption modulator based sampling gates are used. For correct symbol detection, the sampling gates are needed to be synchronized with the symbol. Another condition of an O-FFT is the requirements of a minimum phase offsets in the phase shifters (used in O-FFT circuit) in order to correctly demultiplex the subcarriers.

An O-FFT have advantages over electronic counterpart. It can be used for processing of high speed incoming signal due to sampling windows of sampling gates are much shorter than

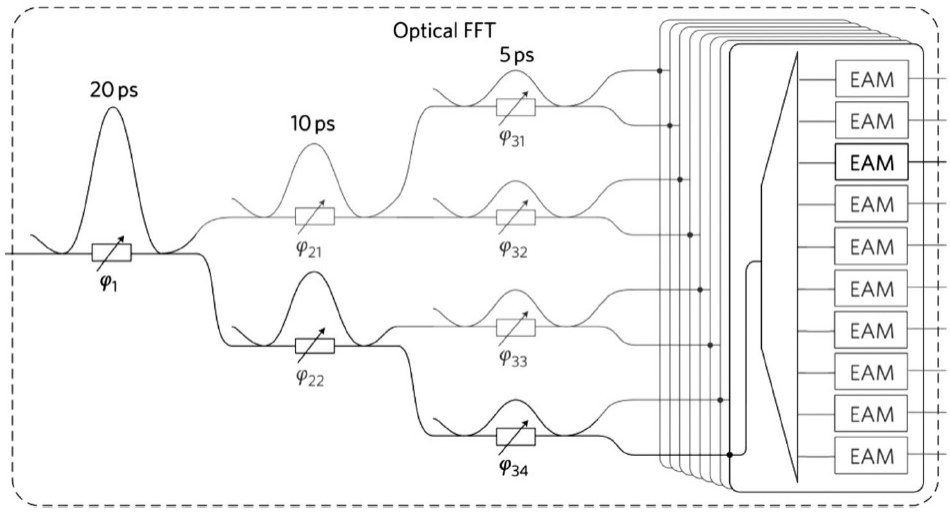

Figure 2.10: Schematic of optical fast Fourier transform based all-optical OFDM composite signal receiver [12].

the sampling windows of ADC in electronic domain. In an O-FFT circuit, the components are passive (delay lines, coupler) and power consumption of these components are much lower. In a case study, the power consumption of 8-point FFT of an incoming signal at the rate of 28 GBd is mainly dominated by an sampling gate driver amplifier, which is 14 W. Additional power is required to compensate the modulation and insertion losses of an optical sampling gates. For the electrical sampling, 160 W is required to process 224 GSa/s signal by using 28 GSa/s ADC (consumes electrical power of 10 W). With the increase of sampling rates, the power consumption (electronic domain) also increases. For performance improvement in electrical OFDM, a guard intervals are normally used. With the guard intervals at the same data rate, power consumption also increases due to processing of guard intervals. In O-FFT, the power consumption remains same with the use of guard intervals [53].

In order to overcome the limitations of ADC and photodiodes bandwidth, the research towards implementation of all-optical transmitter and receiver based on OFDM principle is progressed in [54] - [56] and an all-optical transmitter for superchannel at the data rate of 10.8 Tbit/sec has been reported in [12]. For an all-optical receiver, O-DFT circuits are proposed in [51], [57], which can achieve the FFT function without need of an optical to electrical

domains conversion. In [57], an O-DFT is used to demultiplex 8 subcarrier optically.

In [58], the optical circuits are realized for IFFT and FFT operations by using arrayed waveguide gratings (AWG). Traditionally, AWGs are used in a WDM system for a wavelengths multiplexing and demultiplexing. The main advantage of AWG based FFT/IFFT is a passive integrated device with simple design for large number of subcarriers.

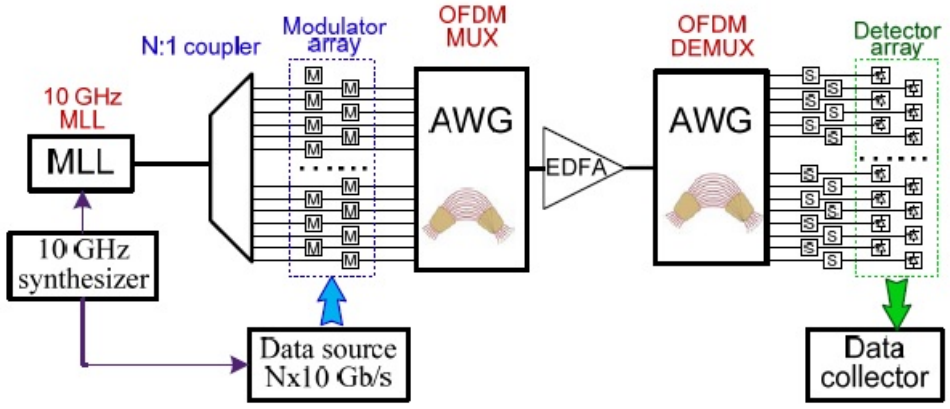

Figure 2.11: Block diagram of AWG based All-Optical OFDM system [58].

The proposed all-optical AWG based FFT/IFFT diagram is shown in Figure 2.11. In the system, the performance is evaluated for 4 and 16 subcarriers and have subcarriers spacing of 10 GHz. The modelocked laser source is used for generation of pulse train at the repetation rate of 10 GHz. The pulse train is splitted by 1:N splitter and each splitted signal is OOK modulated by N independent data sources at 10 Gbaud. After modulation, an AWG is used as IFFT device for incoming parallel modulated data streams. At the receiver side, again AWG is used for FFT function to demultiplex the desired subcarrier(s). An AWG based IFFT/FFT requires the optical sampler for detection of desired demultiplexed subcarrier.

Figure 2.12 shows the eye opening in the results of an AWG based IFFT/FFT in AO-OFDM system. Due to IFFT/FFT operation, the eyes are not much opened which depends on number of subcarriers the system. With the increase in subcarriers, the interference-free regions becomes shrink. For detection of desired subcarrier, a precise and narrow optical sampling gates are required in order to avoid the interference. By using optical sampling gates the system cost increases. The eyes opening is also depends on the modulator bandwidth

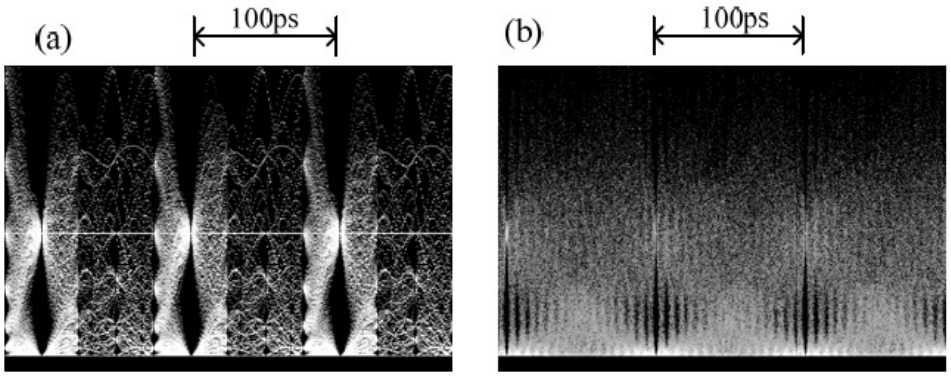

Figure 2.12: Results of proposed AWG based IFFT/FFT for AO-OFDM system [58].

which causes the modulated signal have non-zero symbol rise and fall times. Further, the fabrication imperfections and incoming signal distortions poses challenges to the AWG based AO-OFDM system performance.

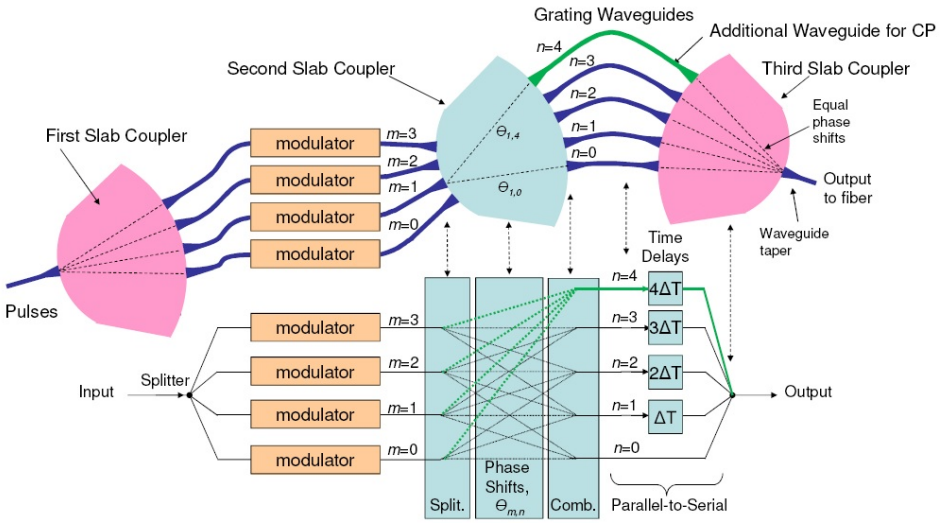

Figure 2.13: AWG-CP based IFFT circuit for AO-OFDM system [59].

In [59], an optical method of inserting cyclic prefix (CP) in an AWG based transmitter for AO-OFDM system is proposed. With the CP, the duration of interference-free region increases which relaxes the need of narrow sampling gates and exact sampling point. In Figure 2.13, the circuit of AWG with CP for IFFT function is shown. An optical signal from pulsed laser source is entered at the input of first slab coupler which works as an optical splitter. After dividing input signal, each signal is modulated to produce a Fourier coefficients,

and then the second slab coupler is used as a phase shifter as per principle of IFFT process. The number of inputs and outputs of second slab coupler depends on number of subcarriers in AO-OFDM system and its design is based on methods of Rowland circle in order to obtain desired phase shifts. For parallel-to-serial conversion, an arrayed waveguides are used for time delays with an additional waveguide (n=4) for the CP insertion. The third slab coupler serves as only an optical combiner [60].

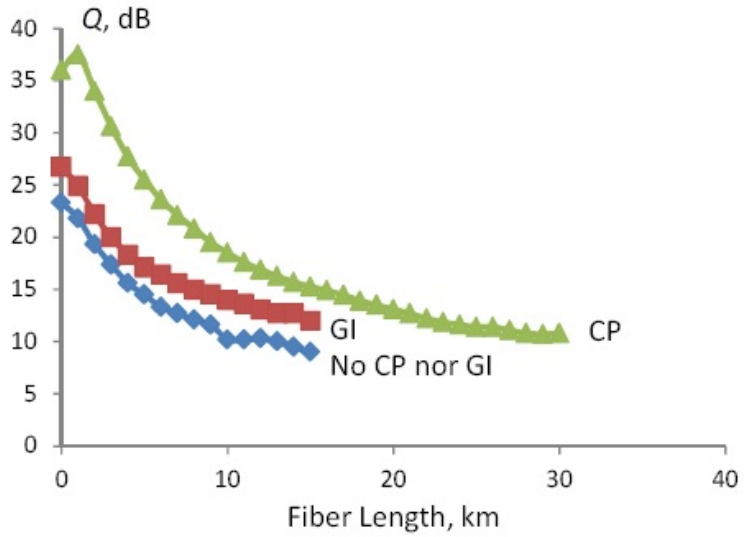

Figure 2.14: Results of proposed AWG-CP based IFFT/FFT for AO-OFDM system without dispersion compensation [59].

In the proposed AWG-CP design for AO-OFDM system, the number of waveguides are required to perform FFT function is same as the number of subcarriers ,N_{SC}, with no CP. The delay between waveguides, τ, is needed to be $\tau = T_{sym}/N_{SC}$. In a performance evaluation of proposed design, number of subcarriers are 4 with spacing of 10 GHz. The data rate of QPSK modulation sources are 10 Gbit/s with the aggregate system transmission rate of 80 Gbit/sec per polarization. The arrayed waveguides are designed to give delay of 12.5 ps. The laser source have pulse duration of 3.25 ps at the rate of 10 GHz. The system simulations shows the received OFDM symbol have some interference due to CP (duration 25 ps) carry the coherent data. The advantage of using system with CP is the broader duration of interference-free region. The proposed system is also simulated with fiber chromatic dispersion (CD) of 16

ps/nm/km. In case of OFDM symbols are perfectly aligned, the dispersion causes the shifting of sampling point and sampling point needs to be tunable to coincide with interference-free region. Another way to reduce the dispersion effects is to use the CP duration slight larger than the delay caused by dispersive link. In Figure 2.14, the performance without dispersion compensation of systems with/without CP and guard interval (GI). Reducing the data rate is an approach of introducing guard interval between symbols in time domain [12]. The system without any CP or GI shows poor performance and Q-factor is reduce by 10 dB at fiber length of 10 km. By using GI, the performance of system is improves by 3 dB with the compromise on reduced symbol rate to 64 Gbit/sec. With CP, the system performance improves with more tolerance to the effects of bandwidth-limitations of photodetector.

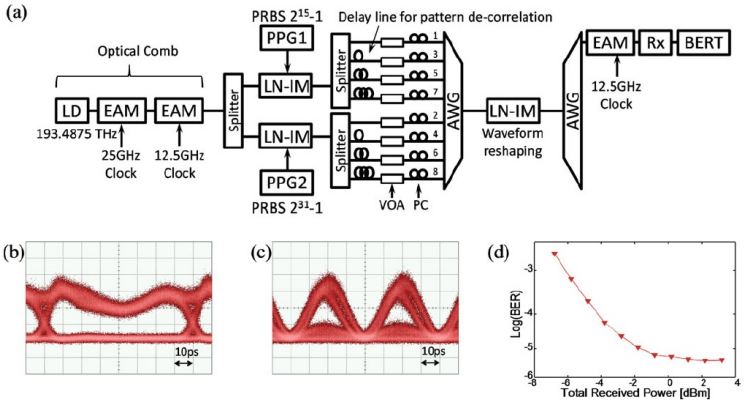

Figure 2.15: Proposed IM-DD AO-OFDM system (a) schematic, (b) desired subcarrier with waveform shaping, (c) ICI with waveform shaping , and (d) BER performance [61].

In [61], an experimental demonstration of an IM/DD AO-OFDM system with eight subcarriers with a spacing of 12.5 GHz is reported. As shown in Figure 2.15(a), The signal is divided and modulated by two modulators in an odd-and-even configuration. The format and data rate of modulation sources are NRZ-OOK and 12.5 Gbit/sec with lengths of pattern are 2^{15}-1 and 2^{31}-1 for odd-and-even subcarriers. After data modulation, each signal is splitted into four signals and decorrelated with an optical delay lines. The polarization controllers and attenuators are used to align the polarisations of subcarriers and maintain the equal powers of subcarriers. The AWG is used to multiplex the signal. To control the point of orthogonality,

waveform shaping based on lithium niobate-intensity modulator (LN-IM) is used to perform equalization in an optical domain. By using a waveform shaping before AWG, the interference from adjacent subcarriers of desired subcarrier is cancelled at the orthogonal point. At the receiver side, an AWG is used for optical FFT device. The desired demultiplexed subcarrier is sampled at an orthogonal point by using sampling gate. Comparing the Figure 2.15(b) and Figure 2.15(c), the eye diagrams confirms that the interference is cancelled at middle of symbol duration by using waveform shaping. Furthermore, BER performance of AO-OFDM system by using technique of equalization is improves from 10^{-4} to 10^{-6} [61]. For BER $<$ 10^{-3}, the minimum received power of AO-OFDM signal have to be -6 dBm, as shown in Figure 2.15(d).

In an experimental demonstrations of AO-OFDM systems, the results sometimes not show the actual system performance due to the off-line signal processing [62] - [65]. In [66], a series of the fiber Bragg gratings (FBG) are used for all-optical OFDM signal transmission over 80 km link, as shown in Figure 2.16. The AO-OFDM composite signal is generated by five channels and each channel is formed by five subcarriers. The subcarriers are differential quadrature phase-shift keying (DQPSK) modulated, and with polarization multiplexing, the aggregate transmission rate of AO-OFDM signal is 1 Tbit/sec. The received signal is detected in real-time by using FBG based optical Fourier transform (OFT) filters.

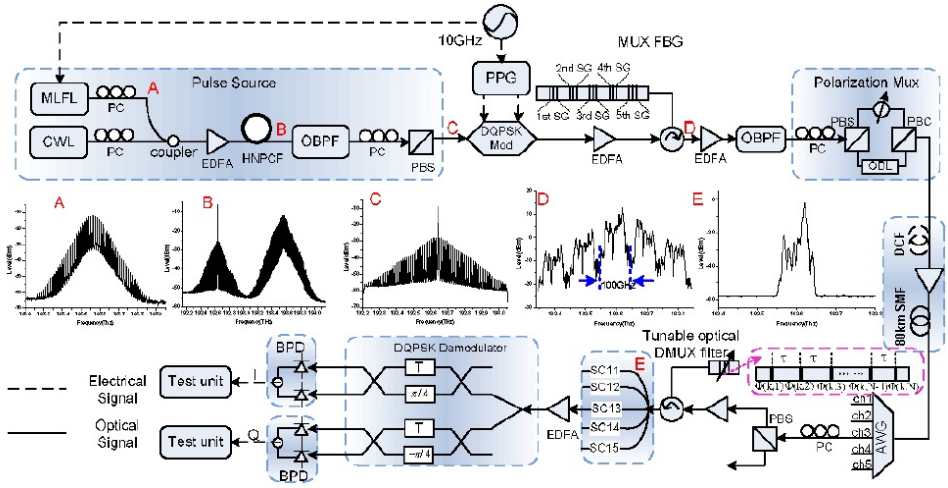

Figure 2.16: Experimental setup of all-optical sampling OFDM system [66].

Figure 2.16 shows the proposed block diagram of an experimental setup. A pulse source transmits a pulses at the repetition rate of 10 GHz and have pulsewidth is 2 ps. After optical signal processing for improving pulse-to-pulse coherence, the inphase and quadrature signals modulated on an optical signals at the total bit rate of 20 Gbit/sec. For AO-OFDM signal generation, FBG based multiplexer of five subcarriers for each WDM channel is used. After polarization multiplexer, all-optical PolMux OFDM signal have line rate of 1 Tbit/sec which is calculated from 2 (polarization multiplexing) $\times$ 5 (WDM channels) $\times$ 5 (subcarriers per channel) $\times$ 20 Gbits/sec (total data rate of inphase and quadrature signals). The AO-OFDM signal is transmitted over 80 km, and the received signal is passed through an arrayed waveguide grating in order to demultiplex the desired WDM channel. After channel demultiplexing, the optical signal is passed through to polarization beam splitter (PBS) and FBG based demultiplexer for desired subcarrier demultiplexing. The function of FBGs is to act as a matched filters. The total bandwidth of each channel is 65 GHz with the spectral efficiency of 3.07 b/s/Hz (corresponding to total data rate of channel 200 Gbit/sec). Figure 2.17 shows the BER performance of 50 subcarriers. The reason of variations in performances is due to fabrication structures of FBGs. After 50 km transmission, the BER of all channels in an AO-OFDM system is lower than the threshold of the FEC limit (10^{-3}). The constellations of received data of 12^{th} subcarrier show that the standard deviations of received symbols after 80 km are within the decision boundary regions. The results show that the proposed system offers high line rate transmission, but with the increase of subcarriers the precise phase control required to prevent loss of orthogonality among subcarriers.

2.4 Disadvantages of OFDM

In the electrical OFDM receiver, an analog signal after down conversion is sampled by ADC. After data conversion, the DSP perform following steps before symbol decision [11]:

- DFT window or symbol time synchronization

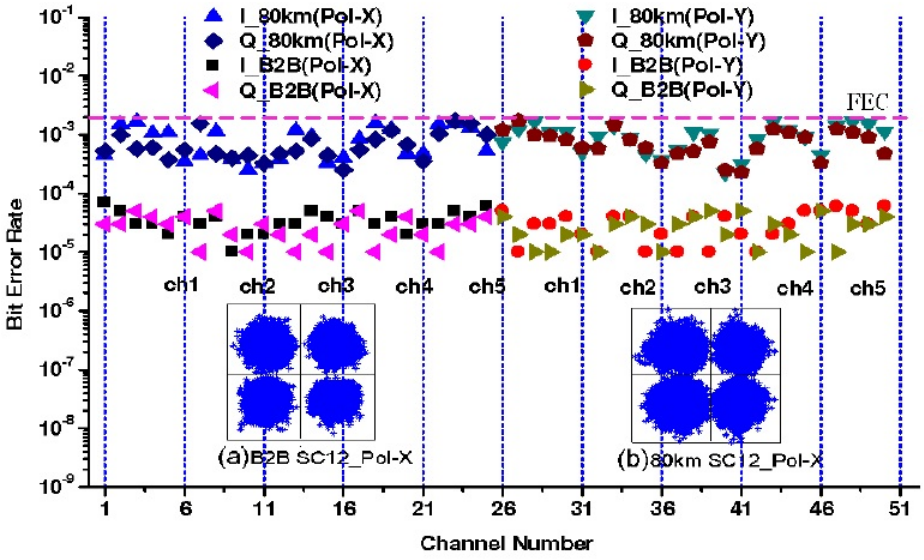

Figure 2.17: BER performances of 50 subcarriers and constellations of 12^{th} subcarrier in (a) B2B and (b) 80 km cases [66].

- Carrier frequency synchronization
- Discrete Fourier transform
- Channel estimation
- Phase noise estimation

In this section, we focus on the synchronization issues which are critical functions in the OFDM systems.

2.4.1 Symbol Time Synchronization

In the presence of time offset between OFDM transmitter and receiver, the received signal is given as [68]

$$\overline{s}(t,\tau) = \begin{cases} s(t+\tau), & 0 \le t \le T_S - \tau, \\ e(t-T_S+\tau), & T_S - \tau \le t \le T_S \end{cases} \tag{2.6}$$

where $e(t)$ is the interference term. Without cyclic extension/prefix (CP) or guard interval (GI), $e(t)$ is the part of OFDM symbol, as shown in Figure 2.18. In case of GI larger than the

time offset τ, the interference term is zero, i.e. $e(t) = 0$. In OFDM system using CP of larger duration than the time offset, the interference term is a part of CP i.e. $e(t) = s(t)$. If the CP duration or guard interval is less than τ, the interference term $e(t)$ mixed with desired OFDM signal.

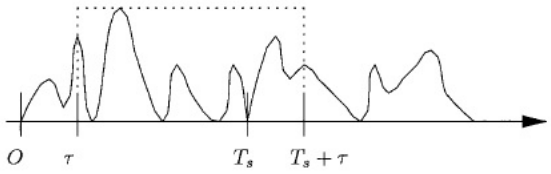

(a) $e(t)$ is a part of the next block

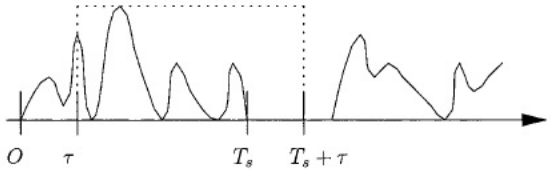

(b) $e(t)$ is a part of guard interval

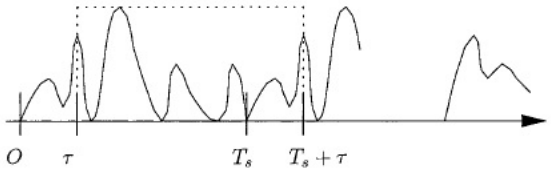

(c) $e(t)$ is a part of cyclic extension

Figure 2.18: Time Offset effects on received OFDM signal [68].

Mathematically, in the presence of time offset ($\tau \neq 0$), the demodulated signal is given as

$$\begin{aligned} X_m &= \frac{1}{T_S}\int_0^{T_S} \bar{s}(t,\tau)e^{-j2\pi f_m t}dt \\ &= \frac{1}{T_S}\int_0^{T_S-\tau} s(t+\tau)e^{-j2\pi f_m t}dt + \frac{1}{T_S}\int_{T_S-\tau}^{T_S} e(t-T_S+\tau)e^{-j2\pi f_m t}dt \\ &= \frac{1}{T_S}\int_0^{T_S} s(t)e^{-j2\pi f_m (t-\tau)}dt - \frac{1}{T_S}\int_0^{\tau} s(t)e^{-j2\pi f_m (t-\tau)}dt + \frac{1}{T_S}\int_0^{\tau} e(t)e^{-j2\pi f_m (t-\tau)}dt \\ &= s_m e^{j2\pi f_m \tau} + \frac{1}{T_S}\int_0^{\tau} [e(t)-s(t)]e^{-j2\pi f_m (t-\tau)}dt \end{aligned} \tag{2.7}$$

Due to the time offset, the detected symbol is phase rotated and have additive interference. Without CP or guard interval, the system performance degrades much with non-zero τ . The average interference terms are $\frac{1}{T_S}\int_0^{\tau} s(t)e^{-j2\pi f_m(t-\tau)}dt$ and $\frac{1}{T_S}\int_0^{\tau} e(t)e^{-j2\pi f_m(t-\tau)}dt$. With proper selection of CP duration, the additive interference terms due to time offset are cancelled.

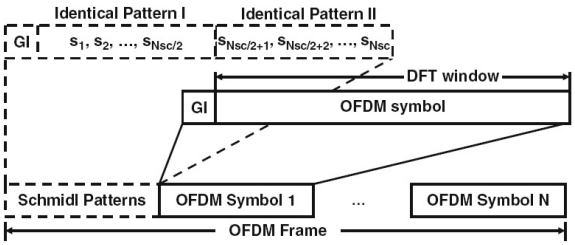

Figure 2.19: OFDM frame synchronization based on Schmidl principle [11].

One of the famous methods for time synchronization is Schmidl-Cox approach in which the pilot symbols is transmitted with data symbols [11]. Figure 2.19 shows the pilot symbols comprises of an identical segments (Schmidl synchronization signal) which can be expressed as

$$s_m = s_{m-N_{SC}}/2, \quad m \in [N_{SC}+1, N_{SC}] \tag{2.8}$$

where s_m is random value of m^{th} sample for m = $1,...N_{SC}/2$. At the receiver, a symbol's delineation is found by following correlation function with the assumption that the constant phase across the received OFDM symbol:

$$R_d = \sum_{m=1}^{N_{SC}/2} r^*_{m+d} r_{m+d+N_{SC}/2}, \tag{2.9}$$

where $r_m = e^{j\Delta\omega t}s_m$ is received sampled signal. The Schmidl's principle of synchronization is based on finding the maximum value of the correlation R_d between the two identical segments.

2.4.2 Sensitivity to Carrier Frequency Offset

OFDM system performance degrades with carrier frequency offset (CFO) which causes not only phase offset in detected symbol but also intercarrier interference (ICI) from other subcarriers in OFDM system. One advantage of long OFDM symbol duration is less sensitive to CFO. If CFO is greater than the maximum tolerable limits, the performance of system is seriously degraded. The sensitivity of OFDM system to CFO is reduced by using DSP for estimation and compensation. In the presence of CFO, the received OFDM signal is given as

$$\widetilde{s}(t) = s(t)e^{j2\pi f_\varepsilon t}, \tag{2.10}$$

where f_ε is CFO between transmitter and receiver. The received signal is demodulated for m^{th} subcarrier and is given as

$$\begin{aligned} X_m &= \frac{1}{T_S}\int_0^{T_S} s(t)e^{j2\pi f_\varepsilon t}e^{-j2\pi f_m t}dt \\ &= \sum_{l=1}^{N} s_l \frac{1}{T_S}\int_0^{T_S} e^{j2\pi f_\varepsilon t}e^{j2\pi(f_l-f_m)t}dt \\ &= s_m e^{j2\pi f_\varepsilon t} + \frac{1}{T_S}\sum_{l\neq m} s_l \int_0^{T_S} e^{j2\pi f_\varepsilon t}e^{j2\pi(f_l-f_m)t}dt \\ &= \eta_0 + \eta_m, \end{aligned} \tag{2.11}$$

where η_0 is the desired signal term with phase offset $e^{j2\pi f_\varepsilon t}$ for m^{th} subcarrier. The ICI term, η_m, after integration is termed as ICI coefficient (considering average power of transmitted symbol s_m on m^{th} subcarrier)

$$\eta_m = \sin\left(\frac{(\pi(m+\delta))}{\pi(m+\delta)}\right)e^{-j\pi(m+\delta)}, \tag{2.12}$$

where $\delta = f_\varepsilon T_S$ is the normalized carrier frequency offset. In Figure 2.20, η_m is plotted in dB at $\delta = 0$ and 0.25 for subcarrier index $m = 0$ to 125. The plot verifies that the contribution to the ICI value is mainly from adjacent subcarrier, which also verifies the expression of η_m.

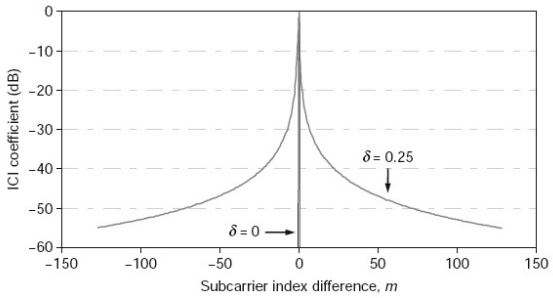

Figure 2.20: ICI due to Carrier frequency offset [11].

In RF OFDM, various methods to estimate and compensate a CFO are proposed [11]. In CO-OFDM system, the correlation function from time synchronization (in Figure 2.19) is used to find the CFO. The samples from s_m to $s_{m+N_{SC}/2}$ have the phase difference of $\pi f_\varepsilon N_{SC}/F_S$, where F_S is the sampling frequency of an ADC. For CFO, the correlation function is given as

$$R_d = \sum_{m=1}^{N_{SC}/2} |r_{m+d}|^2 e^{\pi f_\varepsilon N_{SC}/F_S}. \tag{2.13}$$

The correlation function provides a phase information from which frequency offset is derived as

$$f_\varepsilon = \frac{F_S}{\pi N_{SC}} \angle R_d. \tag{2.14}$$

The range of $\angle R_d$ is from 0 to 2π. The disadvantage of this approach is large CFO is not uniquely identified and only support for -Δf to Δf, where Δf is the subcarrier spacing. To increase the range of CFO estimation, the symbols of synchronization are needed to be further divided. Further various approaches are proposed to perform CFO estimation in [69] - [75].

In [76], a method to estimate the frequency offset in an experimental setup of PDM-QPSK optical communication system of data rate 112 Gbit/sec is presented by using the samples for finding autocorrelation functions. The frequency offset (f_ε) is derived from sampled

autocorrelation function (ACF), $R(l)$, which is given as

$$f_{\varepsilon} = \frac{1}{8\pi T_S} \arg\{\sum_{l=1}^{N} R(l)R^*(l-1)\}, \tag{2.15}$$

and

$$R(l) = \frac{1}{M}\sum_{k=1}^{M} S(k)S^*(k-l), \tag{2.16}$$

where M is the number of received signal samples, l = 1,...,N is the index of sample ACF, and $S(k)$ is the 4^{th} power of received signal. The method of calculating the 4^{th} power of received signal is dominated in QPSK data-modulated symbols for frequency offset estimation. In QPSK data signal, the correlated signal $(x(k)x^*(k-1))^4$ is directly proportional to $exp(4j\Delta\phi[k])$ [101], where $x(k)$ is received signal. By using the mean value of laser phase noise $1/(8\pi T_S)$ and the probability density function of $4\Delta\phi$, the maximum likelihood technique is used to find the estimate of f_{ε}, as given in equation 2.15.

In an experimental setup, 16 subcarriers with spacing of 50 GHz are multiplexed and modulated by QPSK data source at 28 Gsym/sec. After modulation, the modulated signal is polarization-multiplexed. After transmission over 2000 km fiber, the received signal is detected by coherent receiver. The linewidth of LO is 100 kHz and photodetected signal sampled by 50 GSa/sec ADC. In performance evaluation of ACF algorithm, a data set of 56000 symbols for middle subcarrier is used and compared with the FFT-based algorithm. Figure 2.21 shows the histograms for different samples (N) used to estimate frequency offset using ACF algorithm. The difference of ACF algorithm and FFT-based algorithms is used as an estimation error. With the increase in sample ACF, the standard deviation of an estimation error decreases which ultimately increases the accuracy of a CFO estimate. For N = 20, BER = 10^{-4} is reported for PMD-QPSK optical system.

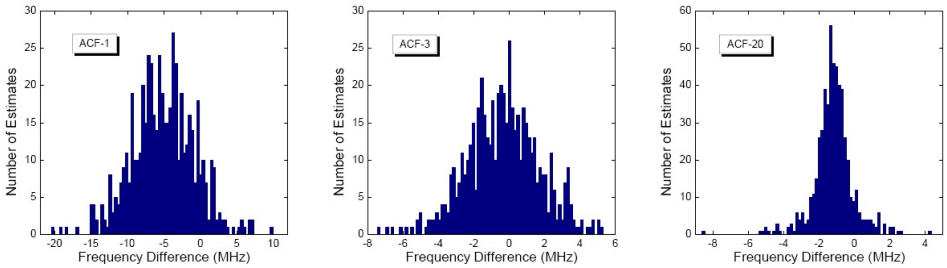

Figure 2.21: Histogram of an error in frequency offset estimation [76].

2.4.3 Joint time and frequency synchronization

In [77], the maximum likehood (ML) estimator of time and frequency offsets is proposed by using the advantage of exploiting the CP in the OFDM symbols without pilot symbols. Figure 2.22 shows the structure of OFDM symbol with cyclic prefix I of data symbols L out of total symbols N. The samples $2N+L$ are observed in the received samples $r(k)$ and have probability density function $f(r|\theta,\varepsilon)$ at given time offset θ and frequency offset ε. The expression of log-likelihood function $\Lambda(\theta,\varepsilon) = \log(f(r|\theta,\varepsilon))$ as a function of time offset θ and frequency offset ε is given as

$$\Lambda(\theta,\varepsilon_{ML}(\theta)) = |\gamma(\theta)| - \rho\Phi(\theta), \tag{2.17}$$

where ρ is the correlation coefficient between received samples $r(k)$ and $r(k+N)$. The joint estimation of θ and ε is given as

$$\theta_{ML} = \arg\max\{|\gamma(\theta)| - \rho\Phi(\theta)\} \tag{2.18}$$

and

$$\varepsilon_{ML} = -\frac{1}{2\pi}\angle\gamma(\theta_{ML}) \tag{2.19}$$

where γ and Φ are the correlation and energy estimation parameters of received samples $r(k)$ and $r(k+N)$, as shown in Figure 2.23. It can be noted that the Φ is independent of ε and only

two parameters affects the estimation of Λ: length of cyclic prefix L, and ρ which ultimately depends on SNR of system. The compensation of magnitude of quantity γ gives a maximum estimate value of θ at the intervals of θ_{ML}, while the phase of γ at the same intervals of θ_{ML} is directly proportional to ε_{ML}. In spite of advantages of joint estimation of time and frequency offsets by using CP, the pilots symbols are required for channel estimation [11] which demands further research towards hybrid estimation schemes.

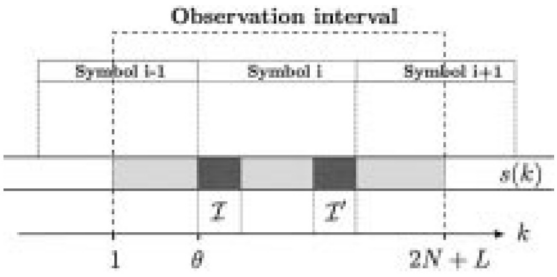

Figure 2.22: i^{th} OFDM symbol structure contains cyclic prefix I of L data symbols I' [77].

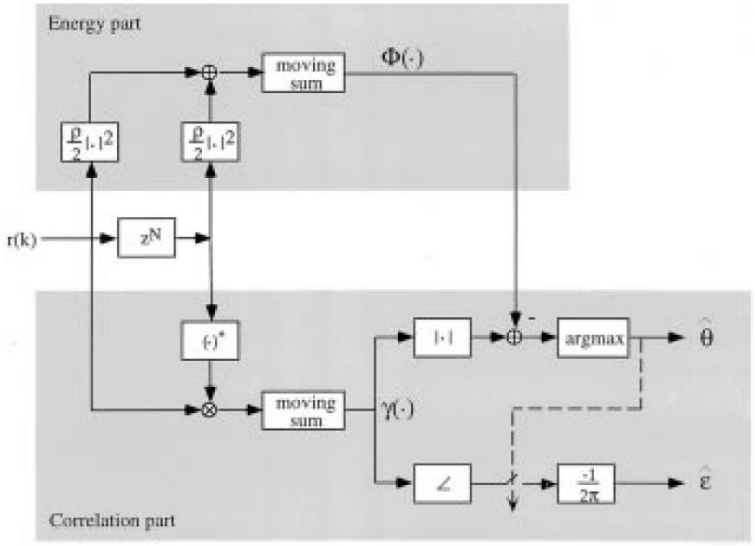

Figure 2.23: Joint estimation of ML time and frequency offsets [77].

The modified synchronization scheme is proposed for CO-OFDM system [78] in order to estimate the time and frequency offsets. In an estimation of time offset, the modified correlation function of Schmidl's principle [11] have impulse-shaped metric with stability in estimation. In the presence of CD in system, the proposed method is not robust to tolerate

the delayed OFDM symbols. In the presence of frequency offset, the estimation range is increased to $\pm N_{SC} \cdot \Delta f/2$ with small number of training symbols are required compared to Schmidl's principle, where N_{SC} is number of subcarrier and Δf is subcarriers spacing. With the CD compensating fiber, the modified synchronization algorithms show stability and the optical SNR (OSNR) of CO-OFDM is increased by 3 dB for required BER = 10^{-3}.

2.4.4 Phase Noise

The impact of laser phase noise is important when using high order modulation in order to achieve high spectral efficiency [79] - [82]. For the system with phase noise, θ_n, the received time domain signal samples are given as

$$y_n = x_n e^{j\theta_n}. \tag{2.20}$$

The system under consideration have constant phase error of θ_0, then we can write the above sampled signal for demodulated signal as [31]

$$Y_m = X_m e^{j\theta_0}. \tag{2.21}$$

In presence of constant phase error, θ_0, the constellation is rotated by θ_0, as shown in Figure 2.24(a). The rotation of constellation is simply corrected by DSP with single tap equalization algorithm. Now, in case of random phase noise and the phase noise between two samples are uncorrelated, $E\{\theta_l \theta_n\} = 0$, where l $\neq$ n and $E\{\}$ is average operator. Then the FFT of received signal, y_m is given as

$$\begin{aligned} Y_m &= \frac{1}{\sqrt{N}} \sum_{n=0}^{N-1} y_m e^{\left(\frac{-j2\pi mn}{N}\right)} \\ &= \frac{1}{\sqrt{N}} \sum_{n=0}^{N-1} x_m e^{j\theta_n} e^{\left(\frac{-j2\pi mn}{N}\right)}. \end{aligned} \tag{2.22}$$

Considering the phase noise is small, then the exponential term, $e^{j\theta_n}$, is approximated to $1+j\theta_n$ and m^{th} subcarrier is given as

$$\begin{aligned} Y_m &= \frac{1}{\sqrt{N}} \sum_{n=0}^{N-1} x_m (1+j\theta_n) e^{\left(\frac{-j2\pi mn}{N}\right)} \\ &= X_m + \frac{j}{\sqrt{N}} \sum_{n=0}^{N-1} x_m \theta_n e^{\left(\frac{-j2\pi mn}{N}\right)} \\ &= X_m + N_m. \end{aligned} \tag{2.23}$$

In presence of phase noise, the received signal contains the desired signal plus noise from all subcarriers in system. The nature of θ_n is random and effects on constellation are shown in Figure 2.24(b).

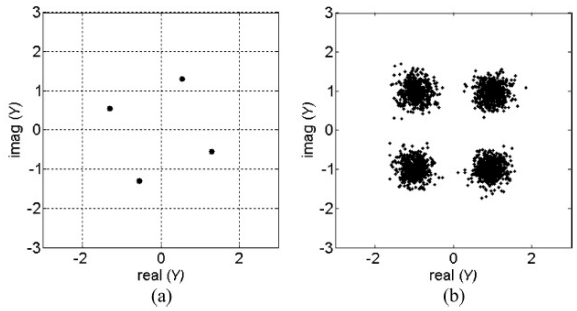

Figure 2.24: Effects of phase noise when (a) θ_n is constant and (b) θ_n is random [31].

In [83], an estimation of maximum likelihood (ML) common phase error (CPE) due to the linewidth of laser sources (range of 100 - 1000 KHz) in CO-OFDM system is proposed. For pilot subcarrier, N_p subcarriers are used to track the CPE. The expression of ML CPE is given as

$$\phi_i = \arg\left(\sum_{k=1}^{N_p} r'_{ki} h_k^* s_{ki}^* / \delta_k^2\right), \tag{2.24}$$

where s_{ki}, r'_{ki}, and h_k are transmitted signal, received received, and transfer function of channel. The indices i and k are for OFDM symbols and subcarriers. The deviation δ_k of constellations points of an k^{th} subcarrier gives an estimation of CPE in order to recover the transmitted data.

2.4.5 Effects of Chromatic Dispersion

Due to signal interaction or passing through an optical fiber over a long distances causes a broadening of pulses. In a high dispersion medium, a bit steam of pulses will be spread in time domain and degrades the system performance if used for transmission through long fiber length. The types of dispersion are: intermodal dispersion, polarization mode dispersion, and chromatic dispersion [102].

The chromatic dispersion (CD) is dependent on the group velocity v_g of signal's wavelength λ and dispersion parameter D [94] is given as

$$D = \frac{d}{d\lambda}\left(\frac{1}{v_g}\right) = -\frac{2\pi c}{\lambda^2}\beta_2 \tag{2.25}$$

where c is the light velocity in vacuum, and β_2 is the group velocity parameter.

In [84], an effects of dispersive channel on OFDM system performance is studied. The time delay between subcarriers causes intercarrier interference (ICI) and intersymbol interference (ISI). In order to reduce the effects of dispersion, a CP can by used in each OFDM symbol, as shown in Figure 2.25. In OFDM symbol with CP, the last part of symbol is copied to the start of OFDM symbol. The addition of CP is done after the inverse FFT function in OFDM system. By using CP, the symbol is able to accommodate the time delay caused by dispersion of fiber in each subcarrier. As a result, the symbol remains periodic in a synchronized FFT window at receiver. Further, the phase errors in frequency domain can be estimated and compensated by a DSP equalizers. The advantage of using CP is the spectral efficiency is compromised.

The effects of CD with fiber nonlinearity over transmission performance for CO-OFDM systems are studied in [85]. In a Monte-Carlo simulations of the CO-OFDM system, the data carrying subcarriers are 128 with symbol duration of 25.6 ns, the modulation format is QPSK, the fiber dispersion (D) is 16 ps/nm/km and a nolinearity coefficient is $2.6 \times 10^{-20} m^2/W$. At OFDM transmitter and receiver, the lasers linewidths are 100 kHz. In Figure 2.26 the

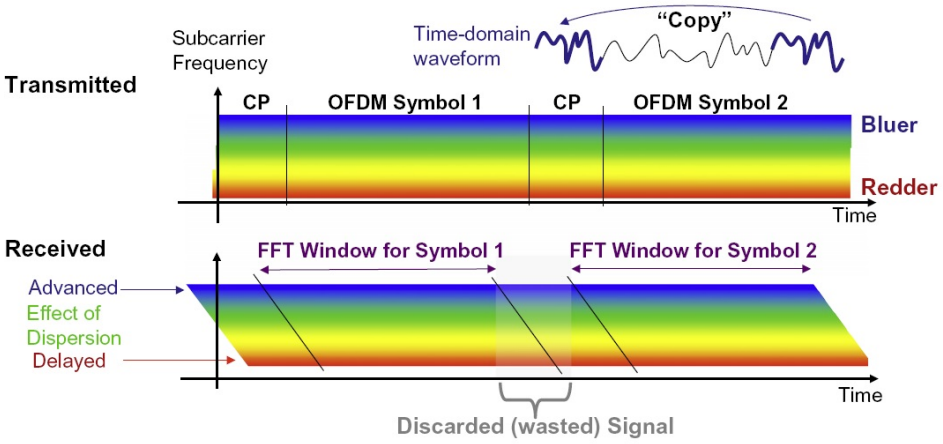

Figure 2.25: Effects of chromatic dispersion on OFDM signal and performance improvement with cyclic prefix (CP) [84]

.

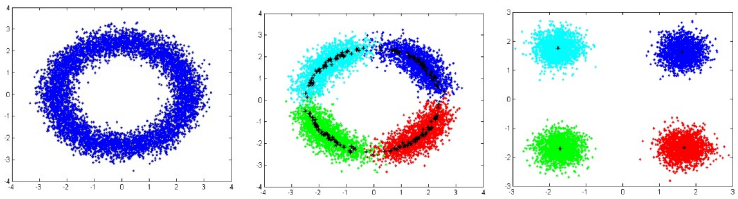

(a) (b) (c)

Figure 2.26: Effects of chromatic dispersion (CD) on received data (a) before (b) after removing CD, and (c) after removing CD and phase noise is averaged [85].

constellations of received 51 OFDM symbols after transmission over 3200 km fiber is shown.

As shown in Figure 2.26(a), the CD causes the rotation of OFDM symbol [86, 46], and the phase shift due to CD is given as

$$\phi = \frac{1}{2}\beta_2 \omega^2 L, \tag{2.26}$$

where ω is frequency of subcarrier and L is length of fiber. The phase shift is commonly estimated and compensated by using training sequences. After CD and average of received 51 OFDM symbols, the performance is slightly improves but phase noise is still dominant in drifting the OFDM symbols, as shown in Figure Figure 2.26(b). After OFDM symbols transmission over 3200 km, the phase noise due to lasers is estimated and compensated and

symbols are recovered with small deviations due to nonlinearity of fiber, as shown in Figure 2.26(c).

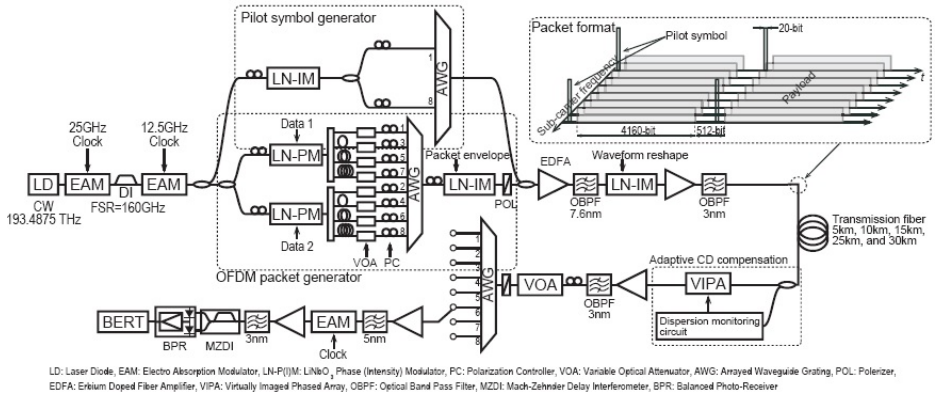

Figure 2.27: Proposed all-optical chromatic dispersion monitoring and compensation in AO-OFDM system [87].

For all-optical CD monitoring and compensation in an AO-OFDM systems is proposed in [87]. In proposed CD compensation technique, a pilot symbols are added to the edge subcarriers (frequency spacing of 87.5 GHz) and after estimation of their relative delays the phased array device is used for CD compensation. The power of pilot symbols are 9 dB higher than the OFDM symbols which can be used for extraction by using threshold circuit at receiver. Figure 2.27 shows the block diagram of proposed experimental setup for CD monitoring and compensation. After transmission over fiber, the subcarriers 1 and 2 are demultiplexed in dispersion monitoring circuit. The pilot symbol of subcarrier 1 is extracted by threshold device after photodetection. The pilot symbol of subcarrier 8 is extracted by using electroabsoption modulator (EAM) with pilot symbol of subcarrier 1 is used as a gate signal. The output of EAM is a pilot symbol with reduced width which depends on relative delay of two edge subcarriers. The BER performance of an AO-OFDM system improved from 10^{-3} to 10^{-6} for signal transmission over 5 km and received signal power -10 dBm, as shown in Figure 2.28.

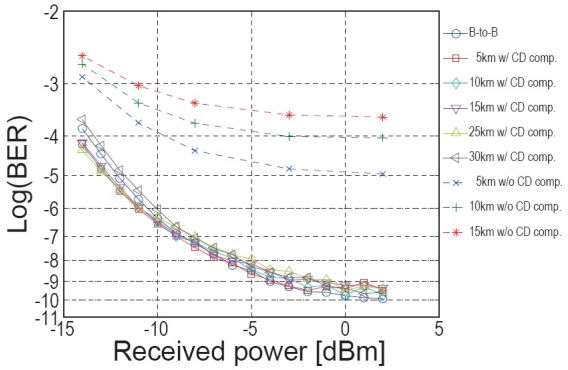

Figure 2.28: BER performance of proposed all-optical chromatic dispersion monitoring and compensation in AO-OFDM system [87].

2.5 DSP Techniques for Single- and Multi-Carrier Optical Communication

In single-carrier optical communication systems, the DSP algorithms for time and/or frequency offset estimation and compensation are well known and are easy to be implemented due to no issue of ICI [101]. The time offset estimation is used to correct the sampling point of ADC in DSP and frequency offset estimate is used to tune the local oscillator (LO) at receiver, as shown in Figure 2.29(a). In AO-OFDM, the estimation and compensation of STM and ScFO by using DSP algorithms of single-carrier doesn't gives accurate received data measure due to presence of ICI in AO-OFDM system. In [88, 33], the ICI is first estimated and then compensated by using pre-filter/filter initialization before CMA algorithms, as shown in Figure 2.29(b). The estimation and compensation of ICI affected desired demultiplexed subcarrier is accurate depends on implementation and performance of DSP algorithms. In [98], the ICI issue in N-WDM system is addressed by using joint DSP algorithms to cancel the linear ICI, as shown in Figure 2.29(c). In the joint DSP based ICI compensation, the desired and adjacent subcarriers are first estimated and compensated by using algorithms of single-carrier optical communication systems. In the DSP based ICI suppression, the algorithms can provide the robustness to AO-OFDM system and enhancing the coherent receiver performance but have high computational requirements which can increase the overall system cost. In this

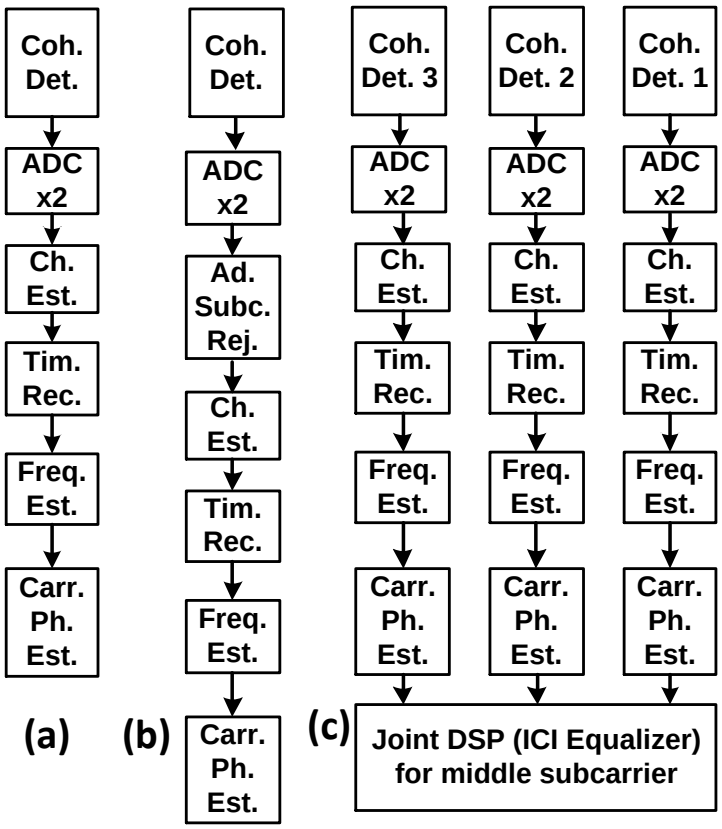

Figure 2.29: Subsystems of DSP for (a) single-carrier optical communication systems [101], (b) AO-OFDM [88, 33], and (c) N-WDM [98]. Coh. Det.: coherent detection; ADC: analog to digital converter; Ch. Est.: channel estimation; Tim. Rec.: timing recovery; Freq. Est.: frequency estimation; Carr. Ph. Est.: carrier phase estimation; Ad. Subc. Rej.: adjacent subcarriers rejection.

thesis, the system performance is investigated with proposed passive optical devices in order to reduce ICI effects. The details of design and operation of proposed devices are presented in Chapter 4 and Chapter 5.

Chapter 3

Time and Frequency Offsets in OOK AO-OFDM System

In wireless communication systems, an orthogonal frequency division multiplexing (OFDM), as a multicarrier transmission technique, has been successfully employed in numerous digital standards which offers high data transmission on multiple subcarriers with high spectral efficiency. Furthermore, in OFDM based multiple subcarrier transmissions have ability to combat the distortion due to intersymbol interference (ISI), and improved tolerance to intercarrier interference (ICI). As discussed in Chapter 2, OFDM is also considered as a promising data transmission technique on multiple carriers in optical communications systems. In this chapter, OOK-modulated AO-OFDM system (AO-OFDM transmitter and digital coherent receiver) is presented and the performance is investigated in the presence of time and frequency offsets in OOK-modulated symbols and optical subcarriers.

3.1 Problem Statement

OFDM based multiple subcarriers transmission offers numerous benefits but these benefits can only be achieved when subcarriers are orthogonal. The orthogonality among subcarriers degrades when synchronization errors exist in OFDM system [88] -[91]. The research on the effects of time and frequency offsets is discussed in Chapter 2. Here we give details of the random nature of synchronization errors in AO-OFDM system perspective.

Figure 3.1 shows the graphical interpretation of symbol time misalignment (STM) and

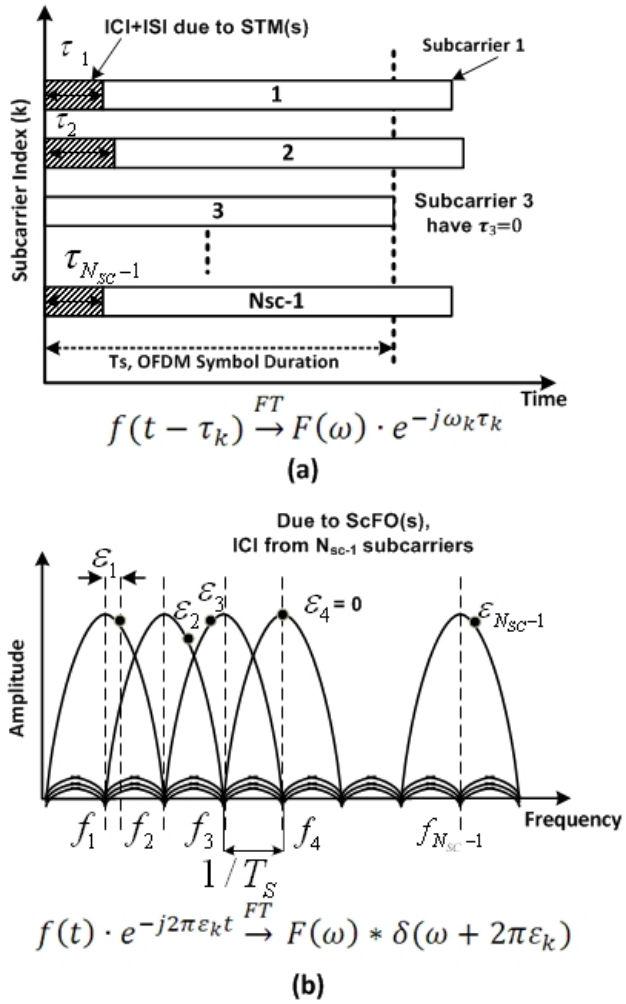

Figure 3.1: Graphical interpretation of STM (a) and ScFO (b) effects on AO-OFDM system with N_{SC} subcarriers.

subcarrier frequency offset (ScFO) effects on AO-OFDM system which comprises of N_{SC} subcarriers. Depending on the arrival of individual subcarriers, the STM causes two interferences i.e. ISI from previous symbol and ICI from $N_{SC}-1$ subcarriers in the desired subcarrier, as shown in Figure 3.1(a). $E(t-\tau_k)$ is the delayed function and have phase offset $e^{-j\omega_k\tau_k}$ in frequency domain which depends on subcarrier index k and its delay τ_k. In the presence of ScFO ε_k between the transmitted subcarrier frequencies ω_k and local oscillator (LO) center frequency ω_{LO}, the center frequency of k^{th} subcarrier is shifted in frequency domain by ε_k which causes degradation of an orthogonality and ultimately ICI occurs, i.e. interference from $N_{SC}-1$ subcarriers, as shown in Figure 3.1(b).

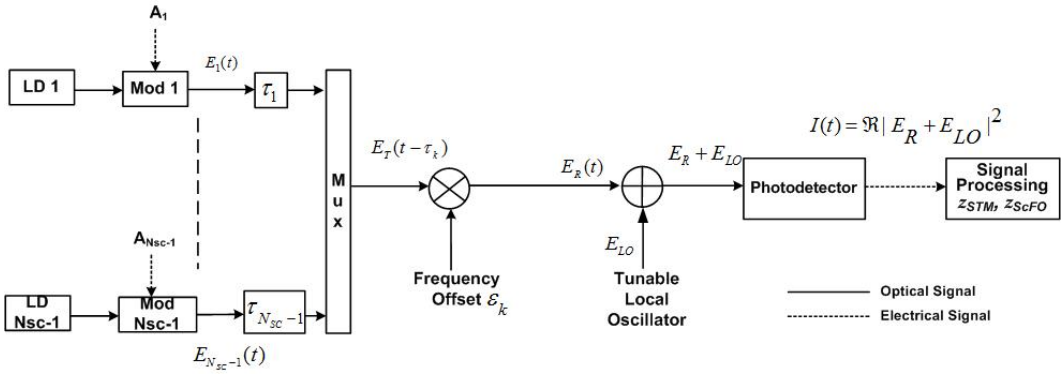

Figure 3.2: Block Diagram of OOK-modulated AO-OFDM system (AO-OFDM transmitter and coherent detection).

In this chapter, we analytically investigate the performance of AO-OFDM system in the presence of random STM and ScFO effects. It is the first time to theoretically evaluate the issues of synchronization in the time and frequency domains. In [88, 92], issues of synchronization in AO-OFDM systems (emulation setups) were considered, and in our work the analytical model with details of the effects of synchronization on AO-OFDM system design parameters are given.

3.2 OOK AO-OFDM System Model Description

In AO-OFDM transmission system model N_{SC} optical subcarriers from continuous wave laser diodes (LD_k) are OOK modulated by Mod_k with independent data sources $A_k \in \{0,1\}$, as shown in Figure 3.2, where k is subcarrier index from 1 to N_{SC}. After modulation, k^{th} optical subcarrier

$$E_k(t) = A_k \sqrt{P_k} \exp(j\omega_k t) \tag{3.1}$$

is time misaligned by τ_k and multiplexed (Mux) to transmit AO-OFDM signal

$$E_T(t) = \sum_{k=1}^{N_{SC}} E_k(t-\tau_k) = \sum_{k=1}^{N_{SC}} A_k \sqrt{P_k} \exp(j\omega_k(t-\tau_k)) \tag{3.2}$$

where A_k and P_k are data symbols (either logical 0 or 1) and average power at given frequency ω_k of k^{th} subcarrier. The phase of LD_k is considered as constant during OOK-modulated symbol duration and the system performance is evaluated w.r.t frequency offset only. A multiplicative noise ScFO ε_k, is introduced in a composite AO-OFDM signal given in equation (3.2) as

$$E_R(t) = E_T(t)e^{j2\pi\varepsilon_k t}. \tag{3.3}$$

The time and frequency offsets (τ_k and ε_k) in the k^{th} subcarrier are modelled as absolute values between transmitter and receiver in AO-OFDM.

Single Branch Coherent Detection In an optical communication, a coherent detection is first introduced for its advantage of receiver sensitivity. Generally, the mixed signal of a LO with received optical signal is equivalent to an optically amplified signal without noise component [93]. If we compare the receiver sensitivity, the amplified signal from an erbium doped fiber amplifier gives lower sensitivity than the coherent detection, in case of OOK modulation. A basic structure of a single branch coherent detection is shown in Figure 3.3. For mixing of optical signals, the polarizations of received optical signal and LO signal must be aligned. For this purpose, an automatic polarization controller is used. In coherent detection, the phase or frequency of LO signal also needs to be locked with received optical signal. The term phase or frequency locked is used for homodyne or heterodyne detection. In our performance evaluations of OOK-modulated AO-OFDM system, we consider the time and frequency offsets and we are assuming that the polarizations are aligned and phases are locked.

Homodyne and Heterodyne Detection Before giving the details of the process of detection for AO-OFDM composite signal, the differences of homodyne and heterodyne detections with their suitability for AO-OFDM are firstly presented. In the technique of coherent detection, the frequency of LO, f_{LO}, is tuned to be same as of received optical signal frequency

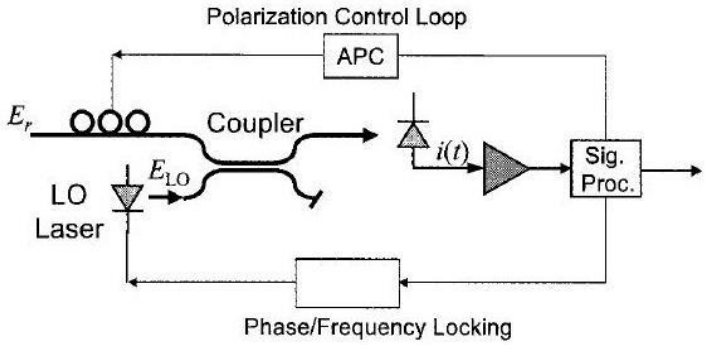

Figure 3.3: Coherent optical receiver for OOK-modulated symbols [93].

f_{RC}. By tuning the LO with the same frequency, the intermediate frequency (IF), f_{IF}= f_{RC}-f_{LO}, is zero. The photocurrent, $I_{HO}(t)$, is produced at the output of a photodetector is given as

$$I_{HO}(t) = 2\Re\sqrt{P_{RC}P_{LO}}. \tag{3.4}$$

In a heterodyne detection, the frequency of LO, f_{LO}, is selected to be not same as the frequency of received optical signal, f_{RC}. In this case the intermediate frequency, f_{IF}, is in the range of approximately 1 GHz [93]. The photocurrent, $I_{HE}(t)$, is produced at the output of a photodetector is given as

$$I_{HE}(t) = 2\Re\sqrt{P_{RC}P_{LO}}\cos(2\pi f_{IF}t). \tag{3.5}$$

In a homodyne detection, the SNR of optical system is higher than the heterodyne detection but at the cost of complex receiver design. In multicarrier transmission systems such as optical OFDM, the received signal contains subcarriers normally greater than 100 and the desired signal needs to be demodulated before optical signal detection. A direct detection gives an alternative but at the cost of high crosstalk from adjacent subcarriers [11].

3.2.1 Homodyne detection for OOK-modulated AO-OFDM system

At the receiver side of AO-OFDM system, the incoming AO-OFDM signal is added with local oscillator $E_{LO}(t) = \sqrt{P_{LO}}e^{j2\pi f_1 t}$ tuned for subcarrier 1 for homodyne detection. For AO-OFDM signal detection, an optical DFT (O-DFT) for subcarrier demultiplexing [12] or a 90^o optical hybrid with coherent detection is used [33]. In O-DFT, we can demultiplex the closely packed optical subcarriers passively (without LO) with the additional burden of the cost of optical sampling gates. A bandpass filter can also be used for subcarrier filtering before direct detection with a photodetector (PD) but its performance remain lower than the O-DFT or coherent detection [12]. In O-DFT based demultiplexing, the desired subcarrier is demultiplexed first and then the sampling gate and the PD are used to sample/extract the demultiplexed subcarrier in the symbol duration and to detect it. The detailed description on O-DFT based subcarrier demultiplexing is explained in the Chapter 2. In this chapter, the subcarriers are OOK modulated at AO-OFDM transmitter side, and at the receiver side LO and PD are used with no need of 90^o optical hybrid [33, 94, 95]. The current produced by the PD comprises of two dc terms and one ac term [94]. In the homodyne detection [95], the third ac term contains the transmitted information of desired subcarrier and interference terms from $N_{SC}-1$ subcarriers and is given as

$$I(t) = 2\Re \sum_{k=1}^{N_{SC}} A_k \sqrt{P_k P_{LO}} \times cos(2\pi(f_k + \varepsilon_k)(t-\tau_k) - 2\pi f_1 t). \tag{3.6}$$

3.2.2 Time Misalignment

After signal detection given in equation (3.6), demodulated time-misaligned signal at receiver is given in a complex form as

$$z_{STM} = (\frac{2\Re\sqrt{P_R P_{LO}}}{T_S}) \times \mathrm{Re}[\underbrace{A_1 \int_{\tau_1}^{T_S} e^{j2\pi f_1(t-\tau_1)} e^{-j2\pi f_1 t} dt}_{\eta_{STM\_1}} + \underbrace{\sum_{k\neq 1} A_k \int_{0}^{\tau_k} e^{j2\pi f_k(t-\tau_k)} e^{-j2\pi f_1 t} dt}_{\eta_{STM\_ICI}}$$
$$+ \underbrace{A_1^p \int_{0}^{\tau_1} e^{j2\pi f_1(t-\tau_1)} e^{-j2\pi f_1 t} dt}_{\eta_{STM\_ISI}}], \quad (3.7)$$

where z_{STM} is demodulated signal containing η_{STM_1}, η_{STM_ICI} and η_{STM_ISI} as desired, ICI and ISI terms in presence of STM. A_1^p is previous bit of symbol at subcarrier 1. Also, $\sqrt{P_R}$ is same for all subcarriers in the received signal, $\Re$ is responsitivity of photodetector, and T_S is symbol duration. The ICI beats in a time misaligned AO-OFDM system are considered as coherent due to the dependence on power and phase. The nature of STMs is random and the random variables τ_k in equation (3.7) are Gaussian independent variables with zero-mean and variance ${\sigma_{\tau_k}}^2$. Simplifying equation (3.7), η_{STM_1} is given as

$$\eta_{STM\_1} = \mathrm{Re}[\mathrm{A_1}(\mathrm{T_S e^{-j2\pi f_1 \tau_1}} - \tau_1 \mathrm{e^{-j2\pi f_1 \tau_1}})]. \quad (3.8)$$

In equation (3.8) the mean of random functions, $e^{-j2\pi f_1 \tau_1}$ and $\tau_1 e^{-j2\pi f_1 \tau_1}$, which depends on τ_1 are computed as

$$\mu_{\eta_{STM\_1}} = T_S e^{-2\pi^2 f_1^2 \sigma_{\tau_1}^2} - \frac{2\sigma_{\tau_1} e^{-2\pi^2 f_1^2 \sigma_{\tau_1}^2}}{\sqrt{2\pi}}. \quad (3.9)$$

In equation (3.7) the ICI term is integrated and given as

$$\eta_{STM\_ICI} = \sum_{k=2}^{N_{SC}} A_k g(\tau_k) \quad (3.10)$$

where

$$g(\tau_k) = \sum_{k=2}^{N_{SC}} \frac{e^{-j2\pi f_k \tau_k}}{j2\pi(f_k - f_1)} \left[e^{j2\pi(f_k - f_1)\tau_k} - 1 \right]. \tag{3.11}$$

With the derivation given in Appendix B, the mean and variance of ICI are

$$\mu_{\eta_{STM\_ICI}} = \sum_{h=1}^{N_{SC}-1} \mathrm{P(h)} \times \left(\sum_{\mathrm{k}=2}^{\mathrm{h}+1} \frac{\exp\left(-2\pi^2 \mathrm{f}_1^2 \sigma_{\tau_\mathrm{k}}^2\right) - \exp(-2\pi^2 \mathrm{f}_\mathrm{k}^2 \sigma_{\tau_\mathrm{k}}^2)}{\mathrm{j}\pi(\mathrm{f_k} - \mathrm{f_1})} \right) \tag{3.12}$$

and

$$\sigma^2_{\eta_{STM\_ICI}} = \sum_{h=1}^{N_{SC}-1} \mathrm{P(h)} \times \left(\sum_{\mathrm{k}=2}^{\mathrm{h}+1} \frac{1 - \exp\left(-2\pi^2(\mathrm{f_k} - \mathrm{f_1})^2 \sigma_{\tau_\mathrm{k}}^2\right)}{2\pi^2(\mathrm{f_k} - \mathrm{f_1})^2} \right) - \left| \mu_{\eta_{\mathrm{STM\_ICI}}} \right|^2, \tag{3.13}$$

where $\mathrm{P(h)}$ is a probability that subcarrier(s) carry bit 1 information, i.e. A_k=1.

In equation (3.7) the ISI term after integration is given as

$$\eta_{STM\_ISI} = A_1^p g(\tau_1) \tag{3.14}$$

where $g(\tau_1) = \tau_1 e^{-j2\pi f_1 \tau_1}$. The mean and variance of ISI, derived in Appendix C, are given as

$$\mu_{\eta_{STM\_ISI}} = \frac{\sigma_{\tau_1} e^{-2\pi^2 f_1^2 \sigma_{\tau_1}^2}}{\sqrt{2\pi}}, \tag{3.15}$$

and

$$\sigma^2_{\eta_{STM\_ISI}} = \frac{\sigma^2_{\tau_1}}{2} - (\mu_{\eta_{STM\_ISI}})^2. \tag{3.16}$$

To find the effect of STM on the performance of system, Q-factor used as a performance metric and is given as in general form $Q = (I_1 - I_0)/(\sigma_1 + \sigma_0)$, where $I_1 - I_0$ is difference of mean currents in response to bit 1 and bit 0 carried by k^{th} subcarrier, and $\sigma_1 + \sigma_0$ is their total standard deviation. The parameter Q in shot noise limited synchronous coherent optical systems is related to signal-to-noise ratio (SNR) by $Q = (1/2)\sqrt{SNR}$. For OOK-modulated

optical systems, the bit error rate (BER) is related with Q as $BER = (1/2)\mathtt{erfc}(Q/\sqrt{2})$ [12].

Shot Noise and Thermal Noise In optical receivers, the shot and thermal noises are responsible for fluctuations in a photodetected current. Due to a random generation of electrons which causes random shot noise current adds to the constant photodetected current. The shot noise variance is directly dependent on the photodetected current, I_p, and the bandwidth of receiver, BW_{RX}, and is given as

$$\sigma^2_{shot} = 2\, q\, \Re\, P_{LO}\, BW_{RX}\ , \tag{3.17}$$

where q is the electron charge, and BW_{RX} is the receiver bandwidth. The thermal noise is generated due to thermally random motion of an electron in a load (resistor). The load resistor adds the thermal current in the photodetected current. The thermal noise variance is only dependent on the bandwidth of receiver, BW_{RX}, and is given as

$$\sigma^2_{thermal} = (4k_BT/R_L)BW_{RX}, \tag{3.18}$$

where k_B is the *Boltzmann constant*, T is the absolute temperature, and R_L is the load resistance.

STM: Q-factor and BER expressions

In AO-OFDM system design, Q expression related to derived mean currents and variances of ICI and ISI due to STM is given as

$$Q = \frac{\alpha(T_S e^{-2\pi^2 f_1^2 \sigma^2_{\tau_1}} - 2\sigma_{\tau_1} e^{-2\pi^2 f_1^2 \sigma^2_{\tau_1}}/\sqrt{2\pi})}{(\sigma_1 + \sigma_0)} \tag{3.19}$$

where

$\alpha = \frac{2\Re\sqrt{P_R P_{LO}}}{T_S}$

$$\sigma_1 = (\sigma^2_{shot-1} + \alpha^2\sigma^2_{\eta_{STM\_ISI}} + \alpha^2\sigma^2_{\eta_{STM\_ICI}} + \sigma^2_{thermal})^{1/2}$$
$$\sigma_0 = (\sigma^2_{shot-0} + \alpha^2\sigma^2_{\eta_{STM\_ISI}} + \alpha^2\sigma^2_{\eta_{STM\_ICI}} + \sigma^2_{thermal})^{1/2}.$$

In equation (3.19), the numerator contains the desired signal including the power penalty term due to STM in desired subcarrier. In the denominator, variances of shot noises, thermal noise and interference terms (ICI and ISI) for bit 1 and 0 are considered. The shot noise for bit 1 and bit 0 is $\sigma^2_{shot-1} = 2\,q\,\Re\,P_{LO}\,BW_{RX}\,(1+\sigma^2_{\eta_{STM\_ICI}})$ and $\sigma^2_{shot-0} = 2\,q\Re\,P_{LO}\,BW_{RX}\,\sigma^2_{\eta_{STM\_ICI}}$, where q is the electron charge, and BW_{RX} is the receiver bandwidth. The thermal noise is given as $\sigma^2_{thermal} = (4k_BT/R_L)BW_{RX}$, where k_B is the *Boltzmann constant*, T is the absolute temperature, and R_L is the load resistance.

3.2.3 Frequency Offset

The ScFO between transmitted subcarrier frequency and local oscillator's frequency degrades the orthogonality and it introduces ICI. By using equation (3.6) for ScFO case, the demodulated received optical signal in complex form have offsets of ε_k is

$$z_{ScFO} = \left(\frac{2\Re\sqrt{P_RP_{LO}}}{T_S}\right)\mathrm{Re}[\underbrace{A_1\int_0^{T_S} e^{j2\pi(f_1+\varepsilon_1)t}e^{-j2\pi f_1 t}dt}_{\eta_{\mathrm{ScFO\_1}}} + \underbrace{\sum_{k\neq 1}A_k\int_0^{T_S} e^{j2\pi(f_k+\varepsilon_k)t}e^{-j2\pi f_1 t}dt}_{\eta_{\mathrm{ScFO\_ICI}}}], \tag{3.20}$$

where z_{ScFO} is demodulated signal for subcarrier 1. The ScFOs, ε_k, are Gaussian independent random variables with zero-mean and variance ${\sigma_{\varepsilon_k}}^2$. After simplifying equation (3.20), means and variances are calculated in ScFO case are

$$\mu_{\eta_{ScFO\_1}} = T_S e^{-2\pi^2\sigma^2_{\varepsilon_1}T_S^2} \tag{3.21}$$

$$\mu_{\eta_{ScFO\_ICI}} = \sum_{h=1}^{N_{SC}-1} \mathrm{P(h)} \times \left(\sum_{\mathrm{k=2}}^{\mathrm{h+1}} \frac{\left[1-\exp(-2\pi^2\sigma_{\varepsilon_\mathrm{k}}^2 \mathrm{T_S^2})\right]}{\mathrm{j}2\pi\left(\mathrm{f_k}-\mathrm{f_1}\right)}\right) \tag{3.22}$$

and

$$\sigma^2_{\eta_{ScFO\_ICI}} = \sum_{h=1}^{N_{SC}-1} \left[\mathrm{P(h)} \times \sum_{\mathrm{k=2}}^{\mathrm{h+1}} \frac{1-\exp(-2\pi^2\sigma_{\varepsilon_\mathrm{k}}^2 \mathrm{T_S^2})}{2\pi^2(\mathrm{f_k}-\mathrm{f_1})^2}\right] - \left|\mu_{\eta_{\mathrm{ScFO\_ICI}}}\right|^2. \tag{3.23}$$

ScFO: Q-factor and BER expressions

The Q expression for ScFO case is given as

$$Q = \frac{\alpha T_S e^{-2\pi^2\sigma_{\varepsilon_1}^2 T_S^2}}{(\sigma_1+\sigma_0)} \tag{3.24}$$

where

$\alpha = \frac{2\Re\sqrt{P_R P_{LO}}}{T_S}$

$\sigma_1 = (\sigma^2_{shot-1} + \alpha^2\sigma^2_{\eta_{ScFO\_ICI}} + \sigma^2_{thermal})^{1/2}$

$\sigma_0 = (\sigma^2_{shot-0} + \alpha^2\sigma^2_{\eta_{ScFO\_ICI}} + \sigma^2_{thermal})^{1/2}$.

3.3 Performance Analysis of AO-OFDM System

In performance analysis, the effects of STM and ScFO are investigated for two cases. In study I, the N_{SC} values are from 8 to 512, while in study II the N_{SC} values are considered from 3 to 128.

3.3.1 Study I: Details of AO-OFDM System

Effects of STM and ScFO on AO-OFDM system performance analyzed with different values of N_{SC} and receiver bandwidth BW_{RX}. The N_{SC} values in our simulations are from 8 to 512 to show the ICI impact in relation with probability of adjacent subcarriers of desired subcarrier carries bit 1 in given symbol duration. The BER performances of AO-OFDM system are given with and without cyclic prefix (CP). The requirements of CP are analyzed in

the presence of STM and ScFO. The relation of CP with T_S is given by CP = $\tau_{CP}/(T_S + \tau_{CP})$, where τ_{CP} is the duration of cyclic prefix [12]. By reducing the data rate, the objective of a CP is achieved while total symbol duration remains constant. Another way of introducing CP in frequency domain in AO-OFDM system is by increasing the subcarrier spacing (Δf) [33]. In our performance evaluations, the CP is added by reducing data rate and increasing Δf in order to reduce STM and ScFO effects. The simulation system parameters are listed in Table 3.1.

Table 3.1: Study I calculation parameters in OOK-modulated AO-OFDM system

Parameter	Value	Unit
numbers of subcarriers (N_{SC})	8 to 512	-
symbol duration (T_S)	0.1	ns
receiver's bandwidth (BW_{RX})	30, 50	GHz
k^{th} subcarrier power (P_k)	1	μW
local oscillator power (P_{LO})	1	mW
cyclic prefix (CP)	0, 22	%

BER performances versus STM and ScFO

The BER performance of AO-OFDM system in the presence of STM and ScFO is evaluated for N_{SC} = 20 and 128, BW_{RX} = 30GHz, and with and without CP. The STM causes interference not only from adjacent subcarriers but also from previous symbol at the desired demultiplexed subcarrier. For N_{SC} = 20 and without CP, the edge and middle subcarriers have same BER performance degradation and maximum acceptable relative deviation for STM (σ_τ/T_S) is 17% for BER = 10^{-3}. With the increase of N_{SC} = 20 to 128 in AO-OFDM system, σ_τ/T_S is nearly same as of N_{SC} = 20 for BER = 10^{-3}, as shown in Figure 3.4. In the presence of STM

in AO-OFDM system the BER increases mainly due to ISI and large number of subcarriers not much contributes in degradation of system performance due to the probability of adjacent subcarriers carry bit 1 is low as N_{SC} increases which shows strong agreement with equation (B.14). For AO-OFDM system with N_{SC} = 128, the BER performance remains same as N_{SC} = 20 case due to much low probability of adjacent subcarriers and tolerance of AO-OFDM system to STM remain same.

The trend of system's performance degradation with STM was reported in [88]. Two-subcarrier QPSK optical communication system was investigated experimentally in the presence of STM. In offline signal processing, relative STM of 50% of symbol duration causes degradation of Q^2 nearly 4.2dB was reported. In our performance evaluations (without any estimation and compensation DSP algorithms), we have presented that the STM causes not only ICI from adjacent subcarriers but also ISI from same desired demodulated subcarrier, and N_{SC} greater than 20 gives no effect on BER performance in presence of STM. The statistical evaluation of the system performance with increase in N_{SC} is to show the STM and ScFO effects in OOK-modulated AO-OFDM system. For advanced modulated (M-QAM, or QPSK) AO-OFDM systems, equation (B.14) will not be applicable due to average power of M-QAM modulated adjacent subcarriers of a desired subcarrier is constant. With the CP value of 22% (T_S is increased from 100 ps to 122 ps as introduced in [12]), effects of ISI and ICI are mitigated and performance of system improved to BER$\approx 10^{-6}$ at $\sigma_\tau/T_S = 17\%$ for N_{SC} = 20 and 128 cases, as shown in Figure 3.4.

In the presence of ScFO in AO-OFDM system, BER performance only depends on ICI from the adjacent subcarriers of desired subcarrier. For N_{SC} = 20, probability of adjacent subcarriers carry bit 1 is high which gives BER = 10^{-3} at maximum relative deviation for ScFO $(\sigma_\varepsilon T_S) = 31\%$. For N_{SC} = 128 case, ScFO tolerance remain the same to $\sigma_\varepsilon T_S = 31\%$, as shown in Figure 3.5. 4. In [92], system performance for an 8-carrier on-off keying (OOK) modulated AO-OFDM system was investigated, and tolerance of frequency mismatch below $\pm 4\%$ of subcarrier spacing for BER $< 10^{-5}$ was reported. The low tolerance of ScFO is

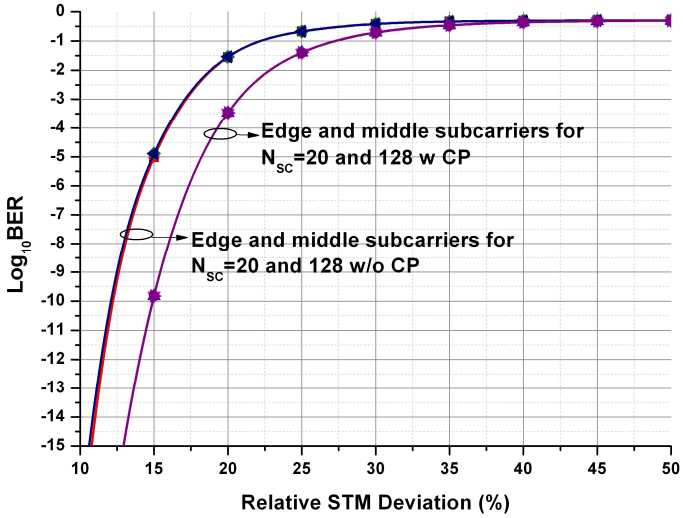

Figure 3.4: Simulated BER performance versus relative deviation for STM (σ_τ/T_S).

due to AWG-based AO-OFDM demultiplexing at receiver side needs orthogonality among all subcarriers should be maintained. Again, our simulation results show the same trend of system's performance degradation with ScFO in experiments. In the presence of ScFO, homodyne detection at receiver side gives more detailed analysis of frequency offset between transmitted subcarriers and LO (not specific to optical device) for AO-OFDM system [33], and also highlight the role of adjacent subcarriers in ICI. In the system with $CP = 22\%$ (Δf is increased from 10 GHz to 12.2 GHz), ScFo tolerance increases to $\sigma_\varepsilon T_S = 40\%$ for BER $< 10^{-3}$.

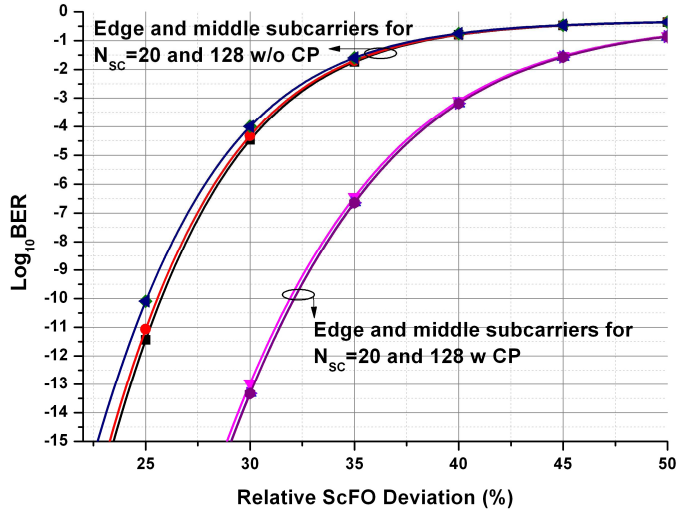

Figure 3.5: Simulated BER performance versus relative deviation for ScFO ($\sigma_\varepsilon T_S$).

The increase of N_{SC} from 8 to 20 gives more STM and ScFO tolerance due to low probability of adjacent subcarriers, and for N_{SC} greater than 20, the ICI variances ($\sigma^2_{\eta_{STM\_ICI}}$ and $\sigma^2_{\eta_{ScFO\_ICI}}$) does not increase due to ICI dependence on adjacent subcarriers only. The performance evaluations with N_{SC} in OOK-modulated AO-OFDM system is statistical by using equation (B.14). In advanced modulated AO-OFDM systems, the equation (B.14) will not be applicable. Furthermore, in our theoretical evaluations the effects of STM and ScFO are presented with derivations of means and variances without any approximations. In experimental demonstrations of AO-OFDM systems, the tolerances of STM and ScFO are different and depends on modulations formats ((de)correlated data symbols on adjacent subcarriers), optical paths ((in)dependent STM effects on adjacent subcarriers), optical subcarriers at transmitter (continuous wave or comb) and demultiplexing (O-DFT, coherent detection or band pass filter). The main reason of our investigations is to present the theoretical model of AO-OFDM transmitter with coherent detection.

Impact of ICI and ISI with N_{SC}

The presence of STM in AO-OFDM system causes not only ICI among desired subcarrier and neighbouring subcarriers but also ISI from previous symbol on desired subcarrier. In case of ScFO, the desired subcarrier have ICI from neighbouring subcarriers. Figure 3.6 shows the plots of ICI and ISI variances (r_1, r_2, and r_3) versus N_{SC} for STM and ScFO cases, where r_1, r_2, and r_3 stands for $\sigma^2_{\eta_{STM\_ICI}}/{T_S}^2$, $\sigma^2_{\eta_{ScFO\_ICI}}/{T_S}^2$, and $\sigma^2_{\eta_{STM\_ISI}}/{T_S}^2$. By observing the effects of ICI and ISI at relative deviations for STM (σ_τ/T_S) and for ScFO $(\sigma_\varepsilon T_S)$ in Figure 3.6, some interesting features can be seen. 1) For N_{SC} = 8, r_2 is 4 dB more than r_1 at relative deviations $\sigma_\tau/T_S = \sigma_\varepsilon T_S$ = 10%, due to high probability of adjacent subcarriers carry 1 bit. Increasing N_{SC} value from 8, r_2 decreases rapidly as compared to r_1. 2) Increase in relative deviations from 10% to 30%, r_1 and r_2 have same ICI level of -9.7 dB while r_3 increases from -14.2 dB to -8.2 dB. 3) STM causes both ICI and ISI so it degrades the system performance

more seriously compared with ScFO which only causes ICI. 4) For $N_{SC} = 64$, r_1 and r_2 values are less than -85 dB while r_3 remains constant and have no effect with increase in N_{SC} value. For large N_{SC} values, the probability of adjacent subcarriers carry 1 bit is low, as per relation in equation (14), which gives low values of ICI variances $\sigma^2_{\eta_{STM\_ICI}}$ and $\sigma^2_{\eta_{ScFO\_ICI}}$.

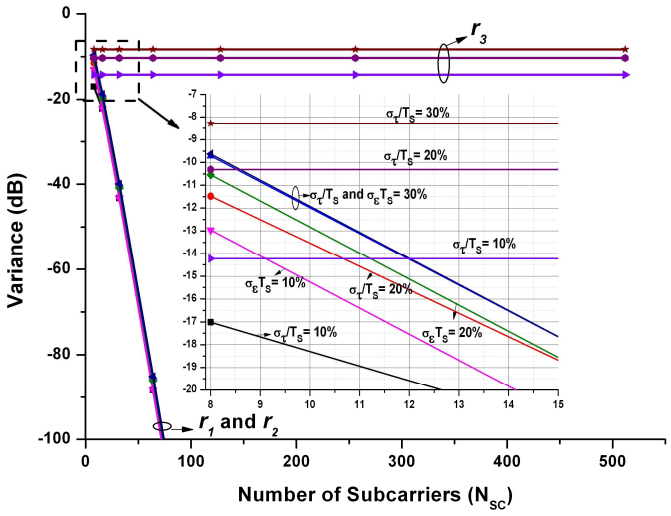

Figure 3.6: The Relationship between ICI and ISI variances (r_1, r_2, and r_3) and N_{SC}. r_1, r_2, and r_3 stands for $\sigma^2_{\eta_{STM\_ICI}}/{T_S}^2$, $\sigma^2_{\eta_{ScFO\_ICI}}/{T_S}^2$, and $\sigma^2_{\eta_{STM\_ISI}}/{T_S}^2$.

CP requirements for AO-OFDM

In the presence of STM and ScFO with relative deviations of $\sigma_\tau/T_S = 17\%$ and $\sigma_\varepsilon T_S = 31\%$, the CP requirements are investigated in AO-OFDM system. The CP is added in time and frequency domains in order to reduce the STM and ScFO effects. In time domain, T_S is increased from 100 ps to 122 ps, and in frequency domain Δf is increased from 10 GHz to 12.2 GHz. Figure 3.7 shows the plots of variances of ICI and ISI (r_1, r_2, and r_3) versus CP for STM and ScFO cases, where r_1, r_2, and r_3 have same relationships as used in Figure 3.6. 1) At CP = 50%, r_1 is reduced by 1.44 dB and r_3 is reduced by 2.32 dB but at the cost of reducing half of data rate of system. 2) At CP = 80%, r_2 is reduced by 5.42 dB but at the cost of increasing spacing between subcarriers from 10 GHz to 18 GHz which ultimately reduces the spectral efficiency. In [33], the subcarrier spacing was increased (as CP was suggested)

in order to get better performance. By properly designing AO-OFDM system considering STM and/or ScFO effects on system performance, we have less requirements of increasing subcarrier spacing or reducing data rate of subcarriers (or increasing CP) and less desire of large sampling rate at receiver side.

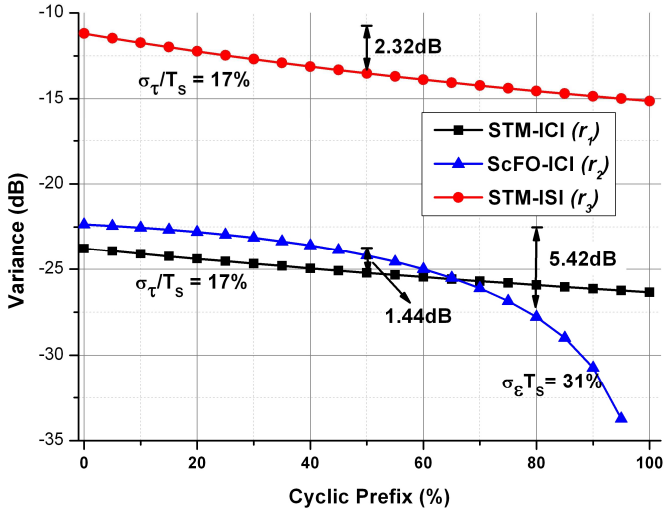

Figure 3.7: CP requirements in presence of STM and ScFO in AO-OFDM.

Effect of Receiver Bandwidth

The presence of STM and ScFO in AO-OFDM system gives rise in ICI power mainly from adjacent subcarriers. By increasing the BW_{RX} from 30 GHz to 50 GHz, more adjacent subcarriers, which carry bit 1, contributes in increasing ICI power. Further, the receiver shot noise is dependent on BW_{RX} [38] and degrades the system performance for large BW_{RX} value.

Figure 3.8 shows the plots of variances of ICI with shot noise and ISI (v_1, v_2, and v_3) versus relative deviations for STM (σ_τ/T_S) and for ScFO ($\sigma_\varepsilon T_S$), where v_1, v_2, and v_3 stands for $(\sigma^2_{\eta_{STM\_ICI}} + \sigma^2_{shot-1})/{T_S}^2$, $(\sigma^2_{\eta_{ScFO\_ICI}} + \sigma^2_{shot-1})/{T_S}^2$, and $\sigma^2_{\eta_{STM\_ISI}}/{T_S}^2$. 1) For BW_{RX} = 30 GHz and N_{SC} = 20 and 128, the ICI with shot noise in both cases of STM and ScFO gives same values v_1 = v_2 = -12.5 dB. The increase in N_{SC} value from 20 to 128 decreases the ICI power in STM and ScFO cases but v_1, v_2 levels remain same due to shot noises. 2) The increase in BW_{RX} to 50 GHz increases v_1, v_2 to -10.6 dB for N_{SC} = 20 due to 4 subcarriers

contributes in ICI. With the increase of N_{SC} from 20 to 128 gives slight decrease of 0.8 dB in v_1, v_2 for relative deviations of STM and ScFO greater than 10%. It is observed that AO-OFDM system with large N_{SC}, the system performance limited to shot noise. 3) The ISI value v_3 increases to nearly -11 dB at relative deviation of STM $(\sigma_\tau/T_S) = 17\%$ regardless of BW_{RX} value.

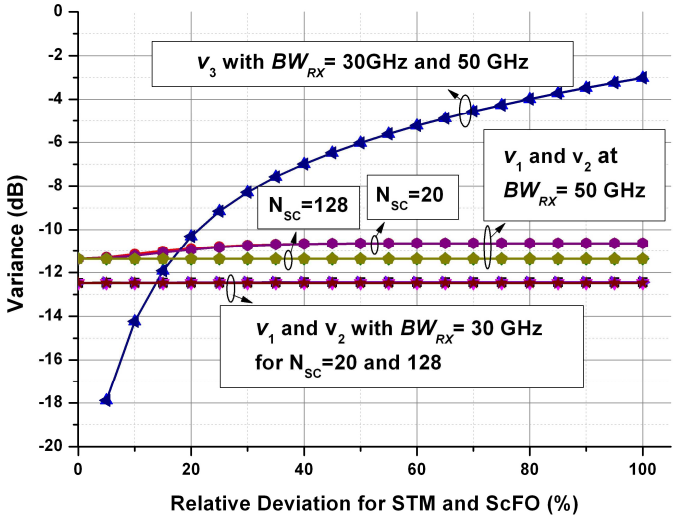

Figure 3.8: Effects on ICI and ISI variances (v_1, v_2, and v_3) with increase in BW_{RX}. v_1, v_2, and v_3 stands for $(\sigma^2_{\eta_{STM\_ICI}} + \sigma^2_{shot-1})/{T_S}^2$, $(\sigma^2_{\eta_{ScFO\_ICI}} + \sigma^2_{shot-1})/{T_S}^2$, and $\sigma^2_{\eta_{STM\_ISI}}/{T_S}^2$.

3.3.2 Study II Details of AO-OFDM System

In this study, the theoretical model is optimized towards the parameters of photodetectors with practical considerations, and the evaluations are started with N_{SC} = 3 in case of BW_{RX} = 30 GHz. The N_{SC} values in our simulations are from 3 to 128 to show the ICI impact in relation with the probability of adjacent subcarriers of desired subcarrier carries bit 1 in given symbol duration. The Bionomial coefficient terms are $\binom{2}{h}$, $\binom{19}{h}$, and $\binom{127}{h}$ in equation (B.14) for chosen values of N_{SC}, where h = 1, 2. The BER performances of AO-OFDM system are given with and without cyclic prefix (CP). The simulation system parameters are listed in Table 3.2.

Table 3.2: Study II calculation parameters in OOK-modulated AO-OFDM system

Parameter	Value	Unit
data rate	10	Gbps
symbol duration (T_S)	0.1	ns
receiver's bandwidth (BW_{RX})	30, 50	GHz
k^{th} subcarrier power (P_k)	1	μW
local oscillator power (P_{LO})	1	mW
cyclic prefix (CP)	0, 22	%

3.3.3 Results and Discussions

BER performances versus STM and ScFO

The BER performance of AO-OFDM system in the presence of STM and ScFO is evaluated for N_{SC} = 3, 20 and 128, BW_{RX} = 30GHz, and with and without CP. For N_{SC} = 3 and without CP, the edge and middle subcarriers have BER performance degradation and maximum acceptable relative deviations for STM (σ_τ/T_S) are 15% and 11% for BER = 10^{-3}, as shown in Figure 3.9. The STM tolerance of middle subcarrier in this study is lower than the Study I due to higher probability of adjacent subcarriers carry 1. The increase in N_{SC} value increases the tolerance as per relationship for OOK-modulated subcarriers is given (B.14).

In the presence of ScFO in AO-OFDM system, BER performance depends only on ICI from the adjacent subcarriers of desired subcarrier. For N_{SC} = 3, the maximum relative deviations for ScFO $(\sigma_\varepsilon T_S)$ for edge and middle subcarriers are 21% and 14%. For N_{SC} = 20 and 128, probability of adjacent subcarriers carry bit 1 is low which gives BER = 10^{-3} at $\sigma_\varepsilon T_S$ = 32%, as shown in Figure 3.10. In the presence of ScFO, homodyne detection at receiver side gives more detailed analysis of frequency offset between transmitted subcarriers and LO at receiver for AO-OFDM system [88], and also highlight the role of adjacent subcarriers in

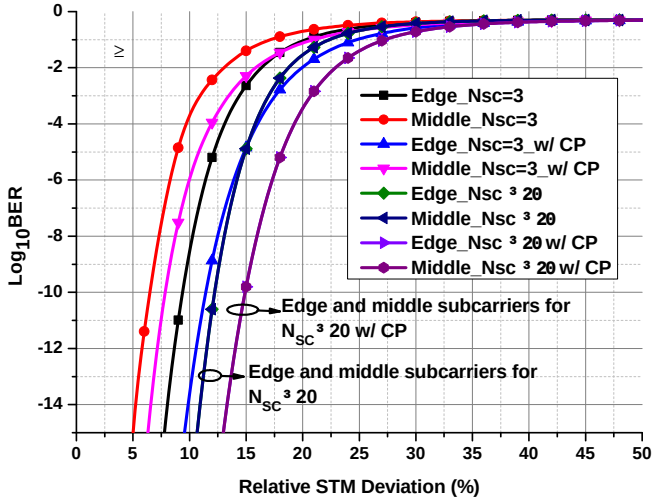

Figure 3.9: Simulated BER performance versus relative deviation for STM (σ_τ/T_S).

ICI. In the system with CP = 22%, ScFo tolerances of the middle subcarrier increases to $\sigma_\varepsilon T_S$ = 18% and 40% for BER $< 10^{-3}$ in N_{SC} = 3 and 128 cases.

The increase in σ_τ/T_S with the increase in N_{SC} value is only applicable to statistical model of OOK-modulated systems. In the case of all subcarriers are ON (carry 1) at the same time (in non-statistical model of OOK-modulated system), the effect of increase in N_{SC} value decreases the STM tolerance (σ_τ/T_S). The above argument is also valid for the ScFO tolerance $\sigma_\varepsilon T_S$.

Impact of ICI and ISI with N_{SC}

In Figure 3.11, the plot shows the variances of ICI and ISI (r_1, r_2, and r_3) versus N_{SC} for STM and ScFO cases, where r_1, r_2, and r_3 stands for $\sigma^2_{\eta_{STM\_ICI}}/{T_S}^2$, $\sigma^2_{\eta_{ScFO\_ICI}}/{T_S}^2$, and $\sigma^2_{\eta_{STM\_ISI}}/{T_S}^2$. By observing the effects of ICI and ISI on middle subcarrier in Figure 3.11, some interesting features can be seen. 1) For N_{SC} = 3, r_1 and r_2 are nearly equal and are 5 dB more than r_3 at relative deviations $\sigma_\tau/T_S = \sigma_\varepsilon T_S$ = 10%. 2) Increase in relative deviations from 10% to 30% for N_{SC} = 3, the r_1 and the r_2 are increased by 3.33 dB and 2.37 dB, but the increments are less than the increase of 5.95 dB in r_2. 3) STM causes both ICI and ISI so it degrades the

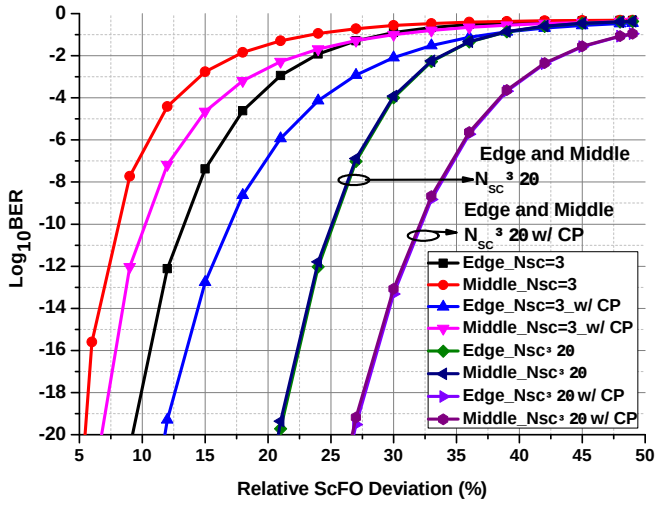

Figure 3.10: Simulated BER performance versus relative deviation for ScFO ($\sigma_\varepsilon T_S$).

system performance more seriously compared with ScFO which only causes ICI. 4) For N_{SC} $\geq$ 32, r_1 and r_2 values are less than -40 dB while r_3 remains constant and have no effect with increase in N_{SC} value.

As shown in Figure 3.11, the performance of AO-OFDM system is mainly degraded due to ICI from adjacent subcarriers, and the contribution in ICI variance is from number of subcarriers depends on bandwidth of photodetectors. It is a major difference between AO-OFDM system and a coherent optical-OFDM system (CO-OFDM) [38]. In CO-OFDM system, multicarrier RF signal (OFDM) is modulated on an optical carrier/tone, and in the presence of time and/or frequency offset in OFDM symbol and/or optical carrier will degrades the performance of received OFDM signal [31, 90, 91]. For the rest of AO-OFDM system performance evaluations, we use N_{SC} = 3 and 5 for BW_{RX} = 30 GHz and 50 GHz (bandwidth windows) at receiver.

CP requirements for AO-OFDM

In the presence of STM and ScFO with relative deviations of $\sigma_\tau / T_S = 11\%$ and $\sigma_\varepsilon T_S = 14\%$, the CP requirements are investigated in AO-OFDM system with BW_{RX} = 30GHz. Figure 3.12

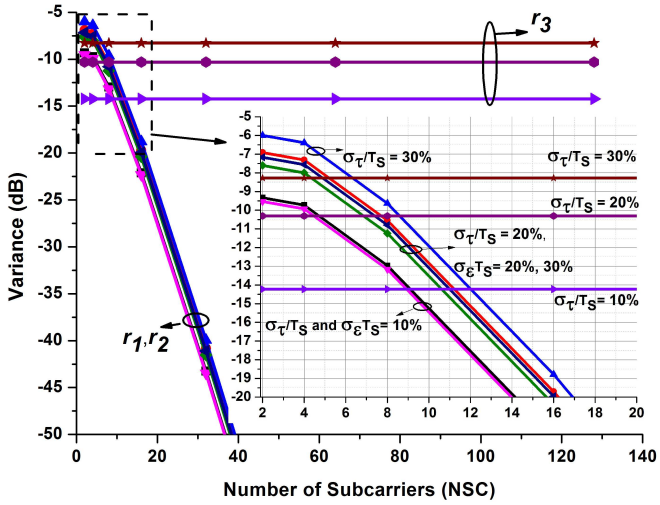

Figure 3.11: The Relationship between ICI and ISI variances (r_1, r_2, and r_3) and N_{SC}. r_1, r_2, and r_3 stands for $\sigma^2_{\eta_{STM\_ICI}}/{T_S}^2$, $\sigma^2_{\eta_{ScFO\_ICI}}/{T_S}^2$, and $\sigma^2_{\eta_{STM\_ISI}}/{T_S}^2$.

shows the plots of variances of ICI and ISI (r_1, r_2, and r_3) versus CP for STM and ScFO cases, where r_1, r_2, and r_3 have same relationships as used in Figure 3.11. 1) At CP = 50% (T_S is increased from 100 ps to 150 ps), r_1 is reduced by 1.62dB and r_3 is reduced by 2.24 dB but at the cost of reducing half of data rate of system. 2) At CP=80% (Δf is increased from 10 GHz to 18 GHz), r_2 is reduced by 6.24 dB but at the cost of increasing spacing between subcarriers from 10 GHz to 18 GHz which ultimately reduces the spectral efficiency. By properly designing AO-OFDM system considering STM and/or ScFO effects on system performance, we have less requirements of increasing subcarrier spacing or reducing data rate of subcarriers (or increasing CP) and less desire of large sampling rate at the receiver side.

Effect of Receiver Bandwidth

The presence of STM and ScFO in AO-OFDM system gives rise in ICI power mainly from adjacent subcarriers. By increasing BW_{RX} from 30 GHz to 50 GHz, more adjacent subcarriers, which carry bit 1, contributes in increasing ICI power. The Figure 3.13 shows the plots

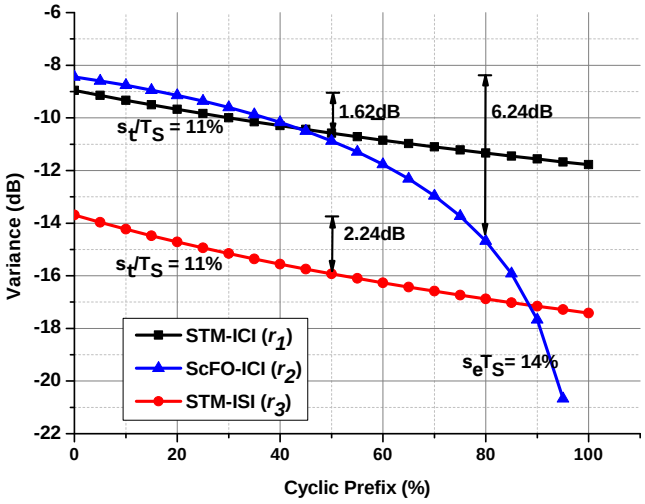

Figure 3.12: CP requirements in presence of STM and ScFO in AO-OFDM.

of variances of ICI and ISI (v_1, v_2, and v_3) versus relative deviations for STM (σ_τ/T_S) and for ScFO ($\sigma_\varepsilon T_S$), where v_1, v_2, and v_3 stands for $\sigma^2_{\eta_{STM\_ICI}}/{T_S}^2$, $\sigma^2_{\eta_{ScFO\_ICI}}/{T_S}^2$, and $\sigma^2_{\eta_{STM\_ISI}}/{T_S}^2$. For BW_{RX} = 30GHz and N_{SC} = 3, the values of v_1 and v_2 at $\sigma_\tau/T_S = 11\%$ and $\sigma_\varepsilon T_S = 14\%$, for the BER = 10^{-3}, are -9 dB and -8.44 dB, while v_3 is -13.7 dB. In order to achieve BER below 10^{-3} for AO-OFDM system with BW_{RX} =50 GHz, the maximum tolerable levels of ICI and ISI variances are required to be same as in case of BW_{RX} = 30 GHz. As shown in Figure 3.13, the ICI variances are increased by the 4 adjacent subcarriers (of the desired subcarrier) at the receiver with BW_{RX} = 50 GHz, and maximum tolerances of σ_τ/T_S and $\sigma_\varepsilon T_S$ are reduced to 5% and 7%.

3.4 Summary

In this chapter, an analytical model of OOK-modulated AO-OFDM system with ISI and ICI effects is presented, and the simulation results show that the STM tolerances are lower than the ScFO tolerances (in Study I and Study II). In Study II, the theoretical model is optimized towards the parameters of photodetectors with practical considerations. The STM tolerance

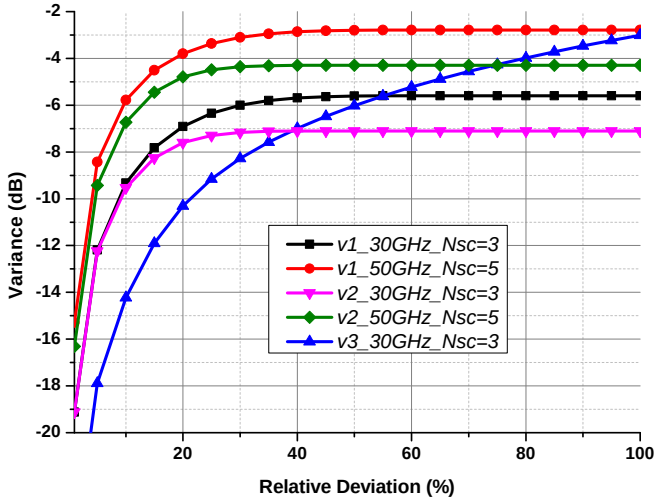

Figure 3.13: Effects on ICI and ISI variances (v_1, v_2, and v_3) with increase in BW_{RX}. v_1, v_2, and v_3 stands for $\sigma^2_{\eta_{STM\_ICI}}/{T_S}^2$, $\sigma^2_{\eta_{ScFO\_ICI}}/{T_S}^2$, and $\sigma^2_{\eta_{STM\_ISI}}/{T_S}^2$.

is low due to STM causes not only ICI among neighbouring subcarriers but also ISI from previous symbol on target subcarrier. Increasing the number of subcarriers reduces the ICI effects from neighbouring subcarriers and only ISI is a dominant factor in system performance degradation. In ScFO case, ICI is only interference which degrades the performance. The increase in receiver bandwidth gives rise of ICI effects (more adjacent subcarriers contributes in ICI variances). To limit BER performance below 10^{-3}, relative deviations for STM and ScFO should be lower than 11% and 14% (Study II). To reduce the effects of STM, the CP gives less than 4 dB reduction of ICI and ISI normalized powers at 50%, which corresponds to reducing the data rate from 10 Gbps to 5 Gbps. In ScFO case, the ICI effects are reduced by 6.24 dB at CP = 80% which corresponds to increasing the subcarrier separation from 10 GHz to 18 GHz. The simulation results from derived analytical model of AO-OFDM system provides the relationships between the major system design parameters (N_{SC}, BW_{RX} and CP), and the ICI and ISI caused by the STM and ScFO.

Chapter 4

Timing and Frequency Offsets in M-QAM All-Optical OFDM System

Orthogonal frequency division multiplexing (OFDM) offers high spectral efficiency (greater than 1 b/s/Hz) with the use of advanced/multilevel modulation formats in optical communication systems [12]. In multilevel signals transmission, we transmit more than two signal waveforms over a communication channel [93]. In this chapter, we investigate M-QAM modulated subcarriers in the presence of time and frequency offsets.

In AO-OFDM, optical subcarriers are multiplexed to transmit composite AO-OFDM signal without phase controller (as required in CoWDM systems). For demultiplexing at the receiver side, an optical discrete Fourier transform (O-DFT) or a coherent detection is used at receiver [12, 33]. The performance of AO-OFDM system is affected by orthogonality among optical subcarriers. The subcarriers' frequencies and the symbol times are required to be synchronized with receiver. If for any reason, symbol time misalignment(s) (STM) and/or subcarrier frequency offset(s) (ScFO) present in AO-OFDM system, the performance of system seriously degraded [88]. In order to overcome the performance degradation due to loss of an orthogonality among subcarriers, cyclic prefix (CP) is commonly used to reduce the ISI and the ICI at the cost of reduced data rate and/or spectral efficiency. Another way by using a digital signal processor (DSP) at the receiver, the effects of ICI from adjacent subcarriers can be reduced [88]. Previously in [88, 33], pre-filtering with constant modulus algorithm (CMA)-based equalizer in the digital domain was used for the ICI estimation and suppression for QPSK and 16-QAM modulated AO-OFDM system (emulation setups). Due to random

nature of STMs and ScFOs in multiple subcarriers, a joint DSP based ICI estimation and suppression in Nyquist wavelength division multiplexing (N-WDM) system is proposed in [98]. The DSP based ICI estimation and reduction improves performance of overall system (as explained in Section 2.5) but it poses challenges on cost-effective and high performance DSP algorithms for AO-OFDM system [38].

In this chapter, the STM and ScFO effects on the performance of M-QAM AO-OFDM system are studied using both analytical and Monte-Carlo (numerical) simulations, and compared with results of an odd-and-even and a decorrelated setups [33]. The effects of number of subcarriers (N_{SC}) on ICI in AO-OFDM system is evaluated. Furthermore, the existing methods like the CP, the optical delay lines (ODL), the tunable laser diode (TLD), and the DSP based methods to reduce the effects of STM and ScFO on desired subcarrier are described, and a delay line interferometer (DLI) for ICI suppression is proposed and results are discussed.

4.1 Problem Statement

In AO-OFDM system, τ_k and ε_k are STM and ScFO effects, and they are independent Gaussian random variables which varies from 0 to T_S and 0 to $1/T_S$, where T_S is the symbol duration. In order to maintain the BER performance, the relative deviations, σ_{τ_k}/T_S and $\sigma_{\varepsilon_k}T_S$, of τ_k and ε_k are required to be below the tolerable limits. In ideal case of no offsets i.e. $\sigma_{\tau_k}/T_S = \sigma_{\varepsilon_k}T_S = 0$, 16-QAM symbol is at point A with no ISI and ICI, as shown in Figure 4.1(a). In case of the STM and ScFO effects below the maximum tolerable limits of σ_{τ_k}/T_S and $\sigma_{\varepsilon_k}T_S$, QAM symbol moves to point B. With these deviations where orthogonality among subcarriers is preserved, the phase of k^{th} subcarrier is rotated by ϕ' from the origin and ICI occurs (with ISI in STM case), shown as region C, but QAM symbols are still within the decision regions/boundariers and the BER performance of AO-OFDM system is not much degraded. In case of σ_{τ_k}/T_S and $\sigma_{\varepsilon_k}T_S$ are deviated above the tolerable limits then orthog-

onality among overlapped subcarriers is not maintained and the ISI and the ICI occurs, as shown in Figure 4.1(b).

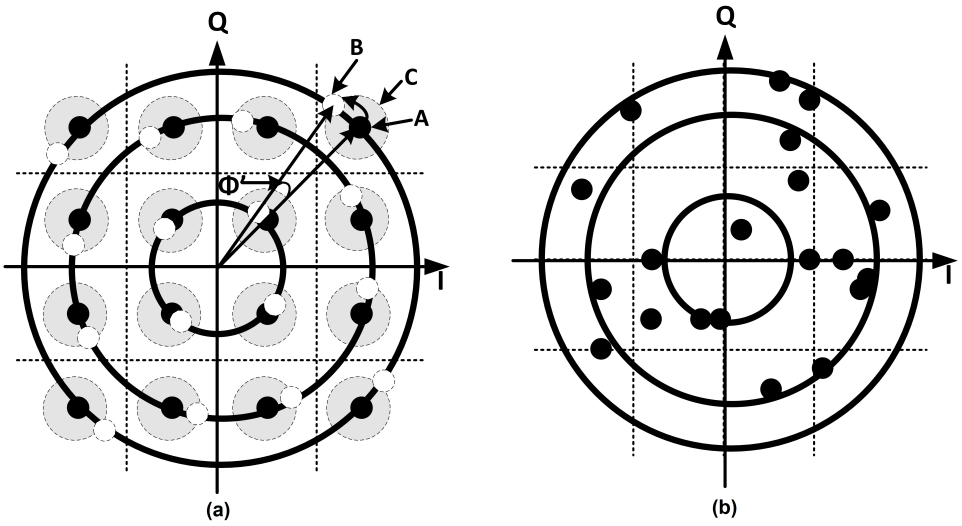

Figure 4.1: Graphical interpretation of STM and ScFO effects on 16-QAM constellations of AO-OFDM signal in (a) and (b).

In AO-OFDM system, the number of optical subcarriers (N_{SC}) are normally larger ($N_{SC} > 100$) and each subcarrier is generated by individual optical source (CW laser) or from comb source (such as modelocked laser). To modulate each optical subcarrier, N_{SC} independent data modulation sources and modulators are needed. Due to limited cost and resource availability of modulators and data converters, the subcarriers are interleaved before data modulator(s) in odd and even subcarriers and modulated with two data modulators to give proof-of-concept in the experimental or emulation setups, as shown in Figure 4.2(a) [12, 58, 66]. If any modulator of odd and even subcarriers is time misaligned or any subcarrier in odd and even subcarriers has frequency offset, then results are not actual. In [33], the issue of incorrect estimation of performance in an interleaved and modulated closely-packed subcarriers is preliminary studied. In this study, a single subcarrier is modulated by 16-QAM modulating signal and by using an optical loop the subcarrier's copies are generated to form AO-OFDM signal, as shown in Figure 4.2(b). The delay in a loop decorrelates a data carrying subcarriers.

In the presence of STM, the subcarriers modulated by independent odd and even modu-

lators have time offset based on two optical paths and an estimate of BER performance will be different if compare with a real system. In a decorrelated system, slight timing error in the optical loop copies a same error in all other the subcarriers, due to single optical path for all modulated subcarriers. This causes unrealistic results than the results of the practical system's configuration which have N_{SC} independent optical modulators and paths to generate composite AO-OFDM signal.

In the presence of ScFO between transmitted subcarrier and LO at a receiver, the performance estimates are different from practical system when single light source is used as seed subcarrier in an experimental system and duplicates generated by means of optical loop [59]. A seed subcarrier with ScFO, transmitted subcarriers N_{SC} have same ScFO. This will cause unrealistic results and give incorrect performance estimates.

The aim of this chapter is to model AO-OFDM system (AO-OFDM transmitter and coherent detection) with each subcarrier on independent optical path is modulated by an independent M-QAM modulation source. The degradation of orthogonality among subcarriers is evaluated by estimation of intercarrier interference in the presence of time and frequency offsets (STM and ScFO). Furthermore, BER performance of M-QAM AO-OFDM system in the presence of random STM and ScFO effects is evaluated and estimated the tolerable limits of σ_{τ_k}/T_S and $\sigma_{\varepsilon_k} T_S$ in AO-OFDM system.

4.2 M-QAM Modulated AO-OFDM System Model

In AO-OFDM system model, N_{SC} optical subcarriers from CW laser sources are M-QAM modulated with independent data sources c_k, as shown in Figure 4.3 , where k is subcarrier index from 1 to N_{SC}.

A M-ary QAM signal $c_k e^{\varphi_k(t)}$ of k^{th} subcarrier contains both the amplitude c_k and the phase $e^{\varphi_k(t)}$ information from M different waveforms [93]. M-QAM modulation format provides higher spectral efficiency as compare to M-PSK. In M-QAM system, the M signal

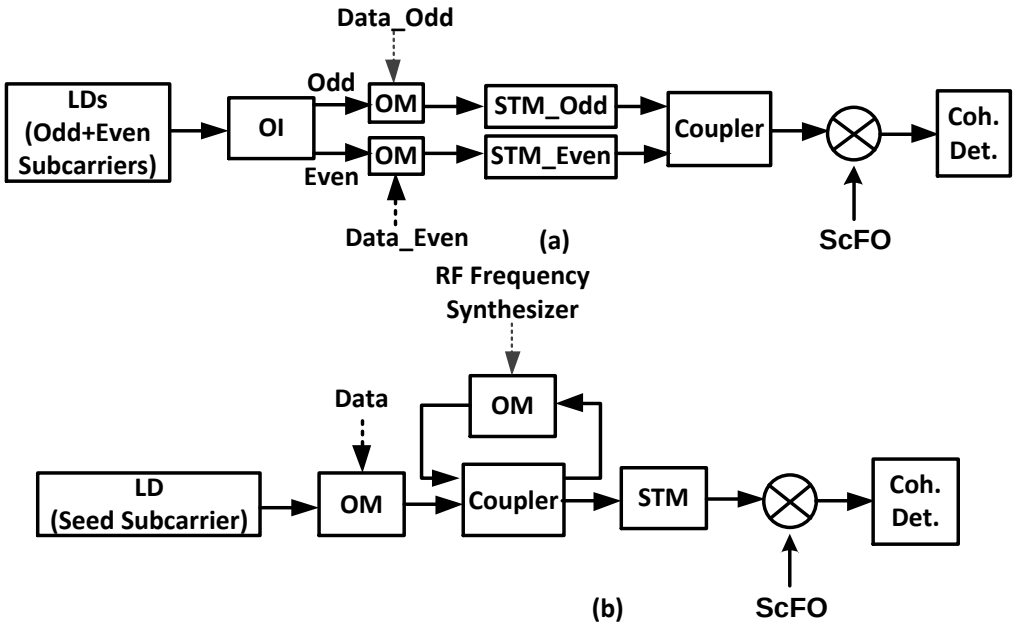

Figure 4.2: Emulation setups of (a) odd-and-even [12] and (b) decorrelated [33] AO-OFDM systems. LD: laser diode; OM: optical modulator; OI: optical interleaver; STM: symbol time misalignment; ScFO: subcarrier frequency offset; Coh. Det.: coherent detection.

waveforms are given as

$$s(t) = c_k e^{j\omega_k t} = a_k \cos \omega_k t - b_k \sin \omega_k t, \tag{4.1}$$

where M is an integer, and $a, b = -\sqrt{M}+1, -\sqrt{M}+3, ..., -1, +1, ..., \sqrt{M}-1$.

Figure 4.4 shows the QAM transmitter based on two Mach-Zehnder modulators (MZM). The optical signal is first splitted into two optical propagation paths and MZM modulates each optical path independently as per quadrature inputs (a and b) [93]. The quadrature inputs have phase difference of $\pi/2$.

After modulation, k^{th} subcarrier

$$E_k(t) = c_k E_k e^{j\omega_k t} \tag{4.2}$$

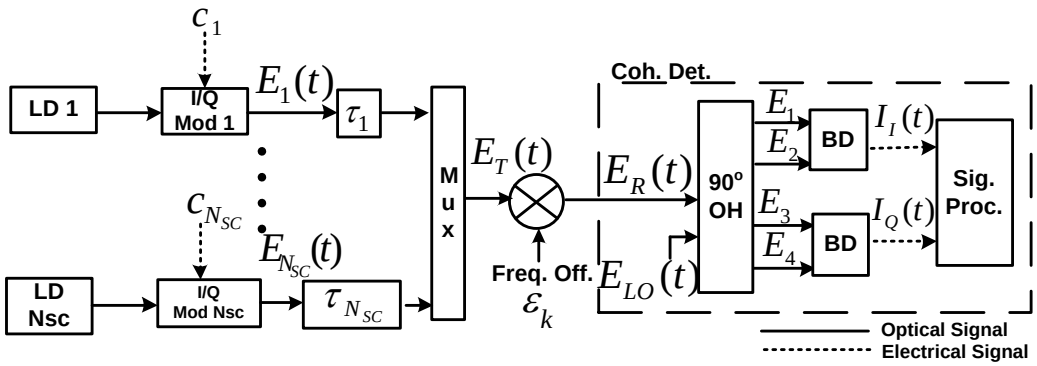

Figure 4.3: Block Diagram of M-QAM AO-OFDM system (AO-OFDM transmitter and coherent detection). LD: laser diode; Freq. Off.: frequency offset; Coh. Det.: coherent detection; LO: local oscillator; OH: optical hybrid; BD: balanced detector; Sig. Proc: Signal Processing.

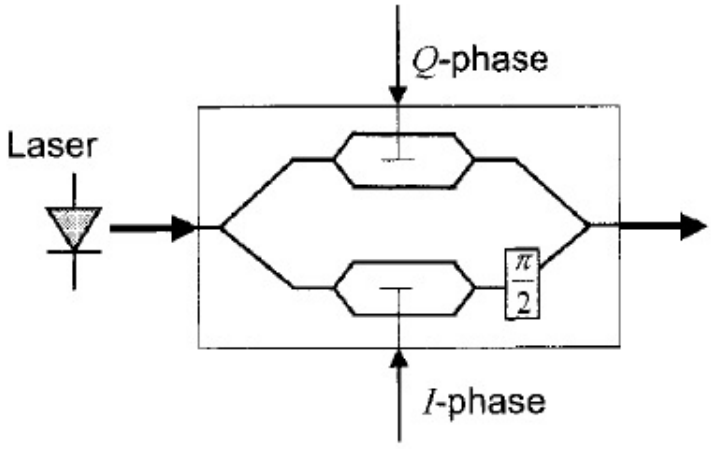

Figure 4.4: QAM Transmitter [93].

is time misaligned by τ_k and multiplexed to transmit AO-OFDM signal which is given as

$$E_T(t) = \sum_{k=1}^{N_{SC}} c_k E_k e^{j\omega_k(t-\tau_k)}, \tag{4.3}$$

where $c_k = a_k - jb_k$ and E_k are complex data symbol (QAM data symbol) and optical field at a given frequency ω_k of k^{th} subcarrier. The frequency offset ε_k is introduced as multiplicative noise in $E_T(t)$ and resultant AO-OFDM signal in the presence of time and frequency offsets

is

$$E_R(t) = \sum_{k=1}^{N_{SC}} c_k E_k e^{j2\pi(f_k+\varepsilon_k)(t-\tau_k)}. \tag{4.4}$$

Quadrature Receiver In order to recover the two quadrature components from incoming optical signal, we need a quadrature receiver comprises of coupler, 90^o optical hybrid and balanced photodetectors, as shown in Figure 4.5. The 90^o optical hybrid comprises of a 3-dB coupler and polarization beam splitter at the each output port of coupler. Mathematically, the input and output of 2x4 90^o optical hybrid have relationship

$$S = \frac{1}{2}\begin{bmatrix} 1 & 1 \\ 1 & j \\ 1 & -1 \\ 1 & -j \end{bmatrix}. \tag{4.5}$$

In a homodyne-quadrature receiver, $i_I(t)$ and $i_Q(t)$ are in-phase and quadrature-phase components and this type of receiver can be used for multilevel modulation formats (M-QAM and M-PSK).

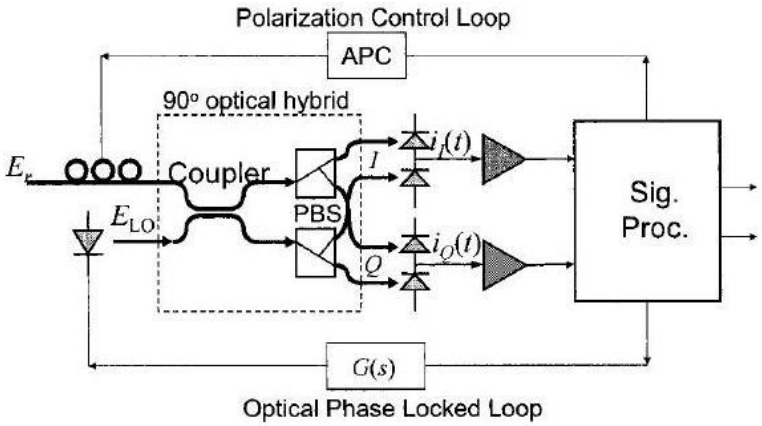

Figure 4.5: Block Diagram of Quadrature Receiver [93].

The output signals E_{1-4} of optical hybrid are related with the received AO-OFDM signal

$E_R(t)$ and the local oscillator signal $E_{LO}(t) = \sqrt{P_{LO}}e^{j2\pi f_{LO}t}$ are given as

$$\begin{aligned} E_1 &= E_R + E_{LO} \\ E_2 &= E_R - E_{LO} \\ E_3 &= E_R - jE_{LO} \\ E_4 &= E_R + jE_{LO}. \end{aligned} \tag{4.6}$$

After the balanced detections, $I_I(t)$ and $I_Q(t)$ can be expressed as

$$I_I(t) = I_1 - I_2 = \frac{1}{4}\Re\{|E_R + E_{LO}|^2 - |E_R - E_{LO}|^2\} \tag{4.7}$$

$$= \Re \sum_{k=1}^{N_{SC}} |c_k|\sqrt{P_k P_L}\cos(2\pi((f_k + \varepsilon_k)(t - \tau_k) - f_{LO}t + \phi_s) \tag{4.8}$$

and

$$I_Q(t) = I_3 - I_4 = \frac{1}{4}\Re\{|E_R - jE_{LO}|^2 - |E_R + jE_{LO}|^2\} \tag{4.9}$$

$$= \Re \sum_{k=1}^{N_{SC}} |c_k|\sqrt{P_k P_L}\sin(2\pi((f_k + \varepsilon_k)(t - \tau_k) - f_{LO}t + \phi_s), \tag{4.10}$$

where $\Re$ is responsitivity of photodetector. Combining equation (4.7) and equation (4.9), total detected current $I(t)$ is given as

$$I(t) = I_I(t) + jI_Q(t) \tag{4.11}$$

$$= \Re \sum_{k=1}^{N_{SC}} c_k \sqrt{P_k P_L} e^{j2\pi((f_k+\varepsilon_k)(t-\tau_k) - f_{LO}t)}. \tag{4.12}$$

4.2.1 Symbol Time Misalignment

We first evaluate the STM effects and rewrite equation (4.11) as

$$I(t) = \Re \sum_{k=1}^{N_{SC}} c_k \sqrt{P_k P_{LO}} e^{j2\pi f_k(t-\tau_k)} e^{-j2\pi f_1 t}. \tag{4.13}$$

The demodulated signal for a symbol with a duration T_S is given as

$$z_{STM} = \frac{1}{T_S}\int_0^{T_S} I(t)\,dt \tag{4.14}$$

$$= \frac{\Re}{T_S}\int_0^{T_S}\sum_{k=1}^{N_{SC}} c_k\sqrt{P_k P_{LO}}e^{j2\pi f_k(t-\tau_k)}e^{-j2\pi f_1 t}dt \tag{4.15}$$

Considering the received power of k^{th} subcarrier, P_R, the demodulated signal can be expressed as,

$$z_{STM} = (\frac{\Re\sqrt{P_R P_{LO}}}{T_S}) \times [\underbrace{c_1\int_{\tau_1}^{T_S} e^{j2\pi f_1(t-\tau_1)}e^{-j2\pi f_1 t}dt}_{\eta_{STM\_1}} + \underbrace{\sum_{k\neq 1} c_k\int_0^{\tau_k} e^{j2\pi f_k(t-\tau_k)}e^{-j2\pi f_1 t}dt}_{\eta_{STM\_ICI}} + \underbrace{c_1^p\int_0^{\tau_1} e^{j2\pi f_1(t-\tau_1)}e^{-j2\pi f_1 t}dt}_{\eta_{STM\_ISI}}], \tag{4.16}$$

where z_{STM} is demodulated signal containing η_{STM_1}, η_{STM_ICI} and η_{STM_ISI} as desired, ICI and ISI terms in the presence of STM. c_1^p is previous symbol of AO-OFDM signal at subcarrier 1. T_S is the symbol duration. The ICI beats are considered as coherent due to dependence on power and phase. The STM random variables τ_k in equation (4.16) are Gaussian independent variables with zero-mean and variance ${\sigma_{\tau_k}}^2$. Simplifying equation (4.16), η_{STM_1} is given as

$$\eta_{STM\_1} = [c_1(T_S e^{-j2\pi f_1\tau_1} - \tau_1 e^{-j2\pi f_1\tau_1})]. \tag{4.17}$$

In equation (4.17) expected values of random functions, $e^{-j2\pi f_1 \tau_1}$ and $\tau_1 e^{-j2\pi f_1 \tau_1}$, which depends on τ_1 are computed as

$$\mu_{\eta_{STM\_1}} = T_S e^{-2\pi^2 f_1^2 \sigma_{\tau_1}^2} - \frac{2\sigma_{\tau_1} e^{-2\pi^2 f_1^2 \sigma_{\tau_1}^2}}{\sqrt{2\pi}}. \tag{4.18}$$

In equation (4.16) the ICI term is integrated and given as

$$\eta_{STM\_ICI} = \sum_{k=2}^{N_{SC}} c_k g(\tau_k) \tag{4.19}$$

where

$$g(\tau_k) = \sum_{k=2}^{N_{SC}} \frac{e^{-j2\pi f_k \tau_k}}{j2\pi(f_k - f_1)} \left[e^{j2\pi(f_k - f_1)\tau_k} - 1 \right]. \tag{4.20}$$

From [97] mean and variance of function $g(\tau_k)$ are

$$\mu_{g(\tau_k)} = \sum_{k=2}^{N_{SC}} \int_{-\infty}^{\infty} g(\tau_k)\, p(\tau_k)\, d\tau_k \tag{4.21}$$

$$\sigma_{g(\tau_k)}^2 = E\left| g(\tau_k) - \mu_{g(\tau_k)} \right|^2 \tag{4.22}$$

where $p(\tau_k) = \frac{1}{\sqrt{2\pi\sigma_{\tau_k}}} \exp(-\tau_k^2/(2\sigma_{\tau_k}^2))$ is probability density function of independent Gaussian distributed variables τ_k. The mean and variance of ICI are given as

$$\mu_{\eta_{STM\_ICI}} = \sum_{k=2}^{N_{SC}} \frac{\exp\left(-2\pi^2 f_1^2 \sigma_{\tau_k}^2\right) - \exp(-2\pi^2 f_k^2 \sigma_{\tau_k}^2)}{j2\pi(f_k - f_1)} \tag{4.23}$$

and

$$\sigma_{\eta_{STM\_ICI}}^2 = \left(\sum_{k=2}^{N_{SC}} \frac{1 - \exp\left(-2\pi^2 (f_k - f_1)^2 \sigma_{\tau_k}^2\right)}{2\pi^2 (f_k - f_1)^2} \right) - \left| \mu_{\eta_{STM\_ICI}} \right|^2 \tag{4.24}$$

In equation (4.16), the ISI term after integration is given as

$$\eta_{STM\_ISI} = c_1^p g(\tau_1) \tag{4.25}$$

where $g(\tau_1) = \tau_1 e^{-j2\pi f_1 \tau_1}$. The mean and variance of ISI are given as

$$\mu_{\eta_{STM\_ISI}} = \frac{2\sigma_{\tau_1} e^{-2\pi^2 f_1^2 \sigma_{\tau_1}^2}}{\sqrt{2\pi}}, \tag{4.26}$$

and

$$\sigma^2_{\eta_{STM\_ISI}} = \sigma^2_{\tau_1} - (\mu_{\eta_{STM\_ISI}})^2. \tag{4.27}$$

STM: ESNR and BER expressions

The effective signal-to-noise ratio (ESNR) expression related to derived mean currents and variances of ICI and ISI due to STM with shot and thermal noises [94] is given as

$$ESNR = \frac{(\mu_{\eta_{STM\_1}})^2}{\sigma^2_{\eta_{STM\_ISI}} + \sigma^2_{\eta_{STM\_ICI}} + \sigma^2_{shot} + \sigma^2_{thermal}}. \tag{4.28}$$

In equation (4.28), the numerator contains the desired signal including the power penalties term due to STM. In denominator, variances of shot noises, thermal noise and interference terms (ICI, and ISI) are considered. The relationships of symbol error probability (P_{M-QAM}) and bit error rate (BER) with ESNR for M-QAM are given as

$$P_{M-QAM} = 2(1 - \frac{1}{\sqrt{M}})erfc\left(\sqrt{\frac{3ESNR}{2(M-1)}}\right), \tag{4.29}$$

and

$$BER = \frac{1}{\log_2 M}(1 - (1 - P_{M-QAM})^2). \tag{4.30}$$

4.2.2 Frequency offset

The ScFO between transmitted subcarrier frequency and receiver local oscillator frequency degrades the orthogonality and it introduces ICI. By using equation (4.11) for ScFO case, the

demodulated received optical OFDM signal has offset of ε_k is given as

$$z_{ScFO} = \left(\frac{2\Re\sqrt{P_R P_{LO}}}{T_S}\right) \underbrace{[c_1 \int_0^{T_S} e^{j2\pi(f_1+\varepsilon_1)t} e^{-j2\pi f_1 t} dt}_{\eta_{ScFO\_1}} + \underbrace{\sum_{k\neq 1} c_k \int_0^{T_S} e^{j2\pi(f_k+\varepsilon_k)t} e^{-j2\pi f_1 t} dt]}_{\eta_{ScFO\_ICI}}, \tag{4.31}$$

where z_{ScFO} is demodulated signal for subcarrier 1. The ScFOs ε_k are Gaussian independent random variables with zero-mean and variance ${\sigma_{\varepsilon_k}}^2$. After simplifying equation (4.31), we calculate the means and variances in ScFO case and derived expressions are

$$\mu_{\eta_{ScFO\_1}} = \sqrt{\pi} T_S \, (\frac{2\pi T_S \sigma_{\varepsilon_1}}{\sqrt{2}}) \tag{4.32}$$

$$\mu_{\eta_{ScFO\_ICI}} = \sum_{k=2}^{N_{SC}} \frac{\left[1 - \exp(-2\pi^2 \sigma_{\varepsilon_k}^2 T_S^2)\right]}{j2\pi\,(f_k - f_1)} \tag{4.33}$$

and

$$\sigma^2_{\eta_{ScFO\_ICI}} = \sum_{k=2}^{N_{SC}} \frac{1 - \exp(-2\pi^2 \sigma_{\varepsilon_k}^2 T_S^2)}{2\pi^2 (f_k - f_1)^2} - \left|\mu_{\eta_{ScFO\_ICI}}\right|^2. \tag{4.34}$$

ScFO: ESNR and BER expressions

The ESNR expression for ScFO is given as

$$ESNR = \frac{(\mu_{\eta_{ScFO\_1}})^2}{(\sigma^2_{ScFo\_ICI} + \sigma^2_{thermal} + \sigma^2_{shot})}. \tag{4.35}$$

4.3 Performance Analysis of AO-OFDM Systems

4.3.1 Details of Simulation Setups

In AO-OFDM system, we first evaluate the variances of the ICI and ISI due to the STM and ScFO for N_{SC} values from 2 to 300 in our proposed analytical model. Each subcarrier is independently 16-QAM modulated with the symbol rate of 10 GBd (single carrier), and the

derived analytical model is verified with numerical simulation. In simulations, the aggregate symbol rate is 3 Tb/s (N_{SC} = 300). In numerical simulations, Monte Carlo method is used with 10^6 random 16-QAM symbols which are sufficient to get the converged BER and the details given in Appendix D. The simulation systems parameters are listed in Table 4.1.

Table 4.1: M-QAM AO-OFDM system simulation parameters

Parameter	Value	Unit
numbers of subcarriers (N_{SC})	2 to 300	-
symbol duration (T_S)	0.1	ns
k^{th} subcarrier power (P_k)	1	μW
cyclic prefix (CP)	0 to 80	%
local oscillator power (P_{LO})	1	mW

For comparison of the performance of AO-OFDM system with an odd-and-even and a decorrelated emulation setups, the numerical simulations are performed with simulation setups as shown in Figure 4.2. For an odd-and-even setup, independent data modulation sources for odd and even subcarriers are used. The ScFO effect is same on all subcarriers with two optical paths gives two independent effects of STM on odd and even subcarriers. The adjacent subcarriers, either from the odd or the even subcarriers, have correlated data due to common modulation source, as shown in Figure 4.2(a). In a decorrelated emulation setup, modulated seed subcarrier is duplicated to decorrelated subcarriers by an optical modulator derived by RF frequency synthesizer. In this setup, we considered cases of decorrelated and correlated subcarriers, and the effects of STM and ScFO are modelled as same for all subcarriers due to single optical path for seed subcarrier is used in this emulation setup, as shown in Figure 4.2(b).

4.3.2 Effects of STM and ScFO with N_{SC}

The effects of STM and ScFO are evaluated for N_{SC} values from 3 to 300. Figure 4.6(a) shows the plot between N_{SC} and variances of ICI and ISI (r_1, r_2, and r_3) due to STM and ScFO effects in an AO-OFDM system, where r_1, r_2, and r_3 stands for $\sigma^2_{\eta_{STM\_ICI}}/{T_S}^2$, $\sigma^2_{\eta_{ScFO\_ICI}}/{T_S}^2$, and $\sigma^2_{\eta_{STM\_ISI}}/{T_S}^2$. At the relative deviations for STM (σ_τ/T_S) = 3% and for ScFO $(\sigma_\varepsilon T_S)$ = 5, r_1 increases from -11.2dB to -10dB and r_2 increases from -11.6 dB to -10.7 dB for N_{SC} from 3 to 10. The corresponding BER performance at N_{SC} = 10 is below 10^{-3}, as shown in Figure 4.6(b). Increasing N_{SC} from 10 to 300 does not affect r_1 and the r_2. The value of r_3 remains the same for N_{SC} from 3 to 300 for σ_τ/T_S = 3% due to the dependence on only the desired subcarrier. The physical interpretation of these simulation results is the interference is rapidly decreases with the increase in frequency separation. Therefore, the performance of the desired subcarrier in AO-OFDM system is mainly degraded due to ICI from adjacent subcarriers [98], and the contribution of number of subcarriers in the ICI variance depends on bandwidth of photodetectors at receiver. For the rest of evaluations of the STM and the ScFO effects, we use N_{SC} = 3 subcarriers and the bandwidth of photodetectors at receiver is 30GHz.

4.3.3 BER performance of AO-OFDM system

In AO-OFDM system, the analytical results based on the derived model shows the BER performance is 10^{-3} of edge and middle subcarriers at the relative deviations for STM (σ_τ/T_S) = 3.8% and 3.2%, as shown in Figure 4.7. The STM tolerance of edge subcarrier is higher than the middle subcarrier due to less number of adjacent subcarriers contributes in ICI. The numerical results of BER by direct symbol error counting in the numerical simulations for AO-OFDM system verifies the same tolerances at σ_τ/T_S = 3.8% and 3.2%. The same trend of degradation of the performance of QPSK modulated AO-OFDM system with coherent detection is reported in [88]. In two-subcarrier transmitter, the STM effects are evaluated and with offline signal processing the relative STM (τ_k/T_S) of 50% of symbol duration Q^2 degra-

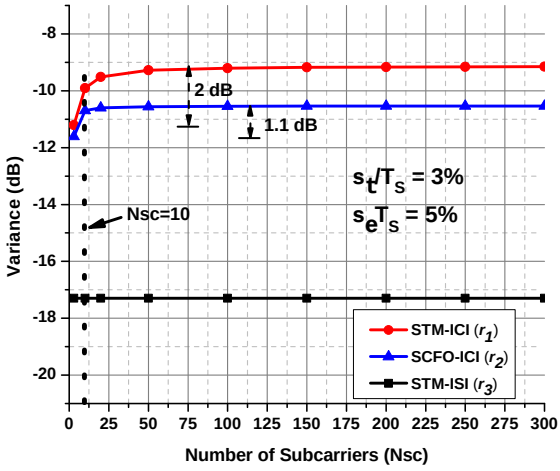

(a)

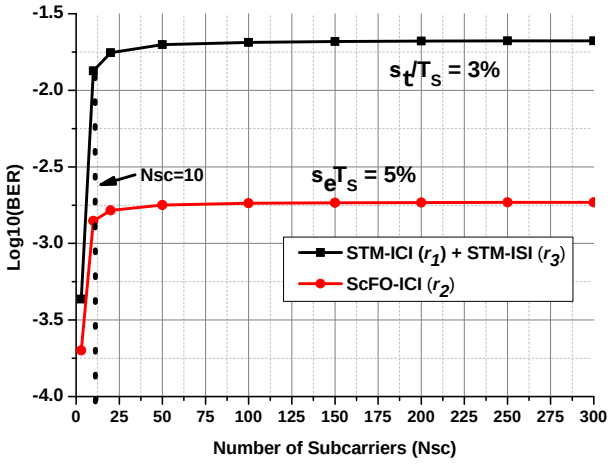

(b)

Figure 4.6: Effects of STM and ScFO with N_{SC} on (a) ICI and ISI variances (r_1, r_2, and r_3) and (b) BER performance. r_1, r_2, and r_3 stands for $\sigma^2_{\eta_{STM\_ICI}}/{T_S}^2$, $\sigma^2_{\eta_{ScFO\_ICI}}/{T_S}^2$, and $\sigma^2_{\eta_{STM\_ISI}}/{T_S}^2$.

dation nearly 4.2dB was reported in an experimental setup. In our analytical model, we have presented that the STM causes not only ICI from adjacent subcarriers but also ISI from same desired subcarrier.

In the presence of ScFO in the system, the BER performance degrades to 10^{-3} at a relative deviations for ScFO $(\sigma_\varepsilon T_S)$ = 6.6% and 5.5% for edge and middle subcarriers, as shown in Figure 4.7. The analytical results are verified by numerical simulations. In [61], tolerance to ScFO for an arrayed waveguide grating (AWG) based on-off keying (OOK) modulated AO-OFDM system was reported, and the frequency mismatch should be below 4% of subcarrier

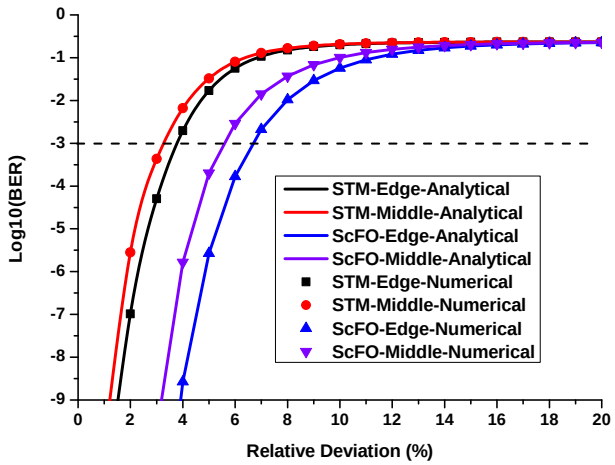

Figure 4.7: BER performance of AO-OFDM system.

spacing for BER $< 10^{-5}$. Further to improve system performance, waveform reshaping scheme was used to reduce the effects of slab-diffraction in an AWG. Our results shows little more tolerance due to desired subcarrier is demultiplexed by using coherent detection which is less sensitive to ScFO.

In experimental demonstrations of AO-OFDM systems, the tolerances of STM and ScFO are different and depends on modulations formats (and (de)correlated data symbols on adjacent subcarriers), optical paths ((un)similar STM effects on adjacent subcarriers), optical subcarriers at transmitter (continuous wave or comb), and demultiplexing and detection method (O-DFT, coherent detection or band pass filter).

In [88], [99], and [100], the multicarrier communication systems are more sensitive to STM than ScFO effects was reported that. In [88], the performance of closely spaced QPSK-modulated optical subcarriers was investigated. In this investigation with adjacent subcarrier rejection filter (as shown in Figure 2.29), at $\sigma_\tau/T_S = \sigma_\varepsilon T_S = 20\%$ the Q^2 is degraded approx. 2 dB in both cases (offsets investigated separately).

4.3.4 Comparison of AO-OFDM system with its emulation setups

In the simulations for an odd-and-even emulation setup, the numerical results gives no errors upto $\sigma_\tau/T_S = 5.7\%$, which is equivalent to 5.7 ps of STM for symbol duration of 100 ps, as shown in Figure 4.8(a). The tolerance is higher than the tolerance of practical AO-OFDM system due to the adjacent subcarriers of desired subcarrier have STM effects based on two optical paths and carry same information, as shown in Figure 4.2(a), which overestimates the system performance. For optical loop simulations, the decorrelated subcarriers gives no errors upto $\sigma_\tau/T_S = 6.5\%$. In the case of adjacent subcarriers are correlated then σ_τ/T_S increases to 8.1% (8.1 ps for 100 ps symbol duration). For ScFO case, the odd-and-even and optical loop systems gives data without an error upto $\sigma_\varepsilon T_S = 7.7\%$ and 10%, as shown in Figure 4.8(b). In [33], both systems were investigated and compared experimentally. The subcarrier spacing was increased (as cyclic prefix was suggested) in order to get better results for optical loop. By proper designing of AO-OFDM system considering STM and/or ScFO effects on system performance, as shown in Figure 4.7, we have less requirements of increasing subcarrier spacing or reducing data rate of subcarriers and less desire of large sampling rate at receiver side.

4.4 Methods of Reducing STM and ScFO Effects

4.4.1 Using Cyclic Prefix

In order to reduce the STM and ScFO effects, the easiest solution is to use CP for all subcarriers in AO-OFDM system, but we have to compromise on spectral efficiency and data rate of AO-OFDM system [12]. T_S is related to the subcarrier spacing Δf by $T_S = 1/\Delta f$ in OFDM systems. We have investigated the CP requirements in AO-OFDM system by reducing the data rate or increasing the subcarrier spacing Δf (method of using CP is similar as applied in Section 3.3). With the CP = 30%, the ICI and ISI variances (r_1, and r_3) due to STM are

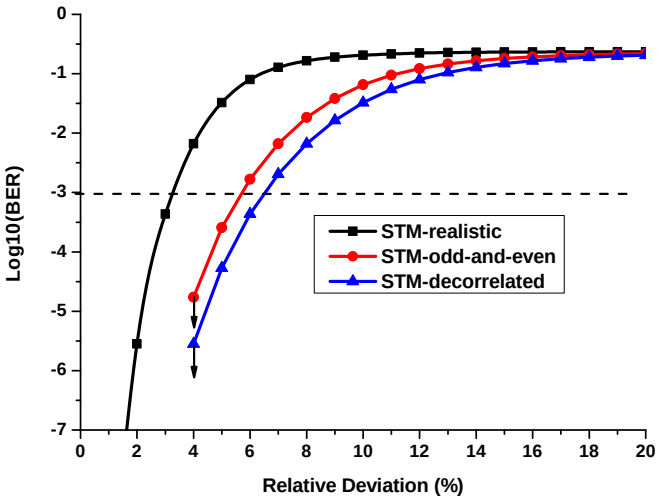

(a)

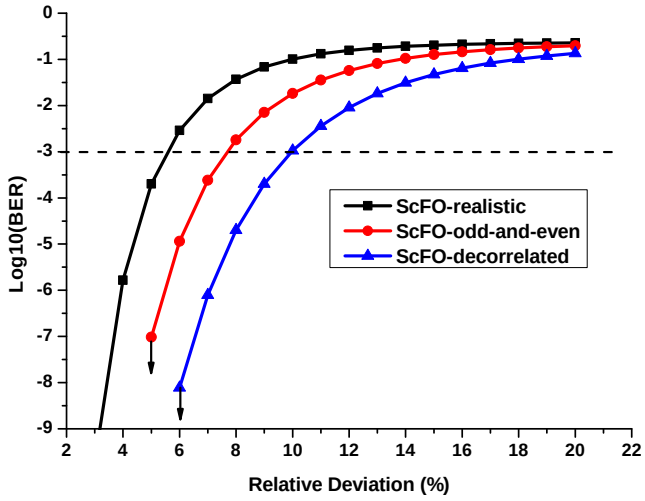

(b)

Figure 4.8: Comparison of BER results versus relative deviation for (a) STM (σ_τ/T_S), and (b) ScFO ($\sigma_\varepsilon T_S$). Downward arrow shows that no data received error upto given relative deviation.

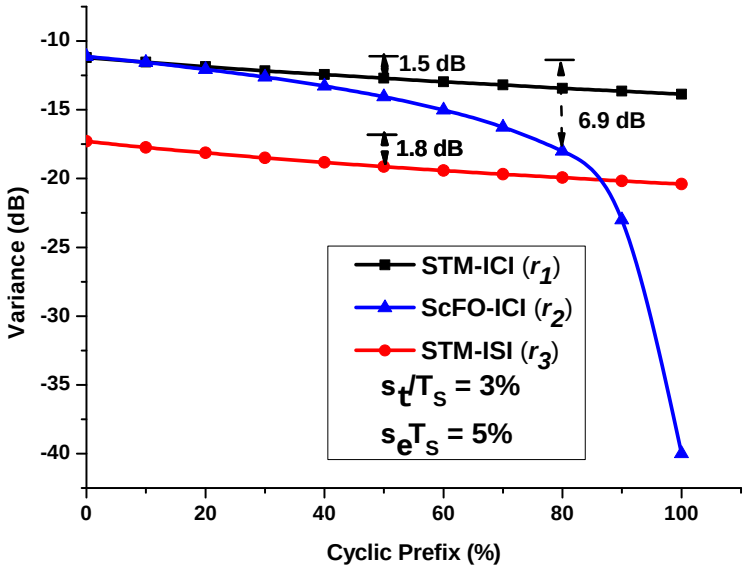

Figure 4.9: CP requirements in presense of STM and ScFO in an AO-OFDM.

reduced by 1 dB and 1.2 dB, while the ICI variance (r_2) due to ScFO is reduced by 1.5 dB, as shown in Figure 4.9. r_1, r_2, and r_3 have same relationships as used in Figure 4.6. The CP = 30% corresponds to increasing T_S from 100 ps to 130 ps or Δf from 10 GHz to 13GHz. It can be seen in Figure 4.9 that by increasing the CP up to 50% gives reduction in r_1, and r_3 to 1.5 dB and 1.8 dB, which causes the data rate is half but the change in variances of ICI and ISI is less than 4 dB. In the ScFO case, r_2 reduces approximately 2 dB at CP = 50% and reduces rapidly from CP = 80% (Δf = 18 GHz). The main reason of rapid reduction in r_2 is the overlapping of adjacent subcarriers with desired subcarrier is minimum, but with the compromise on the spectral efficiency of AO-OFDM system.

4.4.2 Optical Delay Line and Tunable Laser Diode

By using optical delay line (ODL) and tunable laser diode (TLD) for each subcarrier in AO-OFDM system, we can reduce the effects of STM and ScFO. We can use ODL and TLD at either transmitter or at receiver but to avoid the error in ICI measurement at receiver, due to

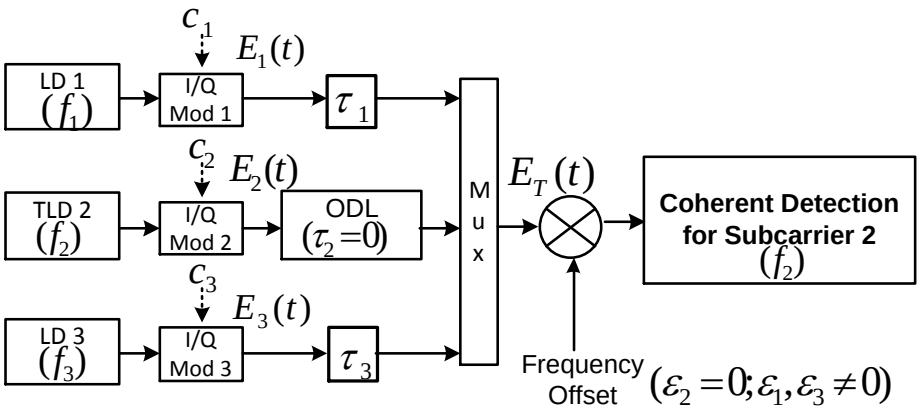

Figure 4.10: Block diagram of optical delay line (ODL) and tunable laser diode (TLD) based STM and ScFO compensation of middle subcarrier.

incorrect estimates of the STM and the ScFO of the adjacent subcarriers, we have used at the transmitter. The block diagram of AO-OFDM system with ODLs and TLDs for middle subcarrier at transmitter is shown in Figure 4.10. We have evaluated the performance of the middle subcarrier in the presence of ICI from adjacent subcarriers. The τ_2 and ε_2 of desired subcarrier are equals to 0, by using ODL and TLD, while adjacent subcarriers have non-zero STM and ScFO values.

With the aligned desired middle subcarrier ($\tau_2 = 0$), the effects of phase offset and the ISI are mitigated and STM tolerance increase from 3.2% to 5.3%. The results of aligned middle subcarrier are compared with system of misaligned all three subcarriers with CP. With the CP = 30%, T_S is increased from 100 ps to 130 ps in all three subcarriers, the tolerance of STM is increased from 3.2% to 4.5%, as shown in Figure 4.11. The ODL based aligned middle subcarrier gives slight increased in tolerance then misaligned subcarriers with CP but gives some interesting finding: 1) For the relative deviation of STM less than or equal to 3%, the tolerance of aligned middle subcarrier is less than misaligned subcarriers with CP, 0.5 dB, due to the ICI is dominated; 2) CP for STM reduction doesn't gives much improvement in BER performance as described in terms of variance of ICI due to STM in Figure 4.11.

In an investigation of ICI due to ScFO in an adjacent subcarriers, the ε_2 between TLD_2 and LO for subcarrier 2 is equal to 0. The ScFO tolerance is increased from 5.5% to 6%.

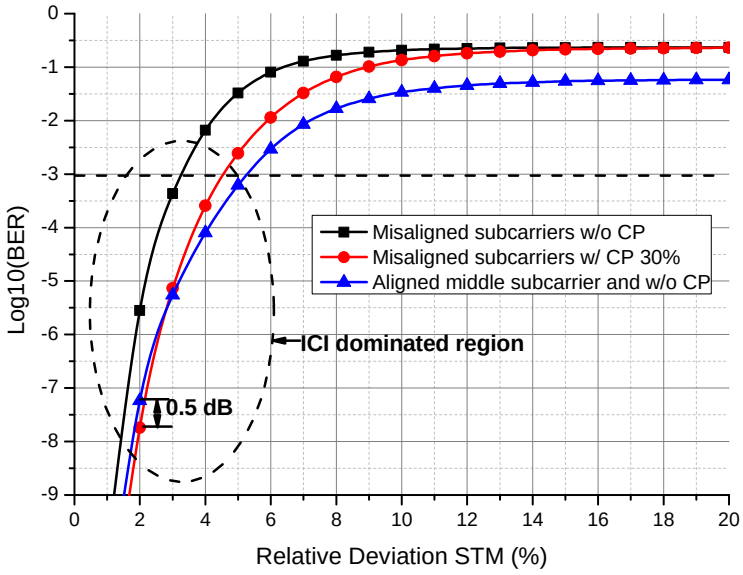

Figure 4.11: optical delay line (ODL) based STM compensation of middle subcarrier.

By comparing this result with three subcarriers have non-zero ScFOs with CP = 30%, the CP provides more tolerance of 7% due to increases in subcarriers spacing which reduces the ICI and the phase offset penalty in desired subcarrier, as shown in Figure 4.12. The difference in BER performances between middle subcarrier compensated and subcarriers with ScFOs and CP is 1.8 dB. The middle subcarrier compensation gives less ScFO tolerance due to phase offset penalty is reduced but ICI still high, and the CP gives better BER performance but at the cost of reduced spectral efficiency. For AO-OFDM system with large N_{SC}, the method of using ODL and TLD for STM and ScFO compensation makes the system design complex.

4.4.3 DLI based ICI suppression

DLI Theory and Operation

A delay line interferometer (DLI) is a passive device that is based on an interference of two optical beams coming from two paths of different lengths. The interference of beams is used to filter/demultiplex the different wavelengths [102]. It can be a Mach-Zehnder interferometer

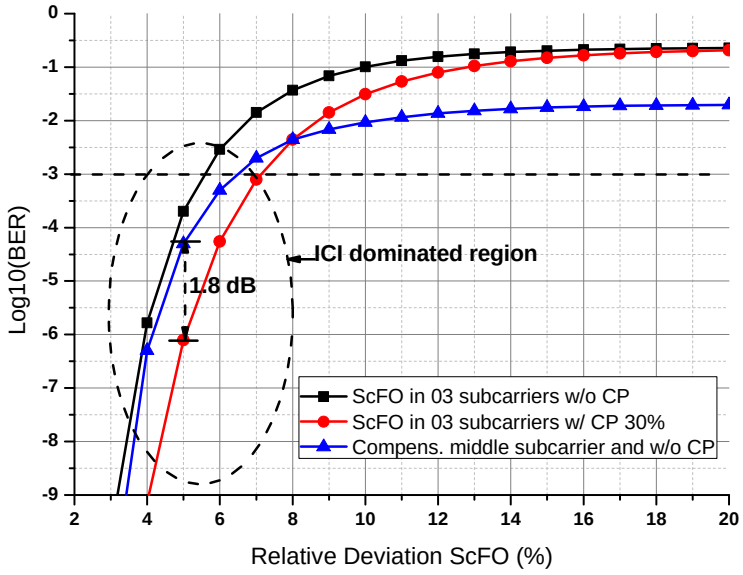

Figure 4.12: TLD based ScFO compensation of middle subcarrier.

(MZI) based or a Michelson interformeter based passive device. The typical construction of a DLI is an integrated optics and it comprises of two 3 dB couplers interconnected by two fibers with different lengths, as shown in Figure 4.13. A DLI is constructed in an integrated optics and the substrate is normally silicon with the silica (SiO_2) material for the waveguide and region of cladding. For the filtering and multiplexing/demultiplexing, MZIs are very useful passive device. In comparison, the other filtering devices like thin-film filters (for narrow band filtering) are better technologies and MZI are much useful for wide band filtering [95]. In our theoretical model, the labels of inputs and outputs of DLI device are given in Table 4.2.

Figure 4.13: Structure of DLI [102].

Table 4.2: DLI Input and Output ports Labels

3 dB Coupler	Port Number	Label
input	1^{st}	E_{in1}
input	2^{nd}	E_{in2}
input	3^{rd}	$\widetilde{E}_{out1}$
input	4^{th}	$\widetilde{E}_{out2}$
output	1^{st}	$\widetilde{E}_{in1}$
output	2^{nd}	$\widetilde{E}_{in2}$
output	3^{rd}	E_{out1}
output	4^{th}	E_{out2}

The input and output of an input lossless 3 dB coupler of the DLI can be given as

$$\begin{bmatrix} \widetilde{E}_{out1} \\ \widetilde{E}_{out2} \end{bmatrix} = \frac{1}{\sqrt{2}} \cdot \begin{bmatrix} 1 & j \\ j & 1 \end{bmatrix} \cdot \begin{bmatrix} E_{in1} \\ E_{in2} \end{bmatrix}. \tag{4.36}$$

Solving the right hand side of above equation, we have

$$\begin{bmatrix} \widetilde{E}_{out1}(t) \\ \widetilde{E}_{out2}(t) \end{bmatrix} = \frac{1}{\sqrt{2}} \cdot \begin{bmatrix} E_{in1}(t) + jE_{in2}(t) \\ jE_{in1}(t) + E_{in2}(t) \end{bmatrix}. \tag{4.37}$$

After incoming signal is equally splitted by input 3dB coupler of the DLI, the signals passes the two fiber of different lengths with delay of symbol duration T_S and we have

$$\begin{bmatrix} \widetilde{E}_{in1}(t) \\ \widetilde{E}_{in2}(t) \end{bmatrix} = \frac{1}{\sqrt{2}} \cdot \begin{bmatrix} E_{in1}(t - T_S) + jE_{in2}(t - T_S) \\ jE_{in1}(t) + E_{in2}(t) \end{bmatrix}. \tag{4.38}$$

The output 3 dB coupler have same input and output relationship as for input 3 dB coupler, and we have output signals at the DLI output ports are given as

$$\begin{bmatrix} E_{out1}(t) \\ E_{out2}(t) \end{bmatrix} = \frac{1}{2}. \begin{bmatrix} E_{in1}(t-T_S) + jE_{in2}(t-T_S) - E_{in1}(t) + jE_{in2}(t) \\ jE_{in1}(t-T_S) - E_{in2}(t-T_S) + jE_{in1}(t) + E_{in2}(t) \end{bmatrix} \tag{4.39}$$

In order to find the optical power of each port of the DLI, we have to take the complex conjugates of output signals of the DLI which are given as

$$P_{out1}(t) = E_{out1}(t).E^*{}_{out1}(t) = P_0 \sin^2\left(\frac{\phi(t-T_S) - \phi(t)}{2}\right) \tag{4.40}$$

and

$$P_{out2}(t) = E_{out2}(t).E^*{}_{out2}(t) = P_0 \cos^2\left(\frac{\phi(t-T_S) - \phi(t)}{2}\right) \tag{4.41}$$

In case of $\phi(t-T_S) - \phi(t)$, the power at port 1 is zero, i.e. $P_{out1}(t)$=0 and only even numbered wavelengths are appeared at port 2. The spectra of both output ports of DLI is shown in Figure 4.14.

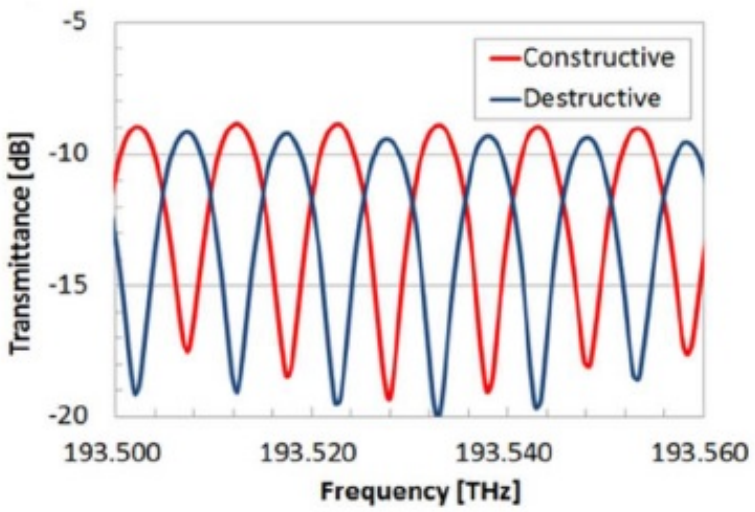

Figure 4.14: Spectra of constructive and destructive ports of DLI [103].

The DLI is used to separate the odd and even subcarriers from received composite AO-

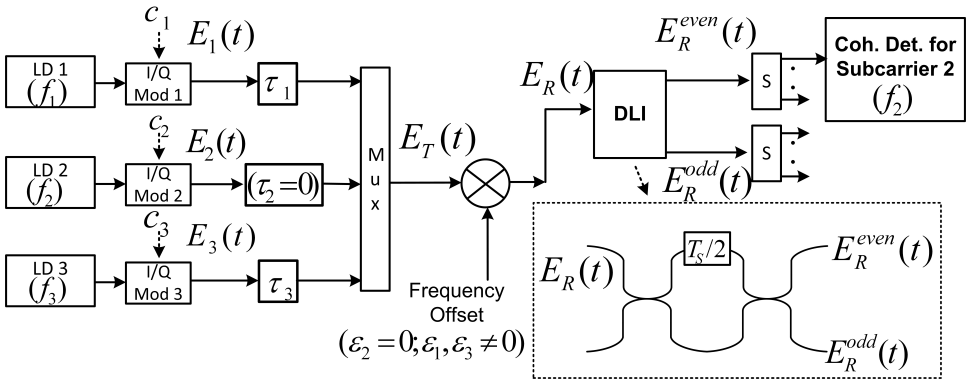

Figure 4.15: Proposed DLI based ICI suppression method in AO-OFDM system. S: splitter.

OFDM signal $E_R(t)$ before coherent detection stage in order to minimize the ICI from adjacent subcarriers caused by STM and ScFO. The advantage of using the DLI based passive method of ICI suppression in an optical domain is to reduce the requirements of DSP based algorithms for ICI suppression. The block diagram of a proposed DLI based ICI suppression is shown in Figure 4.15. In AO-OFDM composite signal $E_T(t)$, the middle desired subcarrier with index $k = 2$ have τ_2 and ε_2 equals to 0, while adjacent subcarriers ($k = 1,3$) have non-zero STM and ScFO values. The main reason of setting adjacent subcarriers with offsets only is to suppress ICI first. The received AO-OFDM signal $E_R(t)$ is first split by an input coupler, and a propagation delay of $T_d = T_S/2$ is introduced in one arm before the signals in two arms are recombined by an output coupler. The electric fields of even, $E_R^{even}(t)$, and odd, $E_R^{odd}(t)$, subcarriers, without STM and ScFO effects, are given as

$$E_R^{even}(t) = \frac{j}{2} \cdot E_R(t)(e^{-j2\pi f_k T_d} + 1), \tag{4.42}$$

and

$$E_R^{odd}(t) = \frac{1}{2} \cdot E_R(t)(e^{-j2\pi f_k T_d} - 1). \tag{4.43}$$

The $E_R^{even}(t)$ contains only even subcarriers and the power of DLI port for even subcarriers ($|E_R^{even}(t)|^2/P_k = [\cos(\pi f_k T_S/2)]^2$) is plotted in Figure 4.16. In the presence of STM and ScFO, the photodetected signals for subcarrier 2 (middle subcarrier) are derived using same

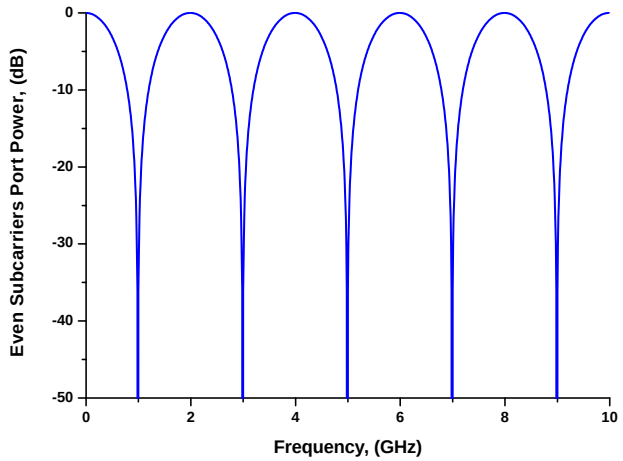

Figure 4.16: Simulated power transmission for even subcarriers at delay line interferometer (DLI) output port.

procedure given in section 4.2 and expression are given as

$$z_{STM-DLI} = \left(\frac{\Re\sqrt{P_R P_{LO}}}{T_S}\right) \times \left[\eta_{STM\_2} \cdot \left(e^{-j\pi f_2 T_S} + 1\right) + \sum_{k\neq 2} \eta_{STM\_ICI} \cdot \left(e^{-j\pi f_k T_S} + 1\right) + \eta_{STM\_ISI} \cdot \left(e^{-j\pi f_2 T_S} + 1\right)\right], \quad (4.44)$$

and

$$z_{ScFO-DLI} = \left(\frac{2\Re\sqrt{P_R P_{LO}}}{T_S}\right) \left[\eta_{ScFO\_2} \cdot \left(e^{-j\pi (f_2+\varepsilon_2) T_S} + 1\right) + \sum_{k\neq 2} \eta_{ScFO\_ICI} \cdot \left(e^{-j\pi (f_k+\varepsilon_k) T_S} + 1\right)\right], \quad (4.45)$$

where η have same relations used in equation (4.16) and in equation (4.31) for subcarrier 2. In equation (4.44) the STM doesn't change the transmission of even and odd subcarriers through the DLI respective port, and equation (4.45) shows that the ScFO change the transmission characteristics of DLI for even and odd subcarriers.

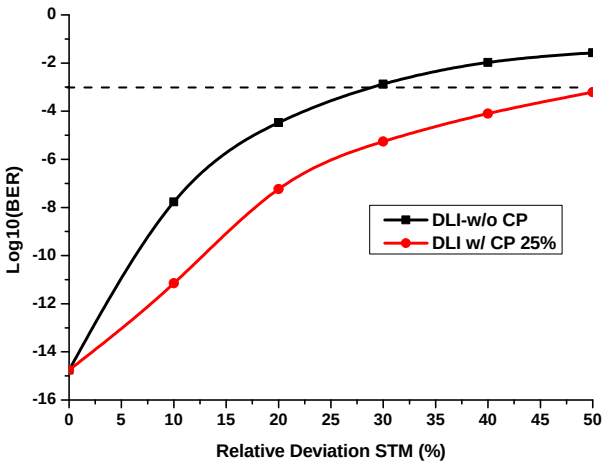

Figure 4.17: DLI based STM-ICI suppression.

STM-ICI suppression

With the DLI, the tolerance to ICI is increased to $\sigma_\tau/T_S = 29\%$, as shown in Figure 4.17. With CP = 20% (T_S increased from 100 ps to 120 ps), which is less than the CP = 50% required in Figure 4.9, the tolerance of σ_τ/T_S is increased to 50%. At $\sigma_\tau/T_S = 50\%$, the symbols are misaligned by $T_S/2$ and at this point the ICI is maximum and normally termed as complete loss of orthogonality [88]. The DLI based STM-ICI suppression provides the more tolerance to σ_τ/T_S with less requirements of CP. With the increase in N_{SC} the design of DLI based passive device for ICI suppression will be same $T_d = T_S/2$.

ScFO-ICI suppression

In AO-OFDM system, the ScFO between free running lasers at transmitter and receiver causes ICI and DLI based ICI suppression increases the $\sigma_\varepsilon T_S$ from 5.5% to 10% without CP, as shown in Figure 4.18. The low tolerance improvement with DLI is due to the DLI ports outputs are dependent on ScFO which prevent the complete cancellation of adjacent subcarriers of desired subcarriers, as derived in Eq. 34. With CP = 15% (Δf increased from 10 GHz to 11.5 GHz), the $\sigma_\varepsilon T_S$ increased to 13%. The ScFO tolerance of 10% with DLI is

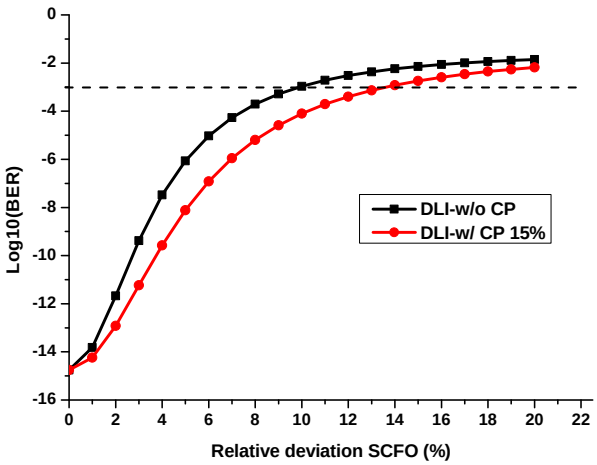

Figure 4.18: DLI based ScFO-ICI suppression.

nearly twice the tolerance of AO-OFDM system without DLI in Figure 4.7. In the presence of ScFO with tolerance of 10% in DLI based AO-OFDM system, the appropriate solution is to use the comb source instead of CW lasers at transmitter. In the comb source, optical subcarriers have same ScFOs and can easily estimated and compensated with single-carrier algorithms [101].

4.5 Summary

In this chapter, we analytically derived M-QAM AO-OFDM system model and compared with numerical simulations. The simulation results show that the orthogonality degrades among subcarriers in the presence of STM and/or ScFO and causes ICI among subcarriers. The results of practical AO-OFDM are compared with the results of odd-and-even and optical loop emulation setups. In practical AO-OFDM model, the modulation sources, modulators and optical paths are considered independent in simulations. In AO-OFDM system model with time and frequency offsets, to keep BER performance below 10^{-3} the relative deviations for STM and ScFO should be lower than 3.2% and 5.5%. With the proposed DLI-based ICI suppression method, the relative deviations for STM and ScFO increase to 29% and 10%

without CP. The STM tolerance improved more than the ScFO tolerance with the proposed method of ICI suppression, and this method is more suitable for AO-OFDM transmitter have optical subcarriers generated from comb source such as MLLD.

Chapter 5

FBG-Assisted ICI Reduction for AO-OFDM Demultiplexed Signal

In Chapter 3 and Chapter 4, we have focused on the time and freqency offsets in the coherently detected received AO-OFDM signal by using local oscillator (LO). In this chapter, the receiver of AO-OFDM signal is an optical discrete fourier transform (O-DFT), which is one of the methods to demultiplex the subcarriers from the received composite AO-OFDM signal [104]. For an N-point O-DFT, a single and compact optical circuit can be utilized to demultiplex all the subcarriers at the same time, as presented in Figure 2.11. Conceptually, an O-DFT circuit comprises of the optical delay lines which are used to convert the incoming serial data stream to parallel data, and the phase shifters are used to perform DFT operation for desired subcarrier. In this concept, the values of the delay lines are same but the values of phase shifters are different for demultiplexing of each subcarrier as per DFT operation explained in Chapter 2. In this chapter, the effects of modulation bandwidth and chromatic dispersion on the performance of AO-OFDM system with O-DFT circuit (optical delay lines and phase shifters) are investigated.

5.1 Optical Discrete Fourier Transform

For the multiplexing and demultiplexing of optical subcarriers, there are several devices for the O-DFT function, such as arrayed waveguide gratings (AWG)[58], coupler-based mesh [104], Mach-Zehnder interferometers (MZI) with phase shifters and couplers [12], and fiber

Bragg gratings (FBG)[54]. The brief details of O-DFT circuits are given here.

5.1.1 Arrayed waveguide gratings

An AWG as WDM demultiplexer and optical codes generation in an optical packet switching and optical code division multiple access (OCDMA) systems, it is utilized with a two star couplers interconnected by arrayed waveguide gratings to produce OFDM symbols (equivalent to OCDMA codes with Fourier coding) [58]. The term of frequency domain is used to define the carriers in OFDM systems are orthogonal in frequency domain. The AWG configuration is shown in Figure 5.1.

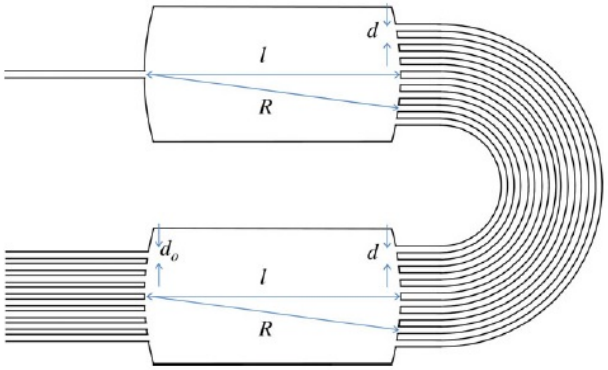

Figure 5.1: Arrayed waveguide gratings schematic [104].

The first star coupler or slab region distributes the incoming optical signal to the array of waveguides. The lengths of interconnecting arrayed waveguides provides an incremental delay of τ = total symbol duration/number of subcarriers in order to perform the serial-to-parallel operation. The second star coupler is designed in such a way that the termination of arrayed waveguides I_m at its input have phase shifts of O_m, as schematic shown in Figure 5.2.

By using an AWG, the DFT operation is in spatial domain which can be equivalent to an imaging system of two-lens system, as shown in Figure 5.2, where a focal length f is equal to a radius of curvature R of the star couplers. In an AWG, the second star coupler performs a DFT operation of inputs from arrayed waveguides. For an AWG based DFT operation, the

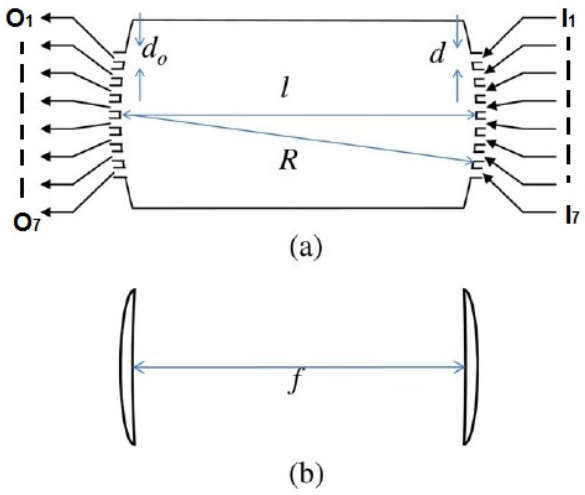

Figure 5.2: Output star coupler of AWG (a) with its equivalent two-lens model[104].

design parameters must satisfy the following condition:

$$d = d_0 = \sqrt{\frac{\lambda R}{N}}, \tag{5.1}$$

where N is number of inputs/outputs, and l is the length of slab which is equal to the radius of curvature R of the star couplers.

5.1.2 Coupler-and-waveguide mesh device

The coupler-and-waveguide mesh (CWM) device comprises of passive optical couplers, waveguides and phase shifters to perform O-DFT operation of an input signal, a_m, to an output signal, b_m, as shown in Figure 5.3(b) [104]. In order to perform N-point DFT with CWM device, $log_2 N$ stages are required with each stage composed of 2×2 optical coupler which is equivalent to the 2-point DFT circuit, as shown in Figure 5.3(a). In order to utilize a CWM device to perform DFT operation in an optical communication system, where the data symbols are transmitted serially, we need a serial-to-parallel converter before a CWM device for a DFT function.

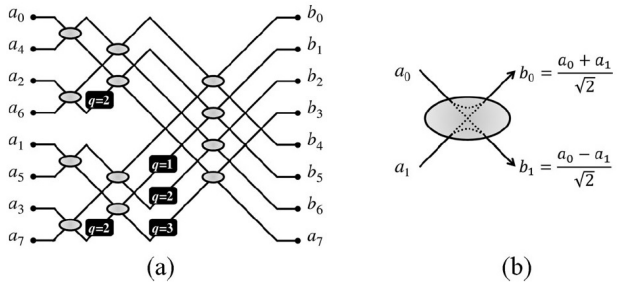

Figure 5.3: Coupler-and-waveguide mech device (a) with its mathematical model (b)[104].

5.1.3 Delay line interferometer with phase shifters

In a CWM based DFT operation, the performance of AO-OFDM system is highly sensitive to phase errors and fabrication errors during design, and with the increase of an order of DFT, a CWM design will be complex [104]. In order to minimize these drawbacks, a novel configuration of MZIs as a time delay array is proposed, as shown in Figure 5.4 [53]. The MZIs are configured in a cascaded or tree architecture in order to demultiplex N subcarriers.

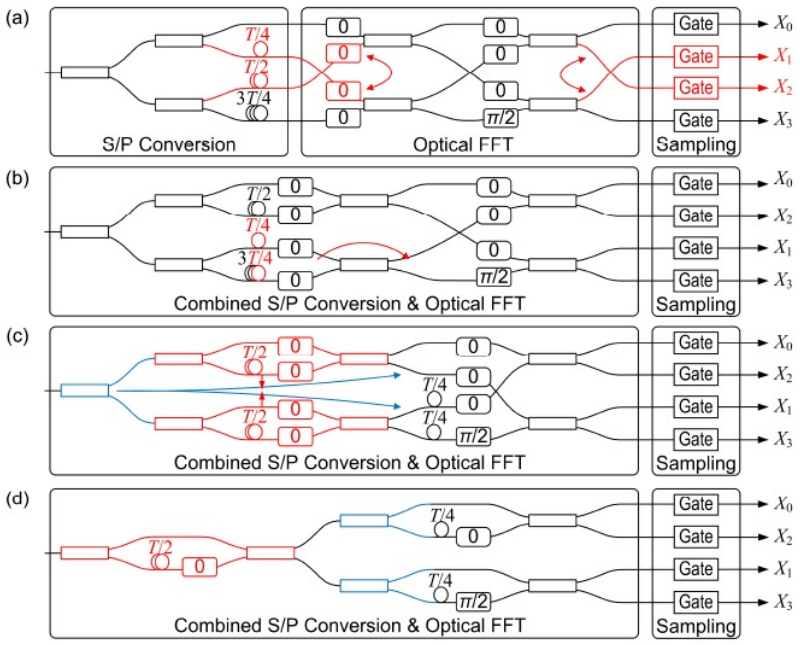

Figure 5.4: Design steps of combined optical DFT and serial-to-parallel Converter; (a) Traditional design, (b)-(c) two DLIs are replaced to one DLI, (d) simple O-DFT design [53]

In Figure 5.4, by re-ordering the delay lines and rearrangement of the output ports of 4-point optical DFT is shown. In step (a), the delays are reordered in a S/P conversion block.

Due to this step the output ports X_1 and X_2 are rearranged. In this way the input stage of an O-DFT circuit consists of two delay paths which have non-equal absolute delays. From step (b) to step (c), the delays of $T/4$ in lower input branch, which are common, are moved to outputs. In step (d), the redundancy of two couplers, $T/2$ delay line, and phase shifter is replaced with one DLI and one coupler. The advantage of this type of O-DFT is small number of couplers, $2(N-1)$, are needed to perform N-point DFT. The transfer function of DLI based O-DFT is given as

$$H_{pm}(\omega) = \underbrace{\frac{1}{\sqrt{2}}\begin{pmatrix} 1 & j \\ j & 1 \end{pmatrix}}_{output\_3dB\_coupler} \cdot \begin{pmatrix} 1 & 0 \\ 0 & e^{-j(\omega T_p+\varphi_m)} \end{pmatrix} \cdot \underbrace{\frac{1}{\sqrt{2}}\begin{pmatrix} 1 & j \\ j & 1 \end{pmatrix}}_{input\_3dB\_coupler} \cdot \underbrace{\begin{pmatrix} 1 & 0 \\ 0 & 0 \end{pmatrix}}_{upper\_input\_isolation}, \quad (5.2)$$

where p, m, T_p, and φ_m, is DLI stage, subcarrier index, interferometer delay, and DLI phase.

5.1.4 Fiber Bragg grating for DFT/IDFT operation

Fiber Bragg grating (FBG) based sampling and processing of ultra-short laser pulses provides all-optical OFDM without the need of sampling gates at a receiver side [54]. In Figure 5.5, the FBGs are shown as O-DFT and O-IDFT modules.

From the ultra-short laser source, the pulse passes through circulator and entered in the FBG device which works as an O-DFT module. The design of the FBG have many subgratings and spatial modulation of the FBG's refractive index is given as

$$\delta n(z) = \sum_{m=0}^{M-1} A(z - mZ_0)\varphi_{km} e^{j\frac{2\pi}{\Lambda}z} + c.c., \quad (5.3)$$

where Λ is the grating period, and Z_0, $A(z)$, and φ_{km} are chip's period, amplitude and phase. The relationship of a pulse entered in the FBG and a reflected signal from the FBG is given as

$$y(t) = x(t) \otimes h(t) = \sum_{m}^{M-1} B(t + m\frac{2n}{c}Z_0)\varphi_{km} \quad (5.4)$$

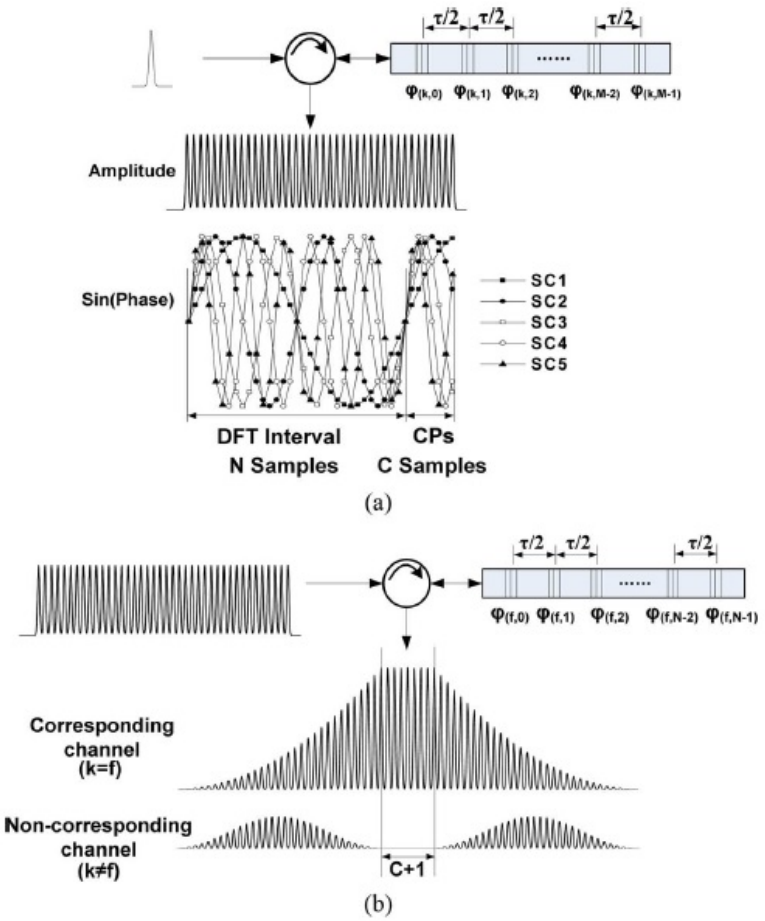

Figure 5.5: FBG designs as (a) O-DFT and (b) O-IDFT modules [54]

where

$$B(t) = 2Kx(t) \otimes \left(A\left(\frac{ct}{2n}\right) \cos\left(\frac{2\pi}{\Lambda}\frac{ct}{2n}\right)\right), \tag{5.5}$$

and

$$h(t) = K\delta n\left(\frac{ct}{2n}\right). \tag{5.6}$$

For the condition that the FBG works as O-DFT and IDFT, the relationship must hold as

$$Z_0 = \frac{cT}{2nM}, \tag{5.7}$$

and

$$\varphi_{km} = e^{-j2\pi mk/M}, \tag{5.8}$$

where m, k, M, and K, is the time sample, the subcarriers index, the total samples in time domain, and the constant. The reflected signal from the FBG have duration equal to OFDM symbol duration which actually contains the multiple copies for input ultra-short pulse with an identical amplitude, and a phase values as per DFT principle. The number of samples in the reflected signal is depends on the number of subgratings in the FBG structure. In Figure 5.5(a), the time-domain waveforms of reflected signals of five subcarriers (SC) show the cycles are integer multiples, as per required principle of OFDM. The O-IDFT at a receiver have same structure of O-DFT at the transmitter, as shown in Figure 5.5(b). The FBG of desired/corresponding SC receives large number of pulses and a reflected signal from desired SC have pulses in middle of OFDM symbol duration while the undesired/non-corresponding FBG have null in the middle. Further, the design of a FBG as O-DFT and O-IDFT for 32 subcarriers is included as an Appendix E.

5.2 Fiber Bragg Grating for ICI Reduction

5.2.1 Theory and Properties

Fiber gratings are passive devices and are produced by an exposition of an optical fiber to an ultraviolet intensity. They are simply an diffraction gratings in an optical domain. Mathematically, the incident light at an angle θ_1 is effected by diffraction grating is given as

$$n \sin \theta_2 = n \sin \theta_1 + m\frac{\lambda}{\Lambda}, \tag{5.9}$$

where θ_2 is a diffracted wave angle and m is an integer which depends on a diffraction order of a wave, as shown in Figure 5.6. This mathematical expression is only useful to find an angle of a diffracted light and a direction of an occurrence of constructive interference, but no information of coupling of modes at a specific wavelength [105].

Fiber gratings have two classes: a Bragg gratings and a transmission gratings. In this

chapter a Bragg gratings are used to reduce the ICI effects in AO-OFDM systems and we focus on theory and operation of a Bragg gratings.

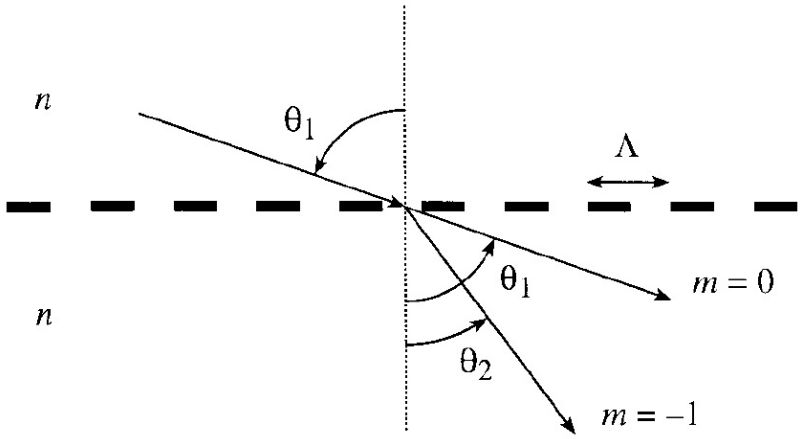

Figure 5.6: Fiber grating as a diffracting device [105].

Fiber Bragg grating (FBG) reflects a narrow band optical field due to index variations. The spatial index perturbation Δn of FBG have length L_{FBG} [105] is

$$\Delta n(z) = \delta n_{eff}(z)\left\{1+\cos(\frac{2\pi}{\Lambda}z)\right\}, \tag{5.10}$$

where Λ, and $\delta n_{eff}(z)$ are nominal period, and refractive index change spatially averaged over a grating period. In Figure 5.7, the reflected mode with θ_2 in $-z$-direction from the FBG is a same as of mode traveling in z-direction with θ_1. The relationship of both modes is θ_2 = -θ_2. The propagation constant of mode is given as

$$\beta = \frac{2\pi}{n_{eff}}, \tag{5.11}$$

where $n_{eff} = n_{core}\sin\theta$. The propagation constant of guided modes is derived as

$$\beta_2 = \beta_1 + m\frac{2\pi}{\Lambda}. \tag{5.12}$$

In single mode fiber, only one mode is dominated and due to reflection from Bragg grat-

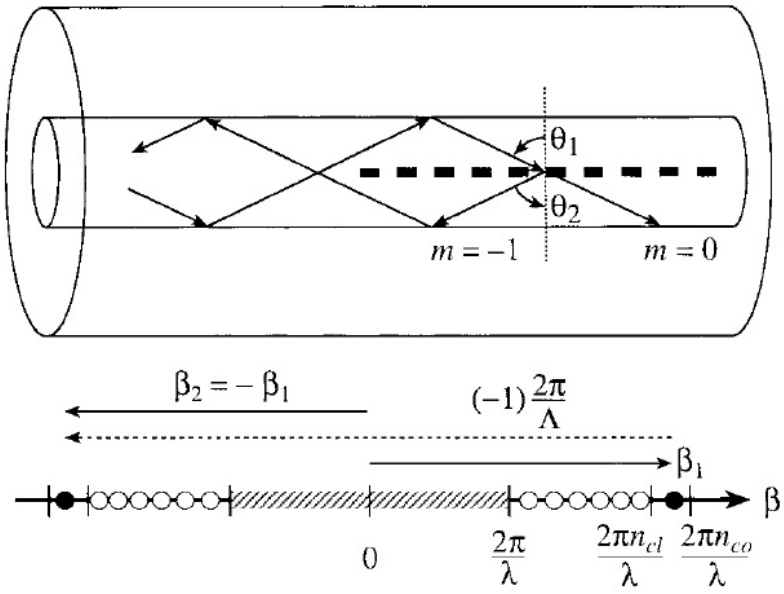

Figure 5.7: Reflected modes illustration in Bragg grating [105]

ing the diffracted mode, *m*=-1, shown on the β axis with solid circles in z and $-z$ directions in Figure 5.7. An effective index, n_{eff} for core modes must have value in range of $n_{cladding} < n_{eff} < n_{core}$. The propagation constant of a reflected mode with β_2 <0, the resonating wavelength reflects for mode of index, $n_{eff,1}$, into mode of index, $n_{eff,2}$ is given as

$$\lambda = (n_{eff,1} + n_{eff,2})\Lambda. \tag{5.13}$$

In case of two identical modes, the above equation becomes the

$$\lambda_B = 2n_{eff}\Lambda. \tag{5.14}$$

The maximum reflectivity, r_{max}, from FBG is related to its length, L_{FBG}, and a coupling coefficient, κ as

$$r_{\max} = \tanh^2(\kappa L) \tag{5.15}$$

5.2.2 Types of Bragg Grating

In this section, common types of Bragg gratings are given which have difference in terms of variation in the index profile along the fiber axis.

Uniform FBG

Uniform Bragg grating have the constant induced index profile (typically, 10^{-5} - 10^{-2}) along the length of grating. The parameters of design uniform FBG in Optigrating Software are given in Table 5.1. In Figure 5.8, the plots of an index profile, with peak index value of 0.0002, and spectrum of an uniform FBG shown. At given parameters, the 3 dB bandwidth ($\Delta\lambda$) of reflected signal from FBG is 0.14 nm. With the increase in δn_{eff} from 0.0001 to 0.0003, the peak index value increases to 0.0006 and 3dB $\Delta\lambda$ increases to 0.4 nm. One way to get the FBG response as a narrowband filter by increase in L_{FBG}. The increase in L_{FBG} from 10000 μm to 15000 μm gives the decrease in $\Delta\lambda$ from 0.14 nm to 0.11nm.

Table 5.1: Parameters of Uniform FBG

Parameter	Value	Unit
grating shape	sine	-
length (L_{FBG})	10000	μm
center wavelength (λ)	1550.0873	nm
index modulation (δn_{eff})	0.0001	-

Chirped FBG

In a chirped FBG (C-FBG), the grating period is monotonically varies along its length, as shown in Figure 5.9. The chirped is introduced axially varying either the grating period Λ or the index of core, n_{core}, or both. The main application of C-FBGs is dispersion compensation

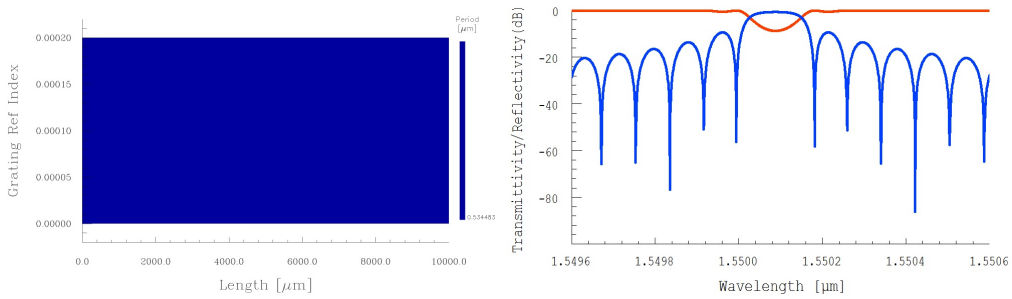

(a) (b)

Figure 5.8: Uniform FBG (a) refractive index profile and (b) transmitted (red) and reflected (blue) signal spectrum

for compression of incoming signal pulse in time domain [102]. A pulse in time domain have wide spectrum, λ_{broad}, and small Λ along C-FBG reflect short wavelength, λ_{short}, and large Λ reflect long wavelength, λ_{short}. The parameters of design C-FBG in Optigrating software are given in Table 5.2. With the given configuration, the 3 dB $\Delta\lambda$ is 3.6 dB to cover the red and blue regions of profile of C-FBG, as shown in Figure 5.10.

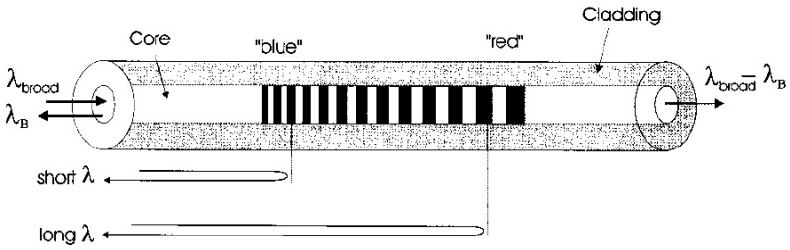

Figure 5.9: Chriped grating structure [106]

Series FBGs as WDM filter

Multiple uniform FBGs in a series configuration can be used in WDM system as a multi-channel filter. The simulated WDM filter have parameter given in Table 5.3. The reflected signal from each FBG have 3 dB $\Delta\lambda = 0.22$nm, as shown in Figure 5.11. The main application of WDM filter is for optical add-drop multiplexer [102].

Table 5.2: Parameters of Chirped FBG

Parameter	Value	Unit
period chirp (total chirp)	linear (2)	nm
length (L_{FBG})	50000	μm
center wavelength (λ)	1550	nm
index modulation (δn_{eff})	0.0006	-

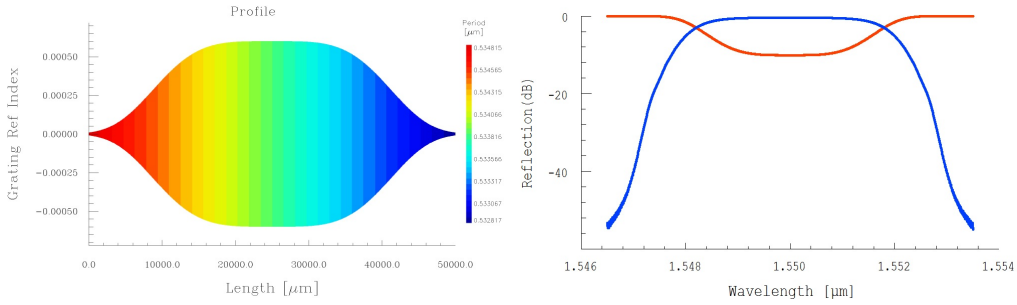

(a) (b)

Figure 5.10: Chirped FBG (a) refractive index profile and (b) transmitted (red) and reflected (blue) signal spectrum.

5.3 Problem Statement

In Figure 5.12(a), the block diagram of serial-to-parallel converter (SP) and N-point DFT with optical sampler (derived with a clock signal) is shown. The received composite AO-OFDM signal is first split at point S into N optical paths and each optical signal is delayed (by an optical delay lines) and phase shifted with multiples of

$$\tau_{SP} = T_S/N$$

and

$$\phi = e^{-j2\pi mn/N},$$

Table 5.3: Parameters of FBGs based WDM filter

Parameter	Value	Unit
index profile and number of FBGs	uniform and 4	-
total length (L)	80000	μm
index modulation (δn_{eff})	0.0004	-

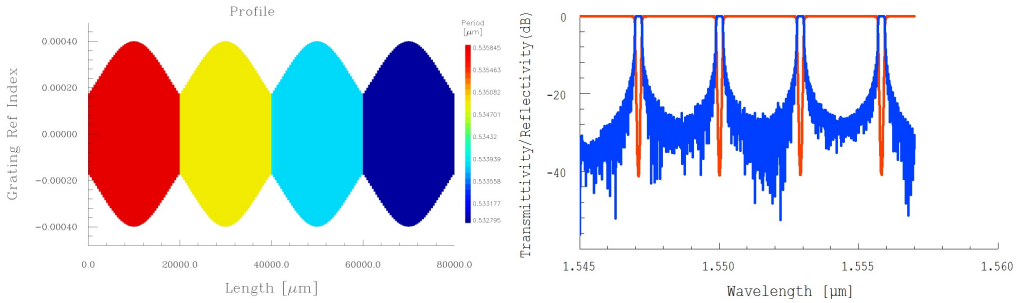

(a) (b)

Figure 5.11: Schematic of series FBG as WDM filter (a) refractive index profile and (b) transmitted (red) and reflected (blue) signal spectrum.

where T_S is the symbol duration, m is sample on DFT circuit path and n is the index of demultiplexed subcarrier. The delayed and phase shifted optical signals are combined at point C and the duration of symbol at point C increased (due to SP conversion) to $2T_S - \tau_{SP}$ contains ICI and ICI-free regions. Main reason of combining the delayed and phased shifted optical signals is to add all the time samples in N paths as per DFT expression for k^{th} subcarrier given as equation (2.4) in Chapter 2. At point C, the constructive interference of delayed optical signals of desired subcarrier gives highest power within duration τ_{SP} (due to SP conversion) while $N-1$ undesired subcarriers have null power [12]. This duration of τ_{SP} is commonly known as ICI-free region. In order to avoid ICI, an optical sampling gate (SG) is required to sample each demultiplexed subcarrier available in a narrow interval of duration τ_{SP}.

The graphical interpretation of modulation bandwidth and chromatic dispersion (CD) effects on the delayed and phase shifted optical signals in the DFT circuit paths (m) and on

the sampled demultiplexed signal at points 1 and 2 are shown in Figure 5.12(b) and Figure 5.12(c). In an ideal case, modulation bandwidth (f_{m-bw}) is infinite (the values of 10-90% of rise time (t_{rise}) and fall time (t_{fall}) of the modulated symbol are equal to 0), and the symbol caused no delay due to CD. The 3 dB modulation bandwidth is related to t_{rise} by

$$f_{m-bw} = \frac{1}{2\pi t_{rise}}.$$

The ICI-free region can be sampled with a SG having sampling instant in the center of demultiplexed signal, as shown in Figure 5.12(b). In a practical case where f_{m-bw} is limited and symbols are delayed due to CD, the ICI free region is narrowed and shifted in time domain. The durations of received symbol of k^{th} subcarrier and ICI-free region of demultiplexed k^{th} subcarrier are reduced to $T_S' = T_S - t_{rise} - t_{fall}$ and $\tau_{SP}' = \tau_{SP} - t_{rise} - t_{fall}$. The shifted and narrowed ICI-free window causes AO-OFDM system performance degradation due to the clock sampling position/instant does not coincide with the ICI-free region. To overcome the shifting problem in the presence of CD, a SG is needed to be tunable which have tunable sampling instant [104]. In AO-OFDM system, the number of subcarriers are normally greater than 100 and to sample each demultiplexed subcarrier a same number of tunable SGs are needed [12]. Furthermore, for a wider interval of ICI-free region, cyclic prefix (CP) is used by increasing symbol duration at the AO-OFDM transmitter in order to broaden the window of ICI-free region. The CP gives tolerance to CD but at a cost of reduced data transmission rate. In this chapter, we theoretically evaluate performance of AO-OFDM system with FBG-assisted ICI reduction in the demultiplexed subcarrier and compare with existing method of SG.

5.4 AO-OFDM System Model Description

In AO-OFDM system model N_{SC} optical subcarriers from CW laser diodes LD_k are modulated with independent data sources A_k, as shown in Figure 5.13. k is subcarrier index from 1

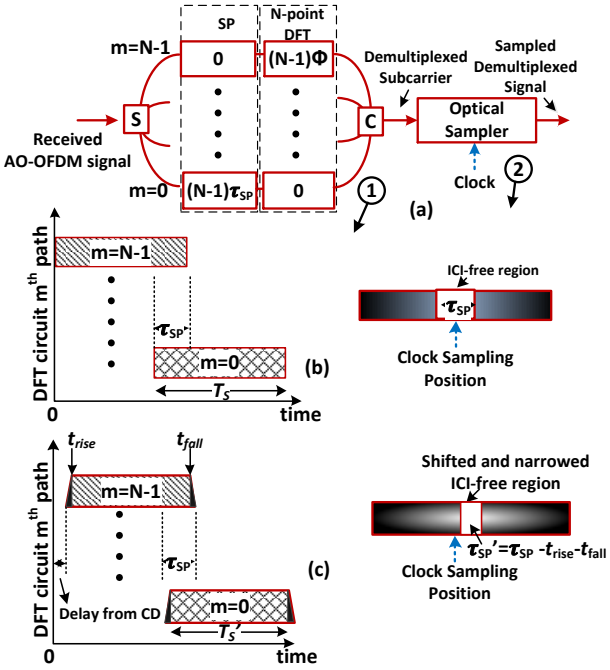

Figure 5.12: (a) Block diagram of subcarrier demultiplexing by O-DFT and sampling at the receiver in AO-OFDM, and graphical interpretation of delayed and phase shifted signals in DFT circuit paths (m) and sampled subcarrier at points 1 and 2 in (b) ideal and (c) practical cases. SP: serial-to-parallel converter.

to N_{SC}. After modulation, electric field of the k^{th} optical subcarrier is

$$E_k(t) = A_k\sqrt{P_k}h_k(t)e^{jk\omega_1 t}, \tag{5.16}$$

where A_k, $h_k(t)$ and P_k are modulated data symbol, rectangular pulse shape of duration T_S and optical subcarrier power at a given frequency $k\omega_1$ of k^{th} subcarrier. The k^{th} subcarrier is combined with $N_{SC}-1$ subcarriers by combiner (or WDM Mux), with no guard bands, to transmit AO-OFDM signal which is given as

$$E_T(t) = \sum_{k=1}^{N_{SC}} A_k\sqrt{P_k}h_k(t)e^{jk\omega_1 t}. \tag{5.17}$$

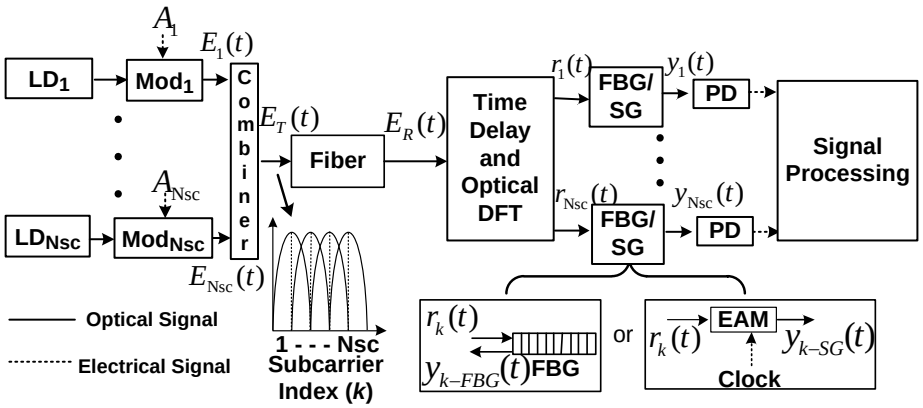

Figure 5.13: AO-OFDM system (with O-DFT) and optical sampling by using fiber Bragg grating (FBG) or electro-absorption modulator (EAM) based optical gate. LD: laser diode; WDM Mux:wavelength division multiplexer; OS: optical sampler; PD: photo detector.

In the frequency domain, transmitted signal E_T can be expressed as

$$E_T(\omega) = 2\pi \sum_{k=1}^{N_{SC}} A_k \sqrt{P_k} H_k(\omega - k\omega_1). \tag{5.18}$$

At the receiver side, the DFT of composite signal is performed to demultiplex the desired subcarrier (phase shifter are set to demultiplex target subcarrier) and the transfer function of DFT for the n^{th} subcarrier [104] is

$$D_n(\omega) = \frac{1}{N} \sum_{m=0}^{N-1} e^{jm\tau_{SP}(\omega - n\Delta)}, \tag{5.19}$$

where τ_{SP}, m, n, N, and $n\Delta = \frac{2\pi n}{N\tau}$ are time delay for serial-to-parallel conversion, DFT circuit path index, desired subcarrier index, total samples in symbol duration, and phase shift for desired demultiplexed subcarrier. Multiplying $E_T(\omega)$ and $D_n(\omega)$ gives $R_{k,n}(\omega) = E_T(\omega)D_n(\omega)$ and the time-domain expression of demultiplexed signal, $r_{k,n}(t) = \mathscr{F}^{-1}R_{k,n}(\omega)$, is written as

$$r_{k,n}(t) = \frac{2\pi}{N} A_k \sqrt{P_k} e^{jk\omega_1 t} \sum_{m=0}^{N-1} e^{j2\pi m(k-n)/N} h_k(t + m\tau_{SP}), \tag{5.20}$$

For a target demultiplexed subcarrier, i.e. $k = n$, equation (5.20) can be written as

$$r_{k,k}(t) = \frac{2\pi}{N} A_k \sqrt{P_k} e^{jk\omega_1 t} \sum_{m=0}^{N-1} h_k(t + m\tau_{SP}). \tag{5.21}$$

5.4.1 Designs of Optical Samplers

In an optical sampling, a sampling gate (SG) based on an electro-absorption modulator (EAM) is used to sample the demultiplexed subcarrier in an ICI-free window, as shown in Figure 5.13. It is driven by electrical clock signal with duty cycle,

$$D_{SG} = \tau_{SG}/T_S, \tag{5.22}$$

where τ_{SG} is a SG sampling time. The SG have sampling function, $h_{SG}(t)$, equals to 1 for t$\leq |\tau_{SG}/2|$ interval, and otherwise is 0.

In the design of FBG, impulse response can be found by using the scaling factor $t = \frac{2n_{eff}\, z}{c}$ for the conversion from spatial- to time-domain, where n_{eff} and c are effective index of grating and speed of light. The scaling factor is commonly used for a low reflectivity or weak FBG. The impulse response of FBG [107] is derived from equation (5.10) is given as

$$h_{FBG}(t) = \Delta n(\frac{ct}{2n_{eff}}). \tag{5.23}$$

For the ICI reduction in the demultiplexed subcarrier, L_{FBG} and bandwidth ($\Delta\lambda$) are related to the FBG interval τ_{FBG} as

$$L_{FBG} = \frac{c\tau_{FBG}}{2n_{eff}} \tag{5.24}$$

and

$$\Delta\lambda = \frac{\lambda^2}{c\tau_{FBG}}, \tag{5.25}$$

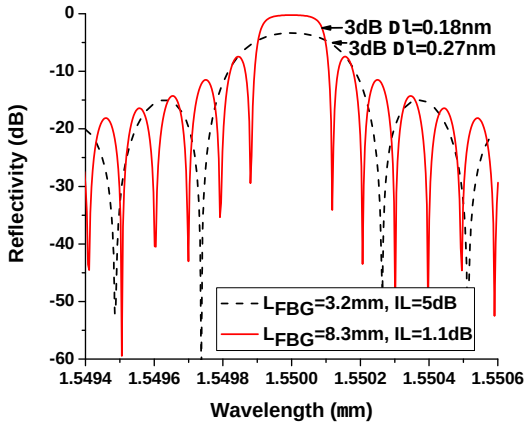

Figure 5.14: Reflection spectra (dB) versus wavelength (μm) for uniform profile FBGs of lengths, L_{FBG}, 3.2 mm (dashed line) and 8.3 mm (solid line).

where λ is wavelength of subcarrier. The $\Delta\lambda$ is derived for weak FBG have relation [105]

$$\frac{\Delta\lambda}{\lambda} = \frac{\lambda}{2n_{eff}L_{FBG}}. \tag{5.26}$$

To evaluate FBG performance in the presence of an ICI, L_{FBG} values from 1.2 mm to 8.3 mm are considered. The reflectivity of designed uniform FBG of rectangular index envelope with L_{FBG} = 3.2 mm and 8.3 mm for an ICI reduction in AO-OFDM system are shown in Figure 5.14. With the increase in τ_{FBG} designed for subcarrier at λ = 1.55μm, the 3 dB bandwidth ($\Delta\lambda$) of reflected signal, and the insertion loss decreases from 0.27 nm to 0.18 nm and 5 dB to 1.1 dB, and reflectivity increases from -3.34 dB to -0.23 dB. The increase in reflectivity for τ_{FBG} = 8.3 mm due to more reflected signal in a given symbol duration.

5.4.2 Chromatic Dispersion

The impulse response and transfer function of CD are given as [53, 94]

$$h_{CD}(t) = \sqrt{\frac{jc}{D\lambda^2 d}} e^{-j\frac{\pi c}{D\lambda^2 d}t^2}, \tag{5.27}$$

and

$$H_{CD}(\omega) = e^{j\frac{D\lambda^2 d}{4\pi c}\omega^2}, \tag{5.28}$$

where D, d, and λ are CD coefficient, length of fiber, and wavelength. For FBG, convolving equation (5.21), (5.23), and (5.28), we have received signal for the k^{th} subcarrier as

$$y_{k-FBG}(t) = r_{k,k}(t) * h_{CD}(t) * h_{FBG}(t), \tag{5.29}$$

and for SG case, convolution of equation (5.21) and (5.28) is multiplied with $h_{SG}(t)$ for k^{th} subcarrier which is as follows,

$$y_{k-SG}(t) = [r_{k,k}(t) * h_{CD}(t)] \cdot h_{SG}(t), \tag{5.30}$$

where $*$ is convolution operator. Mathematically, the incoming signal is convolve with the transfer function of FBG and multiply with the transfer function of SG.

5.4.3 Bit Error Rate Expression

The desired middle subcarrier $y_2(t)$ from SG or FBG is photo detected for bit 1, I_1, and is given as

$$I_1 = \Re \left| y_2(t) + \sum_{k \neq 2} y_k(t) \right|^2, \tag{5.31}$$

and after expanding I_1 is given as

$$I_1 = \frac{\Re}{T_S}[\underbrace{\int_0^{T_S} |y_2(t)|^2\,dt}_{\eta_d} + \underbrace{\int_0^{T_S} \sum_{k\neq 2} |y_k(t)|^2\,dt}_{\eta_{xtalk}} + \underbrace{2\int_0^{T_S} \sum_{k\neq 2} y_2(t)y_k(t)\cdot cos(\phi_2(t)-\phi_k(t))dt}_{\eta_{d\_xtalk}} + \underbrace{\int_0^{T_S} (\eta_{1-3}+\eta_{1-4}+\eta_{3-4})dt}_{\eta_{xtalk\_xtalk}}], \quad (5.32)$$

where η_{1-3}, η_{1-4}, and η_{3-4} is equal to $2y_1(t)y_3(t)\cdot cos(\phi_1(t)-\phi_3(t))$, $2y_1(t)y_4(t)\cdot cos(\phi_1(t)-\phi_4(t))$, and $2y_3(t)y_4(t)\cdot cos(\phi_3(t)-\phi_4(t))$, and $\phi_k(t)$ is phase of k^{th} subcarrier in equation (5.29) or (5.30). The photo detected current for bit 0, I_0, contains only the crosstalk terms $(\eta_{xtalk}, \eta_{xtalk\_xtalk})$. The SNR and BER expressions for AO-OFDM system with SG or FBG are given as

$$SNR = \frac{\eta_d}{|\eta_{d\_xtalk}| + 2|\eta_{xtalk}| + 2|\eta_{xtalk\_xtalk}| + \sigma_{sh}^2 + \sigma_{th}^2}, \quad (5.33)$$

and $BER = \frac{1}{2}erfc(\sqrt{SNR/2})$, where σ_{sh}^2 , and σ_{th}^2 is shot noise and thermal noise modeled in BER calculations for bit 1 and bit 0.

5.5 Performance Analysis of AO-OFDM System

5.5.1 Details of Calculations

In AO-OFDM system, the performance of desired demultiplexed subcarrier is degraded due to ICI from adjacent subcarriers [104]. The number of adjacent subcarriers contribution in ICI depends on bandwidth (window) of photodetector at receiver side. In our performance analysis of SG and FBG, the received AO-OFDM composite signal contains 4 subcarriers and to demultiplex desired subcarrier the 4-point DFT is used. In the simulations, the electrical

NRZ signal composed of a pseudo-random bit sequence (PRBS 2^{10}-1) at 10 Gbit/s is used. The optical delay lines for SP conversion have $\tau_{SP} = T_S/4$ which is required for 4-point DFT operation. To evaluate optimum intervals for SG and FBG (with $\delta n_{eff} = 0.0001$), system performance versus D_{SG} and L_{FBG} are evaluated for $t_{rise} = \{5, 10, 15\}$ ps without CD effects. The simulation parameters are listed in Table 5.4.

Table 5.4: FBG-Assisted AO-OFDM System Simulation parameters

Parameter	Value	Unit
symbol duration (T_S)	0.1	ns
transmitted k^{th}subcarrier power (P_k)	1	mW
fiber chromatic dispersion (D)	16.75	ps/nm/km
k^{th} subcarrier wavelength (λ_k)	1550, 1550.08, 1550.16, 1550.24	nm
symbol rise time (t_{rise})	5, 10, 15	ps
index modulation (δn_{eff})	0.0001	-
bandwidth of photodetector (BW_{RX})	40	GHz

5.5.2 Optimum Sampling Windows with Modulation Bandwidth Limitations and without CD

For an optimum interval of a SG, D_{SG} is varied from 5% to 80% based on τ_{SG} = 5 ps to 80 ps. For t_{rise} = 5 ps, the optimum required $D_{SG-optimum}$ value is 22% with a minimum BER = 10^{-28}, and at this value τ_{SG} is smaller than τ_{SP} due to t_{rise} reduced the ICI-free region, as shown in Figure 5.15(a). The curves in Figure 5.15(a) shows some trends for different values of D_{SG}. D_{SG} values below optimum value gives worse performance due to small optical signal is sampled although ICI level is low, and D_{SG} values above optimum value

gives poor performance due to ICI is also sampled with desired subcarrier. In t_{rise} = 10 ps and 15 ps cases, the optimum required $D_{SG-optimum}$ values are reduced to 17% and 13% due to narrowed ICI-free window, and BER increases to 10^{-19} and 10^{-12}.

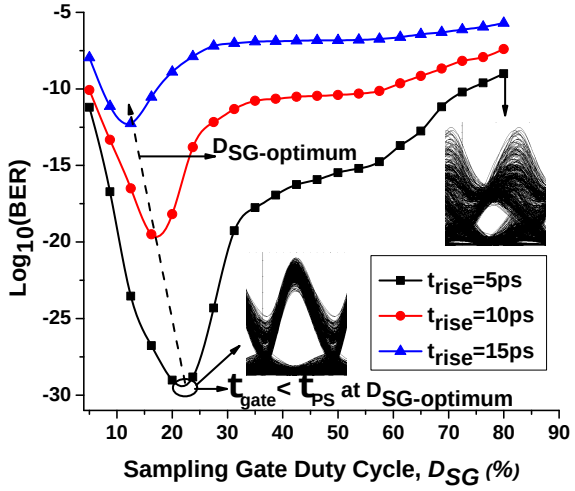

(a)

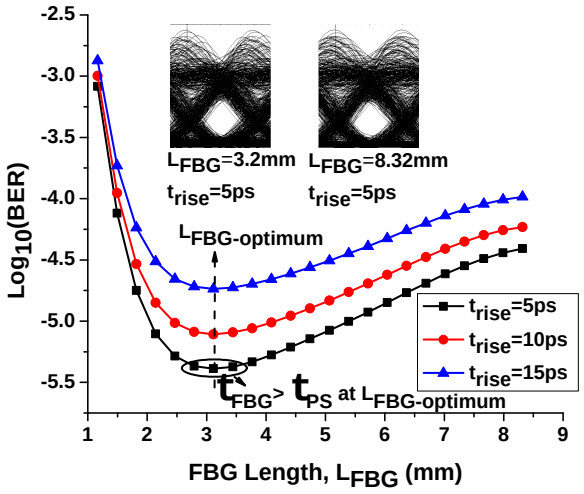

(b)

Figure 5.15: BER performances of (a) optical gate (SG) and (b) fiber Bragg grating (FBG), for t_{rise} = {5, 10, 15}ps and without CD effects.

In a FBG-assisted ICI reduction method, L_{FBG} is varied from 1.2 mm to 8.3 mm corresponding to τ_{FBG} = 11.6 ps to 80.2 ps. For different t_{rise} values, the optimum required

$L_{FBG-optimum}$ values are 3.2 mm and it is same for all three cases of t_{rise}, as shown in Figure 5.15(b). Increasing t_{rise} degrades the BER performance of AO-OFDM system but it does need the FBG to alter its length L_{FBG} in order to get $L_{FBG-optimum}$ value. By comparing the eye diagrams in Figure 5.15(a) and Figure 5.15(b), a timing jitter exist in SG and FBG cases in back-to-back configurations. With the increase in D_{SG} the sampling time at the middle of symbol duration changes, while with the increase in L_{FBG} the eye-opening remains same for FBG case. In AO-OFDM system, the phase errors in an O-DFT operation causes loss of orthogonality and needed to be under tolerable limits to preserve orthogonality among subcarriers [101, 108], as described in Chapter 2.

5.5.3 Effects of Chromatic Dispersion

In the evaluation of CD effects on SG and FBG performances, the values of t_{rise} and t_{fall} are considered to be much less than τ_{SP} in order to maintain orthogonality [53, 104]. In an AO-OFDM system with T_S = 0.1 ns, the values of t_{rise} and t_{fall} are 5 ps ($< \tau_{SP}$ = 25 ps) are considered and corresponding 3 dB modulation bandwidth is 32 GHz which is higher than 10 GHz bandwidth of modulating signal (A_k).

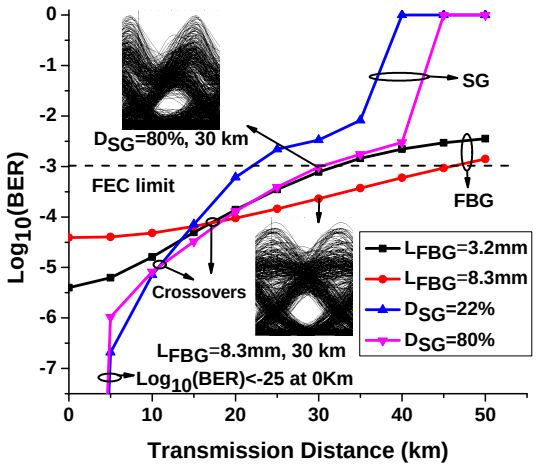

Figure 5.16: BER performances of sampling gate (SG) and fiber Bragg grating (FBG) transmission distance for middle subcarrier λ_2 at t_{rise}=5ps.

The SG with D_{SG} = 22% in AO-OFDM system, the BER in back-to-back case is very low, i.e. $< 10^{-25}$. With the increase in transmission distance (with CD) the BER of the system increases rapidly, as shown in Figure 5.16. The maximum transmission distance with D_{SG} = 22% is 23 km with BER$< 10^{-3}$ for middle subcarrier 2 at λ_2 = 1550.08 nm. The reason of rapid increase in BER is the shifting of ICI-free region and broadening of ICI due to CD. The ICI from $N_{SC} - 1$ subcarriers broaden which causes an incomplete cancellation of ICI at clock sampling position/instant. To keep BER$< 10^{-3}$ for SG with D_{SG} = 22%, tuning of sampling instant is required. When the SG with D_{SG} = 80% is used, the transmission distance is increased from 23 km to 30 km with BER$< 10^{-3}$. The improvement is because the sampling gate with large duty cycle is able to cover the ICI-free region even though it is shifted.

The FBG of L_{FBG} = 3.2 mm is able to support middle subcarrier 2 to transmit up to 30 km with the BER performance $< 10^{-3}$, as shown in Figure 5.16. The FBG of 8.3 mm, provides a large interval is able to support the transmission up to 45km with BER$< 10^{-3}$, because the increment in L_{FBG} leads to more reflected signal in a given symbol duration. Details of FBG length and its relationship with reflected signal is given in Section 5.2.

In our simulations, we investigated the sampling gate by increase in sampling window from 25% to 90%. We have chosen the sampling window of 90% which is less than symbol duration of 100 ps in order to minimize the effects of residual modulation of the subcarriers at symbol boundaries. With sampling gate of duty cycle 90%, the transmission distance is increased from 20 to 30 km with BER$< 10^{-3}$.

By comparing the performances of both optical methods for ICI reduction, the CD causes a shifting of the ICI-free region and the SGs are required to be synchronized/tuned with the shifting of ICI-free region. For synchronization of sampling instant with ICI-free region, complex tuning circuits are required in the SGs. In contrast, FBG is a passive optical device which does not have any issues of tuning interval for ICI reduction in the demultiplexed subcarrier in an AO-OFDM system.

In Figure 5.16, there are two crossovers where BER performance of narrow interval device (SG or FBG) crosses the BER performance of wide interval device (SG or FBG). The crossovers are points where BER of narrow interval device increases rapidly and have worse performance than wide interval device. The reason of increase in BER of narrow interval device is the delay caused by CD which shifts the ICI free region from sampling instant. For SG, the crossover occurred at 10 km while for FBG the crossover occurred at 17 km.

We have further evaluated and compared the BER performances of both ICI reduction methods for four subcarriers. In the case of edge subcarriers 1 and 4 at λ_1 = 1550 nm and λ_4 = 1550.24 nm, the FBG of length 8 mm performs better than SG and gives a maximum transmission distance of 50 km with BER$< 10^{-4}$, as shown in Figure 5.17. The middle subcarriers λ_2 and λ_3 shows the better performance in FBG than SG based sampling, and have BER = 10^{-3} at transmission distance $<$ 45 km. The difference in BER performances of edge (λ_1 and λ_4) and middle (λ_2 and λ_3) subcarriers are due to ICI from one/two interferers (subcarriers) to edge/middle subcarriers.

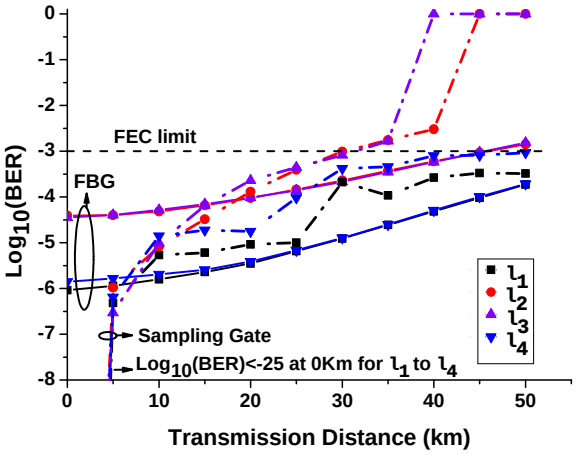

Figure 5.17: Comparison of BER performances of FBG (length 8.3mm, solid lines) and SG (duty cycle 80%, dash-dotted lines) versus transmission distance of four demultiplexed subcarriers.

5.6 Summary

In this chapter, the advantages of O-DFT device based subcarriers demultiplexing are presented and the performance degradation issues are highlighted with consideration of the CD and modulation bandwidth effects. The performance of FBG-assisted ICI reduction is compared with the existing method of optical sampling. Increase in symbol rise times requires the reduced intervals of the SG but the length of FBG remains same. The rise time of 5 ps (total symbol duration 100 ps) and the presence of delay due to CD, the BER performance of FBG is better than that of SG, especially for the transmission distance above 30 km. In the case of middle subcarriers (two adjacent subcarriers), FBG gives BER $< 10^{-3}$ for 45 km. In AO-OFDM system with FBG based passive device, synchronization between the ICI-free region and sampling instant is not needed, which omitting complex tuning circuits and reducing the system cost, and the CP is not required due to tolerance to CD increased.

Chapter 6

Conclusions and Future Works

In this thesis, the performance of OOK-modulated AO-OFDM system with a data rate of 10 Gbit/sec is theoretically evaluated in the presence of symbol time misalignment and subcarrier frequency offset. The performance is evaluated for spectral-efficient AO-OFDM systems which typically use 10 Gbaud M-QAM modulation format for optical subcarriers transmissions. In the presence of chromatic dispersion and limited modulation bandwidth, the synchronization issues in the demultiplexed subcarriers after O-DFT in AO-OFDM system are also discussed.

6.1 Time and Frequency Offsets in OOK AO-OFDM System

In the presence of symbol timing and subcarrier frequency offsets, the overall system performance degrades. Due to limited resources and cost, an odd-and-even and a decorrelated systems are commonly used in experiments to evaluate the performance of AO-OFDM systems. In Section 3.2, we presented the analytical model of OOK-modulated AO-OFDM system (AO-OFDM transmitter and coherent detection) with 10 Gbit/sec data rate. The performance of AO-OFDM system is evaluated for the two cases. In the case I, the numbers of subcarriers are from 8 to 512 with receiver bandwidths 30 GHz and 50 GHz. In the case II, we focused on 3 and 5 number of subcarrier for receiver bandwidths of 30 GHz and 50 GHz. In both studies, the tolerance of subcarrier frequency offset is higher than the symbol time misalignment. In AO-OFDM system with 3 number of subcarriers, the tolerance of the sym-

bol time misalignment and the subcarrier frequency offset is 11% and 14%. We presented that the CP increases the tolerances of symbol time misalignment and subcarrier frequency offset. With CP = 50%, the ISI and ICI variances due to symbol time misalignment are reduced by 4 dB. In the presence of subcarrier frequency offset, the ICI variance is reduced by 6.24 dB at CP = 80%. In this chapter, we have investigated the relationships of AO-OFDM system design parameters (number of subcarriers, receiver bandwidth, cyclic prefix) with the time and frequency offsets.

6.2 Timing and Frequency Offsets in M-QAM All-Optical OFDM System

For high spectral efficiency and data rate, optical subcarriers are normally modulated by using advanced modulation formats such as M-QAM. In this work, we modelled M-QAM modulated AO-OFDM system (AO-OFDM transmitter with coherent detection) with 10 Gbaud symbol rate. The performance of M-QAM AO-OFDM system in the presence of symbol time misalignment and subcarrier frequency offset shows lower tolerance limits than the OOK-modulated AO-OFDM system. In the presence of symbol time misalignment and subcarrier frequency offset, the BER performance of the system is compared with the existing emulation setups in section 4.3. In section 4.4, the existing methods of reducing ICI effects such as CP, optical delay lines, and tunable laser diode are investigated. After evaluation of the effects of the time and frequency offsets on AO-OFDM system performance, a DLI based passive device is proposed for ICI reduction. With the proposed method, the tolerances of the symbol time misalignment and subcarrier frequency offset are increased from 3.2% to 29% and 5.5% to 10%. The proposed method of reducing ICI shows the better performance in the presence of time offset in AO-OFDM system, but the dependance of DLI transfer function on frequency offset gives only 4.5% improvement in tolerance, as discussed in section 4.4.3.

6.3 FBG-Assisted ICI Reduction for AO-OFDM Demultiplexed Signal

An O-DFT based demultplexing of optical subcarriers in AO-OFDM system overcomes the requirement of high-speed data converters, and existing optical circuits of O-DFT with its application in AO-OFDM system is discussed in section 2.3.3 and in section 5.1. The transmitted AO-OFDM composite signal after transmission over fiber have relative delay among the subcarriers due to the CD which degrades the orthogonality among subcarriers. In the presence of CD, the sampling point at the output of O-DFT is shifted and further narrowed if modulation bandwidth is limited. Both ideal and real cases of O-DFT function with sampling clock are discussed in section 5.3. In the theoretical evaluations of AO-OFDM system performance in the presence of CD effect with limited modulation bandwidth, the SG performance shows degradation. We proposed the FBG-assisted ICI reduction method for AO-OFDM system. The differences in the designs of FBGs as an O-DFT/IDFT device and as an ICI reducing device are given with their transfer functions in section 5.1.4 and in section 5.4.1. With the FBG as ICI reducing device, the BER of the system is below 10^{-3} for fiber length 45 km without using CP.

6.4 Future Works

In this section, a brief discussion on future research works is given with some suggestions.

1. OFDM in optical communication system is emerged as the promising technology for spectral-efficient superchannels transmission. In Chapter 4, the theoretical investigation of performance of M-QAM AO-OFDM systems in the presence of time and frequency offsets is conducted, and the simulations show the lower tolerances than the tolerances of emulation setups, such as M-QAM modulated odd-and-even and decorrelated configurations. The future research efforts can be made on an experimental setup

for the performance evaluation of AO-OFDM system with M-QAM modulation format in the presence of time, frequency, and phase offsets. In these efforts, a higher order of modulation format and independent modulation sources for desired and adjacent subcarriers will be considered.

2. In Chapter 4, a DLI based ICI reduction method is proposed and performance of AO-OFDM system is theoretically evaluated. In the future work, the performance improvement of AO-OFDM system in an experimental setup by using DLI based passive device is highly desirable.

3. The methods of ICI reduction by using DSP is studied in this thesis. In future, joint time and frequency offset estimation and compensation by using DSP for superchannels would also be desirable.

4. OFDMA based PON offers flexible channel bandwidth sharing and cost-effective solution. With the increase in number of ONUs in PON, the complexity of algorithms for MAC layer and dynamic bandwidth assignment increases. In Appendix F, the preliminary study of protocols (random access and MAC) is conducted by using commercially available softwares (Matlab and OPNET). Future work on protocols for OFDMA based PON is particularly attractive to get the most of the advantages of using OFDM in optical communication system.

Appendices

A Random Variables

A.1 Gaussian Random Variables

The Gaussian random variables are the most commonly used random variables in many physical phenomena including thermal noise, interference in communication circuits [90, 91, 97]. The probability density function (PDF) $f_X(x)$ of Gaussian random variable X with its mean μ, variance σ^2 and standard deviation σ is given as [97]

$$f_X(x) = \frac{1}{\sqrt{2\pi\sigma^2}} e^{-\frac{(x-\mu)^2}{2\sigma^2}} \tag{1}$$

The cumulative distribution function (CDF) is required to find the probability of deviation σ of a Gaussian random variable from its mean μ which is given as

$$\begin{aligned} F_X(x) &= \int_{-\infty}^{x} f_X(y)dy \\ &= \int_{-\infty}^{x} \frac{1}{\sqrt{2\pi\sigma^2}} e^{-\frac{(y-m)^2}{2\sigma^2}} dy \end{aligned} \tag{2}$$

The CDF expression contains integral which is impossible to be expressed as closed form. One way is to find the integral by numerical simulations which gives approximate CDF of a Gaussian random variable.

Figure A.1(a) shows the Gaussian PDF is centered at mean and width is directly proportional to σ. For $\mu = 0$ and $\sigma = 1$, the random variable X is referred as normal Gaussian random variable. In Figure A.1(b) some useful properties of a Gaussian random variable is

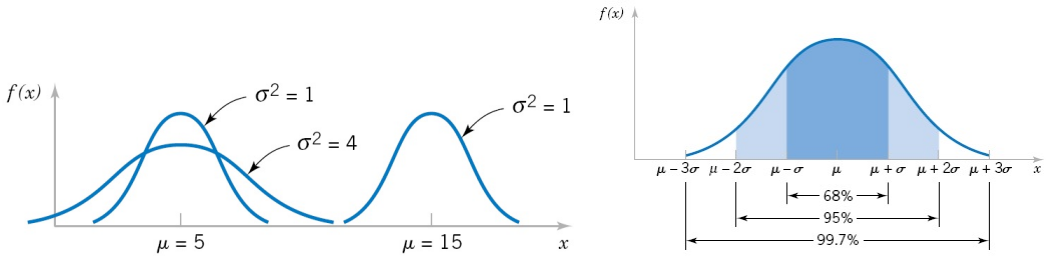

(a) (b)

Figure A.1: Probability density function of Gaussian random variable for (a) different m and σ^2 values and (b) probabilities associated with σ^2 [109].

shown. For a given random variable, the probabilities of random variable are

$$\begin{aligned} P(\mu-\sigma<X<\mu+\sigma) &= 0.6827 \\ P(\mu-2\sigma<X<\mu+2\sigma) &= 0.9545 \\ P(\mu-3\sigma<X<\mu+3\sigma) &= 0.9973. \end{aligned} \tag{3}$$

The PDF of X decreases as it deviates from its μ and area under the PDF beyond 3σ from μ is quite small.

Commonly, the CDF is converted to the standard forms: error function erf(x), complementary error function erfc(x), Φ-function, and Q-function which are given as [97]

$$\begin{aligned} \text{erf}(x) &= \tfrac{2}{\sqrt{\pi}}\int_0^x e^{-t^2}dt \\ \text{erfc}(x) &= 1-erf(x) = \tfrac{2}{\sqrt{\pi}}\int_x^\infty e^{-t^2}dt \\ \Phi(x) &= \tfrac{1}{\sqrt{2\pi}}\int_{-\infty}^x e^{-\frac{t^2}{2}}dt \\ Q(x) &= \tfrac{1}{\sqrt{2\pi}}\int_x^\infty e^{-\frac{t^2}{2}}dt. \end{aligned} \tag{4}$$

The Φ and Q expressions offers straightforward method to express the CDF of a Gaussian random variable. The CDF is related to the Φ-function with the transformation $t = (y-m)/\sigma$

applied to equation (A.2) as

$$\begin{aligned} F_X(x) &= \int_{-\infty}^{x} \frac{1}{\sqrt{2\pi\sigma^2}} e^{-\frac{(y-m)^2}{2\sigma^2}} dy \\ &= \int_{-\infty}^{\frac{x-m}{\sigma}} \frac{1}{\sqrt{2\pi}} e^{-\frac{t^2}{2}} dt \\ &= \Phi(\frac{x-m}{\sigma}). \end{aligned} \tag{5}$$

In order to evaluation the Gaussian CDF, we just need to evaluate the Φ-function from $-\infty$ to $(y-m)/\sigma$. Similar approach is used to find the $\Pr(X > x)$ using Q-function which is given as

$$\Pr(X > x) = \int_{\frac{x-m}{\sigma}}^{\infty} \frac{1}{\sqrt{2\pi}} e^{-\frac{t^2}{2}} dt = Q(\frac{x-m}{\sigma}) \tag{6}$$

The apparent relationship between the Φ-function and the Q-function is

$$Q(\frac{x-m}{\sigma}) = 1 - \Phi(\frac{x-m}{\sigma}). \tag{7}$$

B Derivation of Variance of ICI

In an experiment, the sequence of N independent trials have sample space of 2^N points and each point represent the possible sequence of length N. For example, if N=2 then possible points are 4 in sample space. Here we use the 2^N points to find the relative frequency of an event occurrence [96]. In the direct method, the relative frequency in an experiment of two independent trials, with one event is A and second complementary event is $B = {}^{\Delta}A^C$, is calculated by first counting the number of occurences, $N(A,B)$ and then divide by N which is given as

$$f_N(A,B) = \frac{N(A,B)}{N}. \tag{8}$$

In the indirect method, the conditional relative frequency of B given A is calculated first and multiplied with relative frequency of A which is given as

$$f_N(A,B) = f_N(A) f_N(B|A). \tag{9}$$

Both methods of calculating the relative frequency of two independent trials yields equal values. But in case of large N, the values of $f_N(B)$ and $f_N(B|A)$ have same values and equation (B.9) can be written in an approximate form as

$$f_N(A,B) = f_N(A) f_N(B) \tag{10}$$

Now we find the probabilities of each sequence or sample point, where probability is actually representing the relative frequency of a sample point. Thus, if the probability of A is p then probability of B is $1-p$. The assignment of probabilities and events to the sample points is shown in Table 1. The number $m(A)$ is used to tie the repeated physical experiment with the model which is given as

$$m(A) \stackrel{\Delta}{=} \frac{h}{N}, \tag{11}$$

where h is the total number of A in the sample point.

Table B.1: Probability Assignment

Sample Point	Event	Probability	m(A)
s_1	AAA	p^3	1
s_2	AAB	$p^2(1-p)$	$\frac{2}{3}$
s_3	ABA	$p^2(1-p)$	$\frac{2}{3}$
s_4	BAA	$p^2(1-p)$	$\frac{2}{3}$
s_5	BBA	$p(1-p)^2$	$\frac{1}{3}$
s_6	BAB	$p(1-p)^2$	$\frac{1}{3}$
s_7	ABB	$p(1-p)^2$	$\frac{1}{3}$
s_8	BBB	$(1-p)^3$	0

The probability of a sample points with two A's, P[s_2,s_3,s_4], is given as

$$\mathrm{P}\left[m(A)=\frac{2}{3}\right]=\sum_{i=2}^{4}\mathrm{P}[s_i]=3p^2(1-p) \tag{12}$$

The general expression of probability that $m(A) = h/N$ is given as

$$\begin{aligned}\mathrm{P}\left[m(A)=\frac{h}{N}\right] &= \begin{pmatrix} N \\ h \end{pmatrix} p^h(1-p)^{N-h} \\ &= \frac{N!}{h!(N-h)!}p^h(1-p)^{N-h},\end{aligned} \tag{13}$$

where probability assignment in equation (13) is known as the binomial distribution and the term $\begin{pmatrix} N \\ h \end{pmatrix}$ is binomial coefficients [96].

In equation (3.10) A_k is equally likely to be 1 or 0 with probability 1/2. From [96], probability of h Heads in N tosses of an unbiased coin:

$$\mathrm{P}(h) = \begin{pmatrix} N \\ h \end{pmatrix} \left(\frac{1}{2}\right)^N = \frac{N!}{h!\,(N-h)!}\left(\frac{1}{2}\right)^N. \tag{14}$$

Here, N=N_{sc}-1 and h=1,2,3,..., N_{sc}-1. The total mean and variance of ICI are

$$\mu_{\eta_{STM\_ICI}} = \mu_h \times \mu_{g(\tau_k)|h} = \sum_h \mathrm{P}(h) \times \mu_{\mathrm{g}(\tau_\mathrm{k})|h}, \tag{15}$$

and

$$\begin{aligned} \sigma^2_{\eta_{STM\_ICI}} &= \mu_h \times \sigma^2_{g(\tau_k|h)} - (\mu_h \times \mu_{g(\tau_k)|h})^2 \\ &= \sum_h [\sigma^2_{g(\tau_k|h)} \times \mathrm{P}(h) - \left(\mu_{\mathrm{g}(\tau_\mathrm{k})|\mathrm{h}} \times \mathrm{P}(h)\right)^2]. \end{aligned} \tag{16}$$

In order to elaborate the function P(h) in relation with the receiver bandwidths, BW_{RX} = 30 GHz and 50 GHz, the two cases are explained below:

For BW_{RX} = 30 GHz In this case, the number of adjacent subcarriers of desired subcarrier are 2 and h values are 1 and 2. The expressions of mean and variance for desired edge and middle subcarriers are given as

$$\mu_{\eta_{STM\_ICI\_E}} = \mathrm{P}(h=1) \times \mu_{\mathrm{g}(\tau_\mathrm{k})|h} \quad (\text{edge\_subcarrier}), \tag{17}$$

$$\mu_{\eta_{STM\_ICI\_M}} = 2 \times \mathrm{P}(h=1) \times \mu_{\mathrm{g}(\tau_\mathrm{k})|h} + 2 \times \mathrm{P}(h=2) \times \mu_{\mathrm{g}(\tau_\mathrm{k})|h} \quad (\text{middle\_subcarrier}), \tag{18}$$

$$\sigma^2_{\eta_{STM\_ICI\_E}} = [\sigma^2_{g(\tau_k|h)} \times \mathrm{P}(h=1) - \left(\mu_{\mathrm{g}(\tau_\mathrm{k})|\mathrm{h}} \times \mathrm{P}(h=1)\right)^2] \quad (\text{edge\_subcarrier}), \tag{19}$$

and

$$\begin{aligned}\sigma^2_{\eta_{STM\_ICI\_M}} &= 2\times[\sigma^2_{g(\tau_k|h)}\times \mathrm{P}\,(h=1)-\left(\mu_{\mathrm{g}(\tau_\mathrm{k})|\mathrm{h}}\times \mathrm{P}\,(h=1)\right)^2] \\ &\quad +2\times[\sigma^2_{g(\tau_k|h)}\times \mathrm{P}\,(h=2)-\left(\mu_{\mathrm{g}(\tau_\mathrm{k})|\mathrm{h}}\times \mathrm{P}\,(h=2)\right)^2] \quad \text{(middle\_subcarrier)}.\end{aligned} \tag{20}$$

For BW_{RX} = 50 GHz The number of adjacent subcarriers of desired subcarrier at receiver with BW_{RX} = 50 GHz are 4 and h = 1 to 4. The expressions of mean and variance for desired edge and middle subcarriers are given as

$$\begin{aligned}\mu_{\eta_{STM\_ICI\_E}} &= \mathrm{P}(h=1)\times\mu_{\mathrm{g}(\tau_\mathrm{k})|h}+\mathrm{P}(h=1)\times\mu_{\mathrm{g}(\tau_{\mathrm{k}+1})|h}+\mathrm{P}(h=2)\times\mu_{\mathrm{g}(\tau_\mathrm{k})|h} \\ &\quad +\mathrm{P}(h=2)\times\mu_{\mathrm{g}(\tau_{\mathrm{k}+1})|h} \quad \text{(edge\_subcarrier)},\end{aligned} \tag{21}$$

$$\begin{aligned}\mu_{\eta_{STM\_ICI\_M}} &= 2\times\mathrm{P}(h=1)\times\mu_{\mathrm{g}(\tau_\mathrm{k})|h}+2\times\mathrm{P}(h=1)\times\mu_{\mathrm{g}(\tau_{\mathrm{k}+1})|h} \\ &\quad +6\times\mathrm{P}(h=2)\times\mu_{\mathrm{g}(\tau_\mathrm{k})|h}+6\times\mathrm{P}(h=2)\times\mu_{\mathrm{g}(\tau_{\mathrm{k}+1})|h} \\ &\quad +6\times\mathrm{P}(h=3)\times\mu_{\mathrm{g}(\tau_\mathrm{k})|h}+6\times\mathrm{P}(h=3)\times\mu_{\mathrm{g}(\tau_{\mathrm{k}+1})|h} \\ &\quad +2\times\mathrm{P}(h=4)\times\mu_{\mathrm{g}(\tau_\mathrm{k})|h}+2\times\mathrm{P}(h=4)\times\mu_{\mathrm{g}(\tau_{\mathrm{k}+1})|h} \quad \text{(middle\_subcarrier)},\end{aligned} \tag{22}$$

$$\begin{aligned}\sigma^2_{\eta_{STM\_ICI\_E}} &= \sigma^2_{g(\tau_k|h)}\times\mathrm{P}\,(h=1)-\left(\mu_{\mathrm{g}(\tau_\mathrm{k})|\mathrm{h}}\times\mathrm{P}\,(h=1)\right)^2 \\ &\quad +\sigma^2_{g(\tau_{k+1}|h)}\times\mathrm{P}\,(h=1)-\left(\mu_{\mathrm{g}(\tau_{\mathrm{k}+1})|\mathrm{h}}\times\mathrm{P}\,(h=1)\right)^2 \\ &\quad +\sigma^2_{g(\tau_k|h)}\times\mathrm{P}\,(h=2)-\left(\mu_{\mathrm{g}(\tau_\mathrm{k})|\mathrm{h}}\times\mathrm{P}\,(h=2)\right)^2 \\ &\quad +\sigma^2_{g(\tau_{k+1}|h)}\times\mathrm{P}\,(h=2)-\left(\mu_{\mathrm{g}(\tau_{\mathrm{k}+1})|\mathrm{h}}\times\mathrm{P}\,(h=2)\right)^2 \quad \text{(edge\_subcarrier)},\end{aligned} \tag{23}$$

and

$$\begin{aligned}\sigma^2_{\eta_{STM\_ICI\_M}} &= 2\times\{\sigma^2_{g(\tau_k|h)}\times \mathrm{P}(h=1)-\left(\mu_{\mathrm{g}(\tau_\mathrm{k})|\mathrm{h}}\times \mathrm{P}(h=1)\right)^2\}\\ &+2\times\{\sigma^2_{g(\tau_{k+1}|h)}\times \mathrm{P}(h=1)-\left(\mu_{\mathrm{g}(\tau_{\mathrm{k}+1})|\mathrm{h}}\times \mathrm{P}(h=1)\right)^2\}\\ &+6\times\{\sigma^2_{g(\tau_k|h)}\times \mathrm{P}(h=2)-\left(\mu_{\mathrm{g}(\tau_\mathrm{k})|\mathrm{h}}\times \mathrm{P}(h=2)\right)^2\}\\ &+6\times\{\sigma^2_{g(\tau_{k+1}|h)}\times \mathrm{P}(h=2)-\left(\mu_{\mathrm{g}(\tau_{\mathrm{k}+1})|\mathrm{h}}\times \mathrm{P}(h=2)\right)^2\}\\ &+6\times\{\sigma^2_{g(\tau_k|h)}\times \mathrm{P}(h=3)-\left(\mu_{\mathrm{g}(\tau_\mathrm{k})|\mathrm{h}}\times \mathrm{P}(h=3)\right)^2\}\\ &+6\times\{\sigma^2_{g(\tau_{k+1}|h)}\times \mathrm{P}(h=3)-\left(\mu_{\mathrm{g}(\tau_{\mathrm{k}+1})|\mathrm{h}}\times \mathrm{P}(h=3)\right)^2\}\\ &+2\times\{\sigma^2_{g(\tau_k|h)}\times \mathrm{P}(h=4)-\left(\mu_{\mathrm{g}(\tau_\mathrm{k})|\mathrm{h}}\times \mathrm{P}(h=4)\right)^2\}\\ &+2\times\{\sigma^2_{g(\tau_{k+1}|h)}\times \mathrm{P}(h=4)-\left(\mu_{\mathrm{g}(\tau_{\mathrm{k}+1})|\mathrm{h}}\times \mathrm{P}(h=4)\right)^2\}\quad (\text{middle\_subcarrier}),\end{aligned} \tag{24}$$

where k and $k+1$ are adjacent subcarriers spaced at 10 GHz and 20 GHz from desired subcarrier.

From [97] mean and variance of function $g(\tau_k)$ are

$$\mu_{g(\tau_k)} = \sum_{k=2}^{N_{SC}} \int_{-\infty}^{\infty} g(\tau_k)\, p(\tau_k)\, d\tau_k \tag{25}$$

$$\sigma^2_{g(\tau_k)} = E\left|g(\tau_k)-\mu_{g(\tau_k)}\right|^2 \tag{26}$$

where $p(\tau_k)=\frac{1}{\sqrt{2\pi\sigma_{\tau_k}}}\exp(-\tau_k^2/(2\sigma^2_{\tau_k}))$ is probability density function of independent Gaussian distributed variables τ_k. So, we finally arrive at

$$\mu_{g(\tau_k)} = \sum_{k=2}^{N_{SC}} \frac{\exp\left(-2\pi^2 f_1^2\sigma^2_{\tau_k}\right)-\exp(-2\pi^2 f_k^2\sigma^2_{\tau_k})}{j\pi(f_k-f_1)} \tag{27}$$

and

$$\sigma^2_{g(\tau_k)} = \sum_{k=2}^{N_{SC}} \frac{1}{2\pi^2(f_k - f_1)^2} \times \{1 - \exp\left(-2\pi^2(f_k - f_1)^2\sigma^2_{\tau_k}\right) - 2\left(\exp\left(-2\pi^2 f_1^2\sigma^2_{\tau_k}\right) - \exp(-2\pi^2 f_k^2\sigma^2_{\tau_k})\right)^2\}. \quad (28)$$

Substituting relations given in equation (B.27) and equation (B.28) in equation (B.15) and equation (B.16) yields equation (3.12) and equation (3.13), the desired moments of ICI due to STM.

C Derivation of Variance of ISI

The value of previous symbol A_1^p is either 0 or 1 with equal probability 0.5. Total mean and variance of ISI are given as

$$\begin{aligned}\mu_{\eta_{STM\_ISI}} &= \sum_{A_1^p=\{0,1\}} \mu_{g(\tau_1)|A_1^p} \mathrm{P}(A_1^p) \\ &= \mu_{g(\tau_1)|A_1^p=1} \times \mathrm{P}\left(\mathrm{A_1^p}=1\right)\end{aligned} \tag{29}$$

and

$$\begin{aligned}\sigma^2_{\eta_{STM\_ISI}} &= \sigma^2{}_{g(\tau_1)|A_1^p} \times \mu_{A_1^p} - \left(\mu_{g(\tau_1)|A_1^p} \times \mu_{A_1^p}\right)^2 \\ &= \sum_{A_1^p=\{0,1\}} \sigma^2{}_{g(\tau_1)|A_1^p} \times \mathrm{P}(A_1^p) - \left(\sum_{A_1^p=\{0,1\}} \mu_{g(\tau_1)|A_1^p} \times \mathrm{P}(A_1^p)\right)^2 \\ &= \sigma^2_{g(\tau_1)|A_1^p=1} \times \mathrm{P}\left(\mathrm{A_1^p}=1\right) - [\mu_{\mathrm{g}(\tau_1)|\mathrm{A_1^p}=1} \times \mathrm{P}\left(\mathrm{A_1^p}=1\right)]^2.\end{aligned} \tag{30}$$

The mean and variance of $g(\tau_1)$ are derived and given as

$$\mu_{g(\tau_1)} = 2\sigma_{\tau_1} e^{-2\pi^2 f_1^2 \sigma^2_{\tau_1}} / \sqrt{2\pi} \tag{31}$$

and

$$\sigma^2_{g(\tau_1)} = \sigma^2_{\tau_1} - (\mu_{g(\tau_1)})^2. \tag{32}$$

Substituting equation (C.31) and equation (C.32) in equation (C.29) and equation (C.30) gives equation (3.15) and equation (3.16).

D Monte Carlo Simulation Model

In digital communication system, Monte Carlo simulations are commonly performed for BER performance evaluations in the presence of noise and interference. In the process of estimating a bit error probability, the random variable Y (with mean m and variance σ^2 defined by Gaussian random variable G) is given as

$$Y = m + G. \tag{33}$$

For estimation of probability that $Y < 0$ at given m, the series of experiments based on Monte Carlo method is performed. In an experiments, independent and identically distributed (IID) Guassian random variables are generated G and added with constant value m which can be written as

$$Y_i = m + G_i, \tag{34}$$

where i=1, 2, ... , N. In order to find $P(m) = P(Y < 0|m)$ in an experiment, the value of Y_i is tested for < 0 and a new random variable X_i generate 1 or 0 output which can be mathematically written as

$$X_i = \begin{cases} 0, & \text{if } Y_i \geq 0 \\ 1, & \text{if } Y_i < 0 \end{cases} \tag{35}$$

After testing of state of Y_i, the probability $P(Y < 0|m)$ is estimated as

$$P(m) = \frac{1}{N} \sum_{i=1}^{N} X_i \tag{36}$$

In equation (D.36), the number of received random variables Y_i that are less than zero is divided by total number of Gaussian random variables transmitted.

In Monte Carlo simulation model, the performance of the M-QAM modulation format in an AO-OFDM is evaluated. The main advantage of rectangular constellations of QAM signal is easy generations of two pulse amplitude modulation (PAM) signals which are marked on

quadrature signals [110]. At transmitter, the random numbers are generated uniformly as the information symbols corresponding to required 4-bit combination for 16-QAM symbols, as shown in Figure D.2. The output of 16-QAM signal selector is the signal points with coordinates of (A_{mc}, A_{ms}). The shot and thermal, and interferences from adjacent subcarriers and previous symbol in the desired subcarrier are considered and are modelled as Gaussian random noise and have components $\{n_c, n_s\}$. The received signal is given as

$$r = [A_{mc} + n_c \quad A_{ms} + n_s] \tag{37}$$

The received signal r is detected and computation of distance metric performed in order to find the closest signal point to the r. For BER counter, the detected 16-QAM symbols are compared with transmitted symbols. In Monte Carlo simulations, over 10^6 symbols are used for error counting.

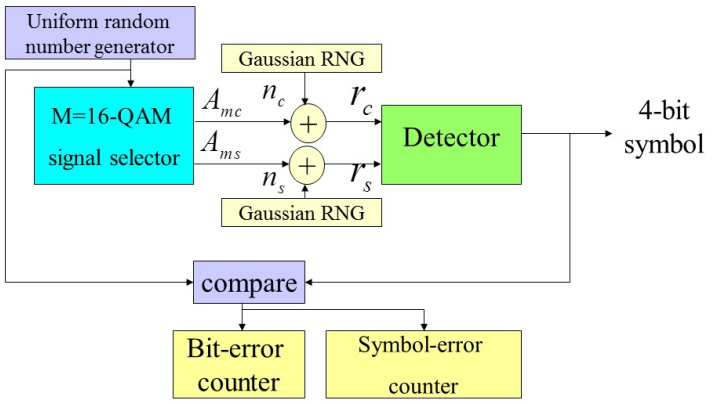

Figure D.2: Monte Carlo model for M-QAM communication system [110].

E SSFBG based optical DFT device

In chapter 2, the requirements of high-speed data converters (ADC and DAC) and complex DSP algorithms for AO-OFDM system are discussed, and needs of optical DFT/IDFT are also studied in chapter 2 and chapter 5. In [12], $N-1$ passive delay interferometers (DI) with N sampling gates are proposed to perform the optical DFT function, as shown in Figure 5.4. For the large number of subcarriers, the design of DI based O-DFT device becomes complex, and we need an integrated and scalable solution based on arrayed waveguide grating (AWG) device for optical DFT and IDFT functions [58]. In an AWG device, two slab regions are interconnected with arrayed waveguides, as shown in Figure 5.1. The drawback of DI- and AWG- based O-DFT functions are the requirement of short and precise optical sampling techniques in order to extract the desired subcarrier in an intercarrier interference (ICI) - free window. Furthermore, the details of O-DFT function with electroabsorption modulator based sampling gate are discussed in section 1.3. The superstructure fiber Bragg grating (SSFBG) based O-DFT/IDFT function provides a real-time system without the needs of a synchronous optical sampling gates and a local oscillator (LO) at the receiver. In this appendix, we give details of design of SSFBG device for O-DFT/IDFT function.

E.1 Realization of SSFBG device for AO-OFDM system

In the SSFBG design, the grating refractive index profile is sinusoidally modulated is given as

$$\delta n_{eff}(z) = A(z - mZ_0) \times \cos\left(\frac{2\pi}{\Lambda}\right)\varphi, \tag{38}$$

where Z_0 is the length of m^{th} segment of the SSFBG device and φ is grating phase term. The steps of derivation of impulse response $h(t)$ of SSFBG are discussed in section 5.1.4. The linear convolution of input signal $x(t)$ and $h(t)$ gives the final expression of the reflected signal $y(t)$ which is given as

$$y(t) = B\left(t - m\frac{2nZ_0}{c}\right), \tag{39}$$

where

$$B(t) = Kx(t) \otimes \left(A\left(\frac{ct}{2n}\right) \cos\left(\frac{2\pi}{\Lambda}\frac{ct}{2n}\right)\right) \varphi. \tag{40}$$

For designed SSFBG O-DFT/IDFT device, the segment length Z_0 and phase φ terms are given as

$$Z_0 = \frac{cT}{2n(N+C}, \tag{41}$$

and

$$\varphi = e^{-j2\pi mk/N}, \tag{42}$$

where m is m^{th} sample of an OFDM symbol, k is k^{th} subcarrier, and C is cyclic prefix (CP).

Required time samples for N = 32

In order to support N = 32 subcarriers, the condition of number of time samples must be equal to N. Figure E.3 shows the plot of sampled input signal of $x(t)$ = [1 1 1 1 1 1 1 1] and k varies from 1 to N. The $x(m)$ with zero-padding gives the linear phase but magnitude plot shows edge subcarriers can be easily demultiplexed. In RF-OFDM systems, zero-padding is usually used as guard interval/CP [10]. In order to design SSFBG for 32 subcarriers, the length is increased from 8 to 32 and phase φ is varied for $m = 0, 1 \cdots 31$, $k = 0, 1 \cdots 31$, and N = 32, as shown in Figure E.4.

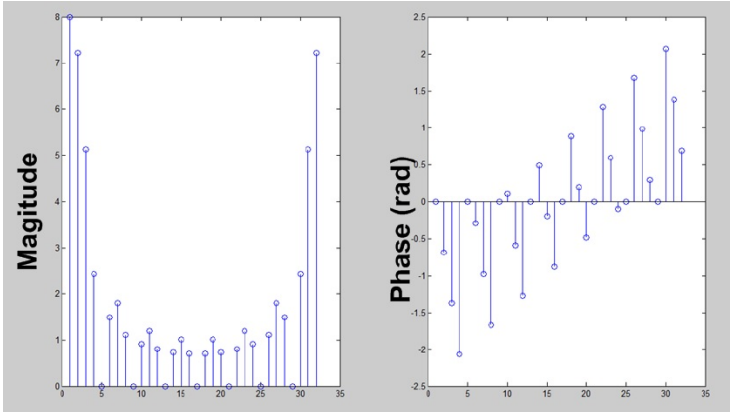

Figure E.3: DFT of $x(m)$ = [1 1 1 1 1 1 1 1] and N=32.

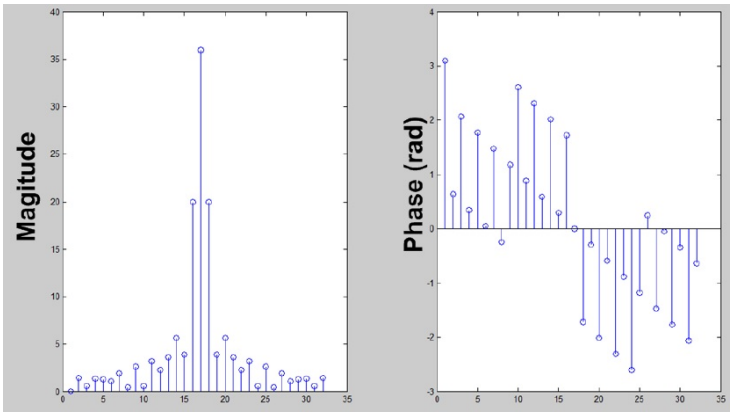

Figure E.4: DFT of $x(m)$ with time samples equal to number of subcarriers without zero-padding.

SSFBG structure for 32 subcarriers

For N = 32 subcarriers, the SSFBG for O-DFT/IDFT functions is designed in Optigrating package and parameters are given in Table E1.

Table E.2: Parameters of SSFBG for DFT/IDFT Functions

Parameter	Value	Unit
data rate	10	Gbit/sec
OFDM symbol duration (T)	0.1	ns
chip period (Z_0)	256	μm
k^{th} subcarrier range	1550.08 to 1552.56	nm
subcarrier spacing (Δf)	0.08	nm
maximum index change	9E-05	-

For subcarrier 1 at λ_1 = 1550.08 nm, the total length of SSFBG is 10.24 mm and phase of each segment is an integer multiple of $\pi/16$. The structure and reflected signal of designed SSFBG for λ_1 are shown in Figure E.5 and Figure E.6. The duration of CP is 20 % of total OFDM symbol duration and can be increase for high dispersive medium.

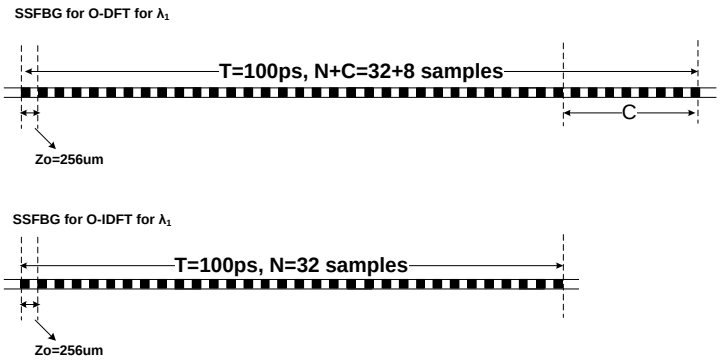

Figure E.5: SSFBG design for all-optical signal generation and detection for subcarrier 1.

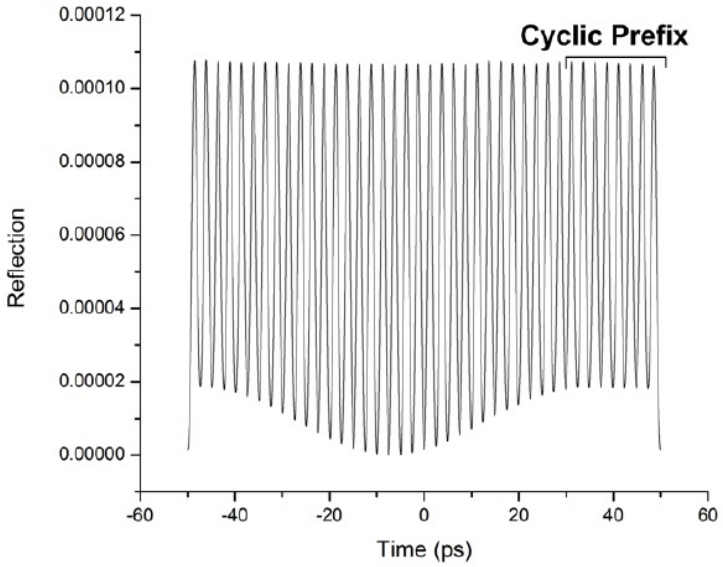

Figure E.6: Reflected time domain signal from SSFBG at transmitter.

E.2 Proposed SSFBG based IM/DD AO-OFDM System

The SSFBG based passive device for O-DFT/IDFG function in AO-OFDM system provides a cost effective solution with more number of subcarriers, as shown in Figure E.7. The multicarrier source such as modelocked laser diode generates $N = 32$ subcarriers that are modulated at 10 Gbit/sec by intensity modulator (IM). The pulse width of optical signal from multicarrier source is varied from 1 ps to 1.12 ps with power of 3 dBm. After modulation, the bank of SSFBGs are used to perform O-DFT function with an optical delay lines (ODL) are used to align the subcarrier in time-domain. Before transmission over fiber, the OFDM signal is filtered by optical bandpass filter (OBPF) with bandwidth 320 GHz (32×10 GHz) in order to reduce the noise. Total fiber length is 10 km with chromatic dispersion of 16.75 ps/(nm.km) is used in simulations. At the receiver side, after splitter (remote node) the SSFBG is used to demultiplex the desired subcarrier. In a direct-detection, the shot, thermal, signal-ASE, and ASE-ASE are considered in receiver noise.

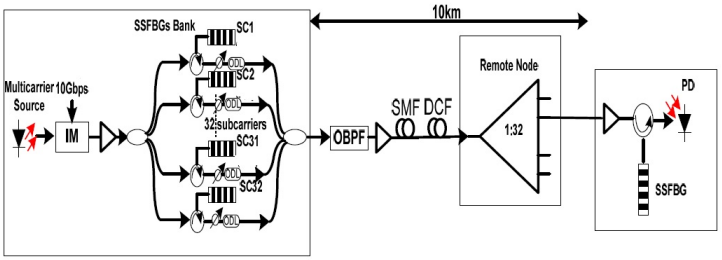

Figure E.7: Proposed SSFBG based All-Optical OFDM system.

Results and Discussions

In the simulations of SSFBG based AO-OFDM system, the BER performance is evaluated with and without OBPF and varying the pulse width of optical signal from multicarrier source. In case of without OBPF and pulse width = 1 ps, the edge subcarriers have BER $< 10^{-4}$ while five middle subcarrier have BER $> 10^{-3}$, as shown in Figure E.8(a). In order to reduce the effects of ASE, OBPF of bandwidth = 320 GHz is used while pulse width remains same as first case. In case of OBPF of 320 GHz, the BER performance of middle

subcarriers becomes better while due to passband's edges of OBPF the edge subcarriers show reduced BER performance, as shown in Figure E.8(b). With the increase in the pulsewidth duration from 1 ps to 1.12 ps, the bandwidth of subcarriers is reduce which ultimately reduces the spectral overlap and the intercarrier interference. In Figure E.8(c), the BER performance of AO-OFDM system with OBPF of bandwidth 320 GHz and pulse width 1.12 ps is shown. With the increase in pulse width, the edge subcarrier have BER$< 10^{-5}$ and also BER performances of middle subcarriers are in between $10^{-4} - 10^{-3}$.

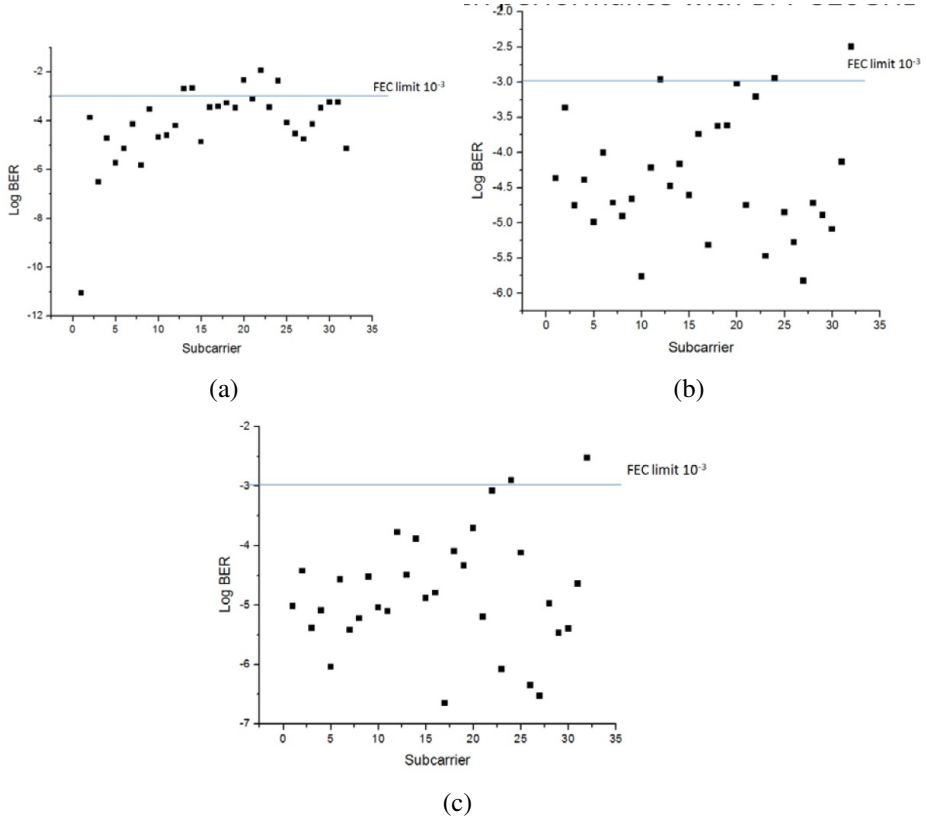

Figure E.8: BER performances of AO-OFDM system with SSFBG based O-DFT/IDFT. (a) Without OBPF and pulse width = 1 ps, (b) with OBPF=320 GHz and pulse width = 1ps, and (c) with OBPF = 320 GHz and pulse width = 1.12 ps.

F MAC Protocols for Next Generation-PON

With the exponential growth in demand of bandwidth hungry multimedia services, the current wire (very high speed digital subscriber line) and wireless (Worldwide Interoperability for Microwave Access, WiMax)techniques cannot support the bandwidth requirements in an access networks. Passive optical networks (PON) are widely adopted as a cost-effective solution for broadband access networks [112, 113]. The multiple access network architectures in the PONs are evolved from time division multiple access (TDMA), wavelength division multiple access (WDMA), hybrid TDMA/WDMA, code division multiple access (CDMA) and orthogonal frequency division multiple access (OFDMA). In an OFDMA PONs, the channel bandwidth is divided into a orthogonal subcarriers and distributed statistically among optical network units (ONU) which can be further exchanged between ONU by using TDM [114].

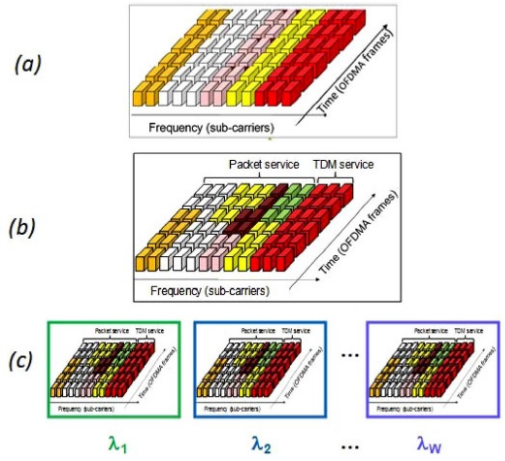

Figure F.9: Variants of OFDMA-PON: (a) Statistically assigned different OFDM subcarriers to different ONUs; (b) Assigned different ONUs different subcarriers and time slots; (c) Assigned different ONUs different subcarriers and time slots on different wavelengths [38].

There are multiple variants of OFDMA in PON which are graphically illustrated in Figure F.9. In the simple architecture of OFDMA-PON, the different subcarriers are assigned to different ONUs from the common OFDM band and the assignment can be adaptive for the real-time traffic demand by using media access control (MAC) algorithms [115]. For the higher flexibility of subcarriers' allocation, the ONU's bandwidth resources are divided

in time which gives the advantage of using same subcarriers to multiple ONUs in different time slots, as shown in Figure F.9(b). This type of architecture is normally referred as OFDMA+TDMA approach and can be implemented by MAC layer protocols. In the three dimensional approach, the OFDM+TDMA approach is implemented on each possible wavelength of WDM by using DSP based algorithms. In the third approach, the wavelength assignments are static if laser sources are generating fixed wavelengths signals which provides a WDM overlay. By adoption of WDM overlay in PON, the aggregate capacity increases which can further be exploited with the novel MAC protocols for OFDMA-PON [116, 117].

In [118], the MAC protocol for the OFDMA-PON is proposed. The OFDMA frame format of proposed system consists of optical line termination (OLT) and several ONUs is shown in Figure F.10. The OFDM subcarriers are assigned dynamically by implementing modified frame format which includes the time slot assignment also. The use of subcarriers by ONU in an allocated time slot is scheduled by OLT.

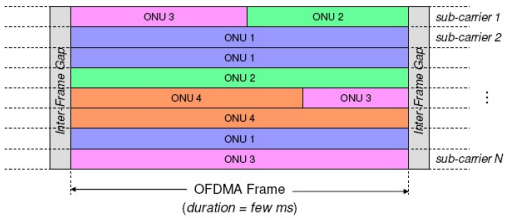

Figure F.10: Proposed architecture of OFDMA-PON [118].

In [119], the control schemes between OLT and ONUs are proposed to avoid the collisions in upstream transmissions. The ONUs transmit data by using allocated subcarriers with one additional dedicated control subcarrier (sc_{co}) between OLT and ONUs. The sc_{co} is normally used for control signalling and can only be used for data transmission if a particular ONU have real-time data request. After data transmission is completed through the sc_{co}, the sc_{co} is released and available to be used for all ONUs in the PON. In Figure F.11(a), the sc_{co} is shown as bus line for dedicated control signalling channel between OLT and ONU. The procedure of request and grant messages between OLT and ONU is shown in Figure F.11(b).

The performance in terms of packet delay and throughput of the proposed MAC protocol

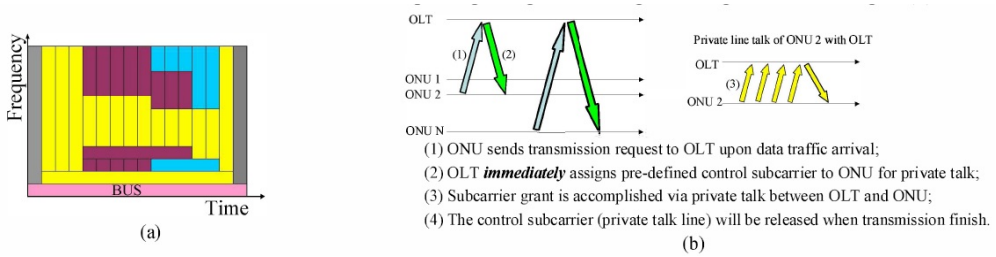

Figure F.11: Proposed Layer 2 (MAC) based control scheme [119].

design for OFDMA-PON is numerically evaluated. In an OFDMA-PON, 128 ONUs are connected with OLT as point-to-point topology and transmission distance of 20 km. Total OFDM subcarriers are 512 including one subcarrier as sc_{co}. The length of message signal is 64 bytes and data transmission rate is 19.53 Mbit/sec. In the bursty uplink transmissions, the ONUs follows the Pareto distribution with mean = 62.37 kbytes. In Figure F.12, the packet transmission delay in proposed scheme is small for traffic load < 0.95. The traffic load is defined as the ONUs traffic over the capacity of network. When load is higher than 0.95, the packet delay eventually increases due to large number of packets are in queue which increases the packet collisions and decreases the throughput.

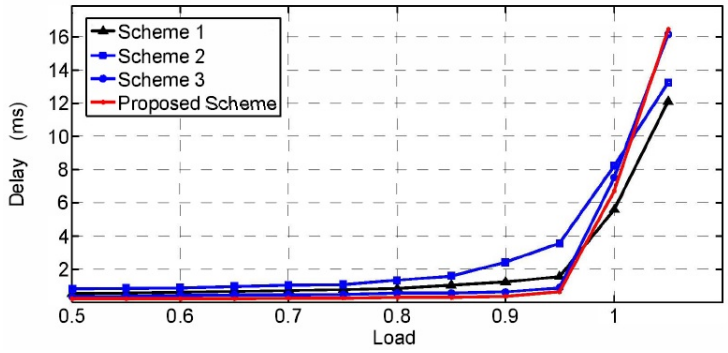

Figure F.12: Packet delay versus traffic load in proposed MAC algorithm [119].

F.1 Random Access Protocol

In our study of random access protocol for NG-PON, the most common protocol pure ALOHA is considered first in which the ONUs transmit the packets when they have packets without

sensing the medium. In this protocol, each ONU hopes that the other ONU are not transmitting to the destination at the same time. In simulations, total number of ONUs are 10, data rate of each ONU is 10 Mbit/sec, and packet frame size is 8000 bits. The performance is evaluated by calculating the total number of successful reception P_s. The throughput, S, of pure ALOHA protocol is given as

$$S = GP_s = Ge^{-2G}, \tag{43}$$

where G is the number of attempts by ONU in given time and e^{-2G} terms shows the ALOHA protocol have the Poisson distribution. Figure F.13 shows the throughput first increases with the increase in arrival rate upto 4 Mbit/sec and then performance of system decrease for arrival rate $>$ 5 Mbit/sec due to no control of packet transmission in the pure ALOHA protocol.

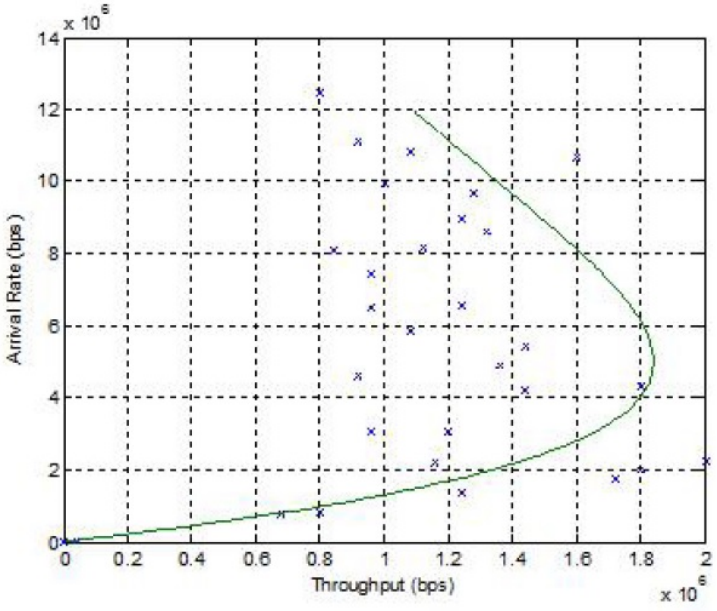

Figure F.13: Simulation results from Matlab for pure ALOHA protocol.

In [120], the MAC protocol based on carrier sense multiple access/collision detection (CSMA/CD) for PON is proposed. In proposed architecture, the upstream and downstream data transmission over two different wavelengths, λ^u and λ^d and WDM multiplexer/demultiplexer is used to combine/seperate the wavelengths at OLT. For uplink transmissions, the an echo

from splitter/combiner is used by ONU to detect the other ONUs' transmissions. For downlink transmission, the most common protocol of broadcast is used [121]. The experimental setup of proposed protocol for PON comprises of two ONUs which generates the packets of 131 bytes at data rate 155 Mbit/sec, as shown in Figure F.14. The signals of ONUs after combiner and transmission over 10m fiber are monitored at OLT. In case of collision, the OLT stops recovering the signals. The other signal from combiner is further splitted by coupler for carrier-sensing circuits in order to detect and compare the signals for extraction of correct time of collision.

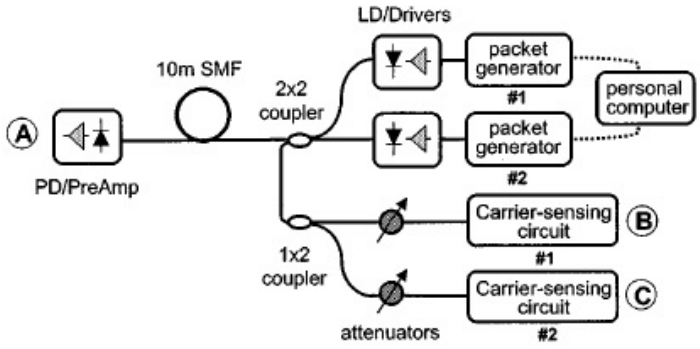

Figure F.14: Experimental setup of proposed optical CSMA/CD protocol[120].

F.2 CSMA based MAC Protocol

For CSMA protocol implementation, the OPNET software package is used with the stages required for transeiver implementation is shown in Figure F.15. The link between OLT and ONUs is configured for following 6 stages:

Tx delay Time required to complete the transmission of packet, $T_d = packet\_length/data\_rate$

Channel Match classify transmission is valid, noise or ignore on the basis DFT operation at receiver

Background Noise Thermal and Shot noise are considered in our system

Noise Defined two conditions: valid packet received and other packet is valid; valid packet received but other packet is invalid. The validity of packet is decided on the basis of Channel Match stage.

SNR Calculation on the basis of stages 7, 8, and 9.

BER Derived from SNR calculations

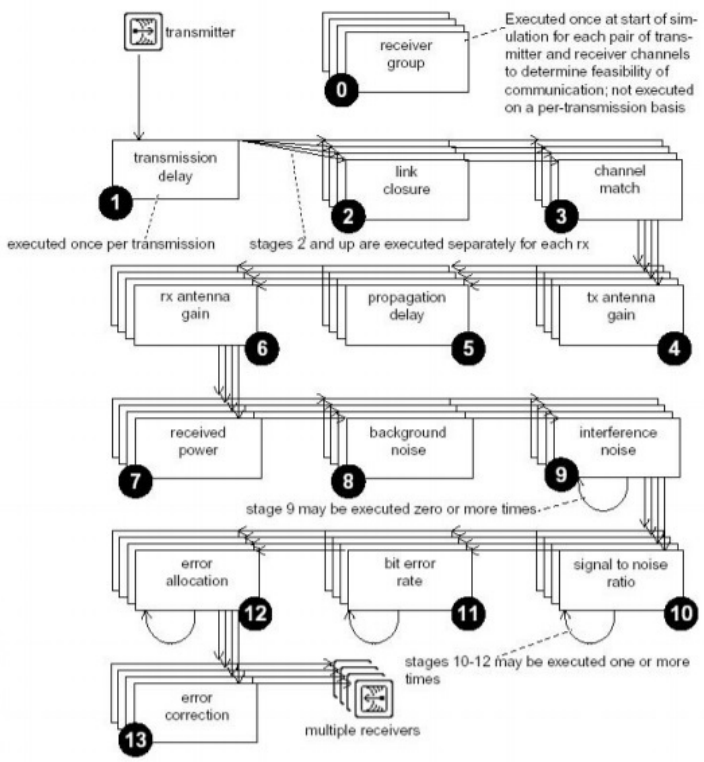

Figure F.15: Transceiver pipeline stages in OPNET software package [122].

After implementation of pipeline stages required for CSMA based MAC protocol for optical network of 20 nodes, the performance is evaluated and compared with ALOHA protocol. Each node transmit data on the allocated subcarrier with equal priority of data transmission. The network architecture in bus topology is shown in Figure **??**. The CSMA protocol provides cost effective solution as each node in the network receives the network traffic which can be utilize for carrier sensing function. In case of more than one packet received at the node, then receiving node decides that the packet is valid, noise/interference, or ignore. De-

spite of different subcarriers assigned to nodes, the simultaneous packet transmissions from more than one node causes interference. The model and simulation results comparison of ALOHA and CSMA protocols is shown in Figure F.16. In CSMA model, the link between the node's receiver (*bus_rx*) and transmitter (*tx_proc*) is enabled in order to implement the packets transmissions from nodes after carrier sensing, while in ALOHA the carrier sensing link is disabled. For perofrmance evaluations, two parameters are configured which are given as

$$\text{Channel Traffic, } G = \frac{\text{Submitted Packets}}{\text{time}} \tag{44}$$

and

$$\text{Channel Throughput, } S = \frac{\text{Received Packets}}{\text{time}}. \tag{45}$$

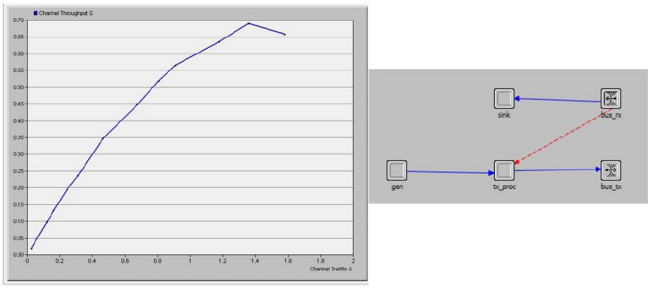

(a)

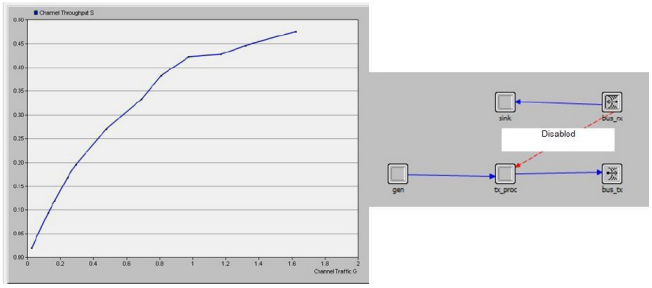

(b)

Figure F.16: Implementation and results of (a) CSMA and (b) ALOHA protocols in OPNET software.

With the increase in G, S increases in both models but ALOHA have low performance of $S = 0.41$ at $G = 1$ than CSMA based MAC protocol which gives $S = 0.6$ at $G = 1$, as shown

in Figure F.16. For $1 \leq G \leq 1.4$, the CSMA protocol still shows better S performance than ALOHA, but for $G > 1.4$ the S reduces for CSMA, due to intercarrier interference from other nodes in the network. In order to further improve the performance of CSMA protocol, the possible ways are use the collision domain feature of nodes, implement the star topology, and time slots assignments [115] to the nodes in the network .

References

[1] P. J. Winzer, "Challenges and Evolution of Optical Transport Networks'", ECOC 2010, Torino, Italy, Paper We.8.D.1

[2] R. W. Tkach, "Scaling optical communications for the next decade and beyond", Bell Labs Technical Journal, **14**, 310 (2010)

[3] A. Odlyzko, "Minnesota Internet Traffic Studies", University of Minnesota, 1-7 (2009) www.dtc.umn.edu/mints/home.php

[4] J. Gray and P. Shenay, "Rules of Thumb in Data Engineering", Microsoft Research Technical Report, **MS-TR-99-100** (2000).

[5] J. L. Hennessy and D. A. Patterson, "Computer Architectures: A Quantitative Approach", Morgan Kaufmann (2003).

[6] A. H. Gnauck, P. J. Winzer, S. Chandrasekhar, X. Liu, B. Zhu, and D. W. Peckham, "10 $\times$ 224-Gb/s WDM transmission of 28-Gbaud PDM 16-QAM on a 50-GHz grid over 1,200 km of fiber", OFC/NFOEC 2010, San Diego, CA, USA, Paper PDPB8.

[7] R. H. Walden, "Analog-to-digital converter survey and analysis", IEEE Journal on Selected Areas in Communications, **17**, 539-550 (1999)

[8] S.K. Korotky, R.-J. Essiambre and R. W. Tkach, "Expectations of optical network traffic gain afforded by bit rate adaptive transmission", Bell Labs Technical Journal, **14**, 285295 (2010)

[9] R.-J. Essiambre, G. Kramer, P. J. Winzer, G. J. Foschini, and B. Goebel, "Capacity Limits of Optical Fiber Networks", Journal of Lightwave Technology, **28**, 662-701 (2010)

[10] Y. S. Cho, J. Kim, W. Y. Yang, C. G. Kang, “MIMO-OFDM Wireless Communications with MATLAB”, Wiley-Blackwell, 2010

[11] W. Shieh , I. Djordjevic, “OFDM for Optical Communications”, Academic Press, 2009

[12] D. Hillerkuss, R. Schmogrow, T. Schellinger, M. Jordan, M. Winter, G. Huber, T. Vallaitis, R. Bonk, P. Kleinow, F. Frey, M. Roeger, S. Koenig, A. Ludwig, A. Marculescu, J. Li, M. Hoh, M. Dreschmann, J. Meyer, S. Ben-Ezra, N. Narkiss, B. Nebendahl, F. Parmigiani, P. Petropoulos, B. Resan, A. Oehler, K. Weingarten, T. Ellermeyer, J. Lutz, M. Moeller, M. Huebner, J. Becker, C. Koos, W. Freude, and J. Leuthold, “26 Tbit s-1 line-rate superchannel transmission utilizing all-optical fast Fourier transform processing”, Nature Photonics, **5**, 364-371 2011

[13] D. Qian, M.-F. Huang, E. Ip, Y.-K. Huang, Y. Shao, J. Hu, and T. Wang “101.7-Tb/s (370×294-Gb/s) PDM-128QAM-OFDM transmission over 3×55-km SSMF using pilot-based phase noise mitigation,” NFOEC 2011, LA California USA, Paper PDPB5

[14] S. L. Jansen, “Multi-carrier approaches for next-generation transmission: Why, where and how?,” OFC/NFOEC 2012, LA California USA, Paper OTh1B.1

[15] H. Nyquist, “Certain topics in telegraph transmission theory”, Proceedings of the IEEE, ROCEEDINGS OF THE IEEE, **90**, 280-305 (2002)

[16] G. Bosco, V. Curri, A. Carena, P. Poggiolini, and F. Forghieri, “On the performance of Nyquist-WDM terabit superchannels based on PM-BPSK, PM-QPSK, PM-8QAM or PM-16QAM subcarriers”, Journal of Lightwave Technology, **29**, 53-61 (2011)

[17] R. Schmogrow, D. Hillerkuss, S. Wolf, B. Buerle, M. Winter, P. Kleinow, B. Nebendahl, T. Dippon, P. C. Schindler, C. Koos, W. Freude, and J. Leuthold, ”512QAM Nyquist sinc-pulse transmission at 54 Gbit/s in an optical bandwidth of 3 GHz”, Optics Express, **20**, 6439-6447 (2012)

[18] J. Zhao and A. D. Ellis, “Offset-QAM based coherent WDM for spectral efficiency enhancement”, **19**, 14617-14631 (2011)

[19] J. Leuthold, R. Schmogrow, D. Hillerkuss, C. Koos, W. Freude, “Super Channels Based on Nyquist Multiplexing”, OECC 2012, Busan, Paper 3B1-2

[20] B. Metcalfe, “Toward Terabit Ethernet”, OFC 2008, San Diego USA, Plenary speech

[21] T. Richter, E. Palushani, C. S.-Langhorst, M. Nolle, R. Ludwig, and C. Schubert, “Single Wavelength Channel 10.2 Tb/s TDM-Data Capacity using 16-QAM and coherent detection”, NFOEC 2011, LA, California USA, Paper PDPA9

[22] R. W. Chang, “Synthesis of band-limited orthogonal signals for multichannel data transmission”, Bell System Technical Journal **45**, 17751796 (1966)

[23] D. Hillerkuss, T. Schellinger, R. Schmogrow, M. Winter, T. Vallaitis, R. Bonk, A. Marculescu, J. Li,M. Dreschmann, J. Meyer, S. Ben Ezra, N. Narkiss, B. Nebendahl, F. Parmigiani, P. Petropoulos, B. Resan, K. Weingarten, T. Ellermeyer, J. Lutz, M. Mller, M. Huebner, J. Becker, C. Koos, W. Freude, J. Leuthold, “Single source optical OFDM transmitter and optical FFT receiver demonstrated at line rates of 5.4 and 10.8 Tbit/s”, OFC 2010, Paper PDPC1

[24] Jianjun Yu, Ze Dong, Xin Xiao, Yan Xia, Sheping Shi, Chao Ge, Weiqing Zhou, Nan Chi and Yufeng Shao, “Generation, transmission and coherent detection of 11.2 Tb/s (112$times$100 Gb/s) single source optical OFDM superchannel”, OFC 2011, Paper PDPA6

[25] S. L. Jansen, I. Morita, T. C. W. Schenk, and H. Tanaka, “Long-haul transmission of 1652.5 Gbits/s polarization-division-multiplexed OFDM enabled by MIMO”, Journal of Optical Networking, **7**, 173182 (2008)

[26] Y. Ma, Q. Yang, Y. Tang, S. Chen, and W. Shieh, "1-Tb/s single-channel coherent optical OFDM transmission over 600-km SSMF fiber with subwavelength bandwidth access", Optical Express, **17**, 94219427 (2009)

[27] W. Shieh, "High Spectral Efficiency Coherent Optical OFDM for 1 Tb/s Ethernet Transport", OFC 2009, San Diego, USA, Paper OWW1

[28] S.L. Jansen, I. Morita, H. Tanaka, "121.9-Gb/s PDM-OFDM transmission with 2-b/s/Hz spectral efficiency over 1000 km of SSMF", OFC 2008, San Diego, USA, Paper PDP2

[29] A. Sano, E. Yamada, H. Masuda, E. Yamazaki, T. Kobayashi, E. Yoshida, Y. Miyamoto, S. Matsuoka, R. Kudo, K. Ishihara, Y. Takatori, M. Mizoguchi, K. Okada, K. Hagimoto, H. Yamazaki, S. Kamei, H. Ishii, "13.4-Tb/s (134 *times* 111-Gb/s/ch) no-guard-interval coherent OFDM transmission over 3,600 km of SMF with 19-ps average PMD", ECOC 2008, Brussels, Paper Th.3.E.1.

[30] E. Yamada, A. Sano, H. Masuda, E. Yamazaki, T. Kobayashi, E. Yoshida, K. Yonenaga, Y. Miyamoto, K. Ishihara, Y. Takatori, T. Yamada, H. Yamazaki, "1 Tbit/s (111 Gbit/s/ch$\times$10ch) no-guard-interval CO-OFDM transmission over 2100 km DSF", Electronics Letters, **44**, 14171418 2008

[31] J. Armstrong, "OFDM for optical communications", Journal of Lightwave Technology, **27**, 189204 (2009)

[32] W. Shieh, H. Bao, Y. Tang, "Coherent optical OFDM: theory and design", Optics Express, **16**, 841859 (2008)

[33] L. B. Du and A. J. Lowery, "The validity of Odd and Even channels for testing all-optical OFDM and Nyquist WDM long-haul fiber systems", **20**, B445-B451 (2012)

[34] S. K. Ibrahim, J. Zhao, F. C. Garcia Gunning, P. Frascella, F. H. Peters, and A. D.

Ellis, “Towards a practical implementation of coherent WDM: analytical, numerical, and experimental studies”, IEEE Photonics Journal, **2**, 833847 (2010)

[35] J. A. C. Bingham, “Multicarrier modulation for data transmission: An idea whose time has come,” IEEE Commun. Mag., vol. 28, 514 (1990)

[36] R. van Nee and R. Prasad, “OFDM for Wireless Multimedia Communications”, Artech House, 2000

[37] W. Y. Zou and Y. Wu, “COFDM: An overview”, IEEE Transactions on Broadcasting, **41**, 18 (1995)

[38] N. Cvijetic, “OFDM for Next-Generation Optical Access Networks”, Journal of Lightwave Technology, **30**, 384 - 398 (2012)

[39] S. B. Weinstein, “The history of orthogonal frequency division multiplexing”, IEEE Communication Magazine, **47**, 2635 (2009)

[40] Y. H. Ma, P. L. So, and E. Gunawan, “Performance analysis of OFDM systems for broadband power line communications under impulsive noise and multipath effects,” IEEE Transactions on Power Delivery **20**, 674682, (2005)

[41] C. Stevenson, G. Chouinard, Z. Lei, H. Wendong, S. Shellhammer, and W. Caldwell, “IEEE 802.22: The first cognitive radio wireless regional area network standard”, IEEE Communication Magazine, **47**, 130138, (2009)

[42] O. Gonzalez, S. Rodriguez, R. Perez-Jimenez, B. R. Mendoza, and F. Delgado, ”Adaptive OFDM system for multi-user communications over the indoor wireless optical channel,” IEE Proceedings Optoelectronics **154**, 139-144 (2006)

[43] N. Cvijetic, D. Qian, and T. Wang, “10 Gb/s free-space optical transmission using OFDM,” OFC 2008, San Diego, USA, Paper OThD2

[44] J. Vucic, C. Kottke, S. Nerreter, A. Buttner, K.-D. Langer, and J. W. Walewski, "White light wireless transmission at Mb/s net data rate by use of discrete-multitone modulation," IEEE Photonics Technology Letters, **21**, 15111513, (2009)

[45] D. Qian, J. Yu, J. Hu, P. N. Ji, and T. Wang, "11.5-Gb/s OFDM transmission over 640 km SSMF using directly modulated laser," ECOC 2008, Brussels, Belgium, Paper Mo.3.E.4

[46] A. J. Lowery, L. Du, and J. Armstrong, "Orthogonal frequency division multiplexing for adaptive dispersion compensation in long haul WDM systems," OFC 2006, Anaheim, Paper PDP39

[47] B. J. C. Schmidt, A. J. Lowery, and J. Armstrong, "Experimental demonstrations of electronic dispersion compensation for long haul transmission using direct-detection optical OFDM," Journal of Lightwave Technology, **26**, 196203 (2008)

[48] W.-R. Peng, X. Wu, V. R. Arbab, B. Shamee, J.-Y. Yang, L. C. Christen, K.-M. Feng, A. E. Willner, and S. Chi, "Experimental demonstration of 340 km SSMF transmission using a virtual single sideband OFDM signal that employs carrier suppressed and iterative detection techniques," OFC 2008, San Diego, CA, Paper OMU1

[49] N. Cvijetic, S. G. Wilson, and D. Qian, "System outage probability due to PMD in high-speed optical OFDM transmission," Journal of Lightwave Technology, **26**, 21182127, (2008)

[50] M. Cvijetic, "Coherent and Nonlinear Lightwave Communications," Artech House, 1996

[51] Y. K. Huang, D. Qian, R. E. Saperstein, P. N. Ji, N. Cvijetic, L. Xu, and T. Wang, "Dual-polarization IFFT/FFT optical signal processing for 100-Gb/s QPSK-PDM all-optical OFDM," OFC 2009, San Diego, CA, Paper OTuM4.

[52] Y.-K. Huang, E. Ip, Z. Wang, M.-F. Huang, Y. S., and T. Wang, "Transmission of Spectral Efficient Super-Channels Using All-Optical OFDM and Digital Coherent Receiver Technologies," Journal of Lightwave Technology, **29**, 3838 - 3844 2011

[53] D. Hillerkuss, M. Winter, M. Teschke, A. Marculescu, J. Li, G. Sigurdsson, K. Worms, S. B. Ezra, N. Narkiss, W. Freude, and J. Leuthold, "Simple all-optical FFT scheme enabling Tbit/s real-time signal processing," Optics Express, **18**, 9324-9340 (2010)

[54] H. Chen, M. Chen, and S. Xie, "All-optical sampling orthogonal frequency-division multiplexing scheme for high-speed transmission system," Journal of Lightwave Technology, **27**, 48484854 (2009).

[55] F. C. Garcia Gunning, S. K. Ibrahim, P. Frascella, P. Gunning, and A. D. Ellis, "High symbol rate OFDM transmission technologies",OFC 2010, San Diego, CA, Paper OThD1

[56] S. Chandrasekhar, X. Liu, B. Zhu, and D. W. Peckham, "Transmission of a 1.2 Tb/s 24-carrier no-guad-interval coherent OFDM superchannel over 7200-km of Ultra-Large-Area Fiber," ECOC 2009, Vienna, Austria, Paper PD2.6

[57] K. Takiguchi, M. Oguma, H. Takahashi, and A. Mori, "PLC-based eight-channel OFDM demultiplexer and its demonstration with 160 Gbit/s signal reception," OFC 2010, San Diego, CA, Paper OThB4

[58] Z. Wang, K. S. Kravtsov, Y.-K. Huang, and P. R. Prucnal, "Optical FFT/IFFT circuit realization using arrayed waveguide gratings and the applications in all-optical OFDM system," Optics Express, **19**, 4501-4512 (2011)

[59] A. J. Lowery, "Inserting a cyclic prefix using arrayed-waveguide grating routers in all-optical OFDM transmitters," Optics Express, **20**, 9742-9754 (2012)

[60] A. J. Lowery, "Design of Arrayed-Waveguide Grating Routers for use as optical OFDM demultiplexers," Optics Express, **18**, 1412914143 (2010).

[61] S. Shimizu, G. Cincotti, and N. Wada, "Demonstration of 8×12.5 Gbit/s All-Optical OFDM System with an Arrayed Waveguide Grating and Waveform Reshaping" ECOC 2012, Amsterdam Netherlands, Paper Th.1.A.2

[62] W. Shieh, Q. Yang, and Y. Ma, "107 Gb/s coherent optical OFDM transmission over 1000-km SSMF fiber using orthogonal band multiplexing," Optics Express, **16**, 63786386 (2008).

[63] S. L. Jansen, I. Morita, T. C. W. Schenk, and H. Tanaka, "121.9-Gb/s PDM-OFDM transmission with 2-b/s/Hz spectral efficiency over 1000 km of SSMF," Journal of Lightwave Technology, **27**, 177 - 188 (2009).

[64] E. Yamada, A. Sano, H. Masuda, E. Yamazaki, T. Kobayashi, E. Yoshida, K. Yonenaga, Y. Miyamoto, K. Ishihara, Y. Takatori, T. Yamada, and H. Yamazaki, "1Tb/s (111Gb/s/ch × 10ch) No-Guard-Interval CO-OFDM Transmission over 2100 km DSF," OECC 2008, Paper PDP.6

[65] K. Takiguchi, M. Oguma, H. Takahashi, and A. Mori, "PLC-based eight-channel OFDM demultiplexer and its demonstration with 160 Gbit/s signal reception," OFC 2010, SanDiego CA, Paper OThB4

[66] H. Chen, X. Gu, F. Yin, M. Chen, and S. Xie, "5200Gbit/s all-optical OFDM transmission using a single optical source and optical Fourier transform real-time detection," Optics Express, **19**, 21199-21204 (2011)

[67] T. M. Schmidl and D. C. Cox, "Robust frequency and timing synchronization for OFDM," IEEE Transactions on Commununcations, **45**, 16131621, (1997)

[68] Y. G. Li, and G. L. Stuber, "Orthogonal Frequency Division Multiplexing for Wireless Communications", Springer 2006

[69] Z. Wang, Y. Qiao, and Y. Ji, "A novel joint frequency offset and channel estimation method for CO-OFDM system," ACP 2010, Shanghai China, 607-608 (2010).

[70] S. Cao, S. Zhang, Y. Shaoliang, K. Changyuan, and P.-Y. Kam, "Full range pilot-assisted frequency offset estimation for OFDM systems," OFC 2013, Anaheim, California United States, Paper JW2A.53

[71] X.-H. Fan, J. Yu, D. Qian, and G.-K. Chang, "A fast and efficient frequency offset correction technique for coherent optical orthogonal frequency division multiplexing," Journal of Lightwave Technology, **29**, 19972004 (2011)

[72] X. Zhou, K. Long, R. Li, X. Yang, and Z. Zhang, "A simple and efficient frequency offset estimation algorithm for high-speed coherent optical OFDM systems," Optics Express, **20**, 73507361 (2012).

[73] H. Y. Rha, B. G. Jeon, and H. Choi, "Simple wide range carrier frequency offset estimation for coherent optical OFDM," IEEE Photonics Technology Letters, **24**, 20642066 (2012)

[74] M. Lei, M. Zhao, J. Zhong, and Y. Cai, "ML-based estimation algorithm of frequency offset for 2×2 STBCOFDM systems," ETRI Journal, **34**, 458461 (2012).

[75] P. H. Moose, "A technique for orthogonal frequency division multiplexing frequency offset correction," IEEE Transactions on Communications, 42, 29082914 (1994).

[76] J. C. Cartledge, J. D. Downie and J. E. Hurley, "Frequency Offset Estimation for 112 Gbit/s PDM-QPSK Systems Using Sample Autocorrelation Functions," IEEE Photonics Society Annual Meeting, 596-597 2010.

[77] J.-J. van de Beek, M. Sandell, and P. O. Borjesson, "ML Estimation of Time and Frequency Offset in OFDM Systems," IEEE Transactions on Signal Processing, **45**, 1800 - 1805 1997

[78] Y. Huang, X. Zhang, and L. Xi, "Modified Synchronization Scheme for Coherent Optical OFDM Systems," IEEE/OSA Journal of Optical Communications and Networking, **5** 584 - 592, 2013

[79] T. Pollet, M. Van Bladel, and M. Moeneclaey, "BER sensitivity of OFDM systems to carrier frequency offset and Wiener phase noise," IEEE Transactions on Communications, **43**, 191193, (1995)

[80] J. Stott, "The effects of phase noise in COFDM," EBU Technical Review, 122, 1998

[81] L. Tomba, "On the effect of Wiener phase noise in OFDM systems," IEEE Transactions on Communications, **46**, 580583, (1998)

[82] A. G. Armada, "Understanding the effects of phase noise in orthogonal frequency division multiplexing (OFDM)," IEEE Transactions on Broadcasting, **47**, 153159, (2001)

[83] W. Shieh, X. Yi, Y. Ma, and Q. Yang, "Coherent optical OFDM: has its time come," Journal of Optical Networking, **7**, 234255 (2008)

[84] A. J. Lowery, and L. B. Du, "Optical orthogonal division multiplexing for long haul optical communications: A review of the first five years," Optical Fiber Technology, **17**, 421438 (2011)

[85] H. Bao and W. Shieh, "Transmission simulation of coherent optical OFDM signals in WDM systems," Optics Express, **15**, 4410-4418 (2007)

[86] W. Shieh and C. Athaudage, "Coherent optical orthogonal frequency division multiplexing," Electronics Letters, **42**, 587 588 (2006)

[87] S. Shimizu, G. Cincotti, and N. Wada, "Chromatic Dispersion Monitoring and Adaptive Compensation in an 8×12.5 Gb/s All-Optical OFDM System," ECOC 2013, London UK, 1 - 3

[88] S. Chandrasekhar and X. Liu, "Experimental investigation on the performance of closely spaced multi-carrier PDM-QPSK with digital coherent detection," Optics Express, **17**, 21350-21361 (2009)

[89] G. Goldfarb, L. Guifang, and M. G. Taylor, "Orthogonal Wavelength-Division Multiplexing Using Coherent Detection," IEEE Photonics Technology Letters, **19**, 2015-2017 (2007)

[90] K. Sathananthan, and C. Tellambura, "Probability of Error Calculation of OFDM Systems With Frequency Offset," IEEE Transactions on Communications, **49**, 1884-1888 (2001)

[91] R. U. Mahesh, and A. K. Chaturvedi, "Closed Form BER Expressions for BPSK OFDM Systems with Frequency Offset," IEEE Communications Letters, **14**, 731-733 (2010)

[92] S. Shimizu, G. Cincotti, and N. Wada, "Demonstration and performance investigation of all-optical OFDM systems based on arrayed waveguide gratings," Optics Express, **20**, B525-B534 (2012)

[93] K.-P. Ho, "Phase-Modulated Optical Communication Systems," Springer 2005

[94] G. P. Agrawal, "Fiber-Optic Communication Systems," John Wiley & Sons 2002

[95] J. M. Senior, and M. Y. Jamro, "Optical Fiber Communications: Principles and Practice" Pearson 2009

[96] J. M. Wozencraft, and I. M. Jacobs, "Principles of Communication Engineering," John Wiley & Sons 1990

[97] S. L. Miller, and D. G. Childers, "Probability and Random Processes: With Applications to Signal Processing and Communications," Academic Press 2012

[98] C. Liu, J. Pan, T. Detwiler, A. Stark, Y.-T. Hsueh, G.-K. Chang, and S. E. Ralph, "Joint digital signal processing for superchannel coherent optical communication systems," Optics Express, **21**, 8342-8356, (2013)

[99] K. Fazel, S. Kaiser, "Multi-carrier and Spread Spectrum Systems: From OFDM and MC-CDMA to LTE and WiMAX," Wiley-Blackwell, 2008

[100] J. M. P.-Borrallo, "Multicarrier vs. Monocarrier Modulation Techniques: An Introduction to OFDM," in Proc. Berkeley Wireless Research Center Retreat, 2000

[101] S. J. Savory, "Digital Coherent Optical Receivers: Algorithms and Subsystems," IEEE Journal of Selected Topics in Quantum Electronics, **16**, 1164-1179, (2010)

[102] R. Ramaswami, K. Sivarajan, G. Sasaki, "Optical Networks: A Practical Perspective," Morgan Kaufmann, 2009

[103] R. Kou, H. Fukuda, T. Tsuchizawa, H. Nishi, T. Hiraki, K. Yamada, "Silicon/Silica-Hybrid-Integrated Delay Line Interferometer for Demodulation of PSK Formats," IEEE Photonics Journal, **5**, 2201508, 2013

[104] J.-K. K. Rhee, N. Cvijetic, N. Wada, and T Wang, "Optical orthogonal frequency division multiplexed transmission using all-optical discrete Fourier transform," Laser & Photon Reviews, **7**, 539-553 (2013)

[105] T. Erdogan, "Fiber Grating Spectra," Journal of Lightwave Technology, **15**, 1277 - 1294 (1997)

[106] A. Othonos, "Fiber Bragg gratings," AIP Review of Scientific Instruments, **68**, 4309 - 4341 (1997)

[107] P. C. Teh, P. Petropoulos, M. Ibsen, and D. J. Richardson, "A Comparative Study of the Performance of Seven- and 63-Chip Optical Code-Division Multiple-Access Encoders and Decoders Based on Superstructured Fiber Bragg Gratings," Journal of Lightwave Technology, **19**, 1352 - 1365 (2001)

[108] S. Schwarz, C. G. Schaeffer, A. Rahim, J. Bruns, and K. Petermann, "Comparison of phase error sensitivities of all-optical discrete Fourier transforms for OFDM demultiplexing," Optical and Quantum Electronics, **45**, 775-781 (2013)

[109] D. C. Montgomery, and G. C. Runger, "Applied Statistics and Probability for Engineers," John Wiley & Sons, 2010

[110] Y. C. Ko, "Quadrature Amplitude Modulation," Communication Systems and Lab, Korea University, 2009

[111] J.G. Proakis, M. Salehi, and G. Bauch, "Contemporary Communication Systems Using Matlab," Thomson Brooks/Cole, 2004

[112] E. Wong, Current and next-generation broadband access technologies, OFC/NFOEC 2011, USA, Paper NMD1.

[113] L. G. Kazovsky, W.-T. Shaw, D. Gutierrez, N. Cheng, and S.-W. Wong, Next-Generation Optical Access Networks, J. Lightwave Technol. **25**, 34283442 (2007).

[114] X.Q. Jin, E. Hugues-Salas, R. P. Giddings, J. L. Wei, J. Groenewald and J. M. Tang, "First real-time experimental demonstrations of 11.25Gb/s optical OFDMA PONs with adaptive dynamic bandwidth allocation," Optics Express, **19**, 20557 - 20570, (2011)

[115] N. Cvijetic, D. Qian, and J. Hu, "100 Gb/s Optical Access Based on Optical Orthogonal Frequency-Division Multiplexing," IEEE Communications Magazine, **48**, 70 - 77, (2010)

[116] W. Wei, T. Wang, D. Qian, and J. Hu, MAC protocols for optical orthogonal frequency division multiple access (OFDMA)-based passive optical networks, IEEE/OSA OFC 2008, San Diego, CA, Paper JWA82.

[117] J. Zhang, T. Wang, and N. Ansari, An efficient MAC protocol for asynchronous ONUs in OFDMA PONs, IEEE/OSA OFC 2011, Los Angeles, CA, Paper JWA071.

[118] K. Kanonakis, I. Tomkos, T. Pfeiffer, J. Prat, and P. Kourtessis, "ACCORDANCE: A Novel OFDMA-PON Paradigm for Ultra-High Capacity Converged Wireline-Wireless Access Networks," ICTON 2010, Munich, Germany, Paper Tu.A1.2

[119] L. Liu, X. Yang, W. Hu, "An efficiency-improved MAC protocol for asynchronous ONUs in OFDMA PONs," ACP 2012, Paper AS1D3

[120] C.-J. Chae, E. Wong, and R. S. Tucker, "Optical CSMA/CD Media Access Scheme for Ethernet Over Passive Optical Network," IEEE Photonics Technology Letters, **14**, 711-713 (2002)

[121] Broadband Optical Access Systems Based on Passive Optical Networks,, Recommendation G.983.1, 1998. http://www.itu.int/rec/T-REC-G.983.1-199810-S/en

[122] J. Prokkola,"OPNET - Network Simulator: Simulations and Tools for Telecommunications," University of Oulu, 2008.